



ANALYTICAL HARMONIC DESCRIPTION OF DEAD-TIME EFFECTS IN
VOLTAGE SOURCE INVERTERS

Jorge Eliécer Caicedo Castaño

Tese de Doutorado apresentada ao Programa de Pós-graduação em Engenharia Elétrica, COPPE, da Universidade Federal do Rio de Janeiro, como parte dos requisitos necessários à obtenção do título de Doutor em Engenharia Elétrica.

Orientador: Mauricio Aredes

Rio de Janeiro
Março de 2020

ANALYTICAL HARMONIC DESCRIPTION OF DEAD-TIME EFFECTS IN
VOLTAGE SOURCE INVERTERS

Jorge Eliécer Caicedo Castaño

TESE SUBMETIDA AO CORPO DOCENTE DO INSTITUTO ALBERTO LUIZ COIMBRA DE PÓS-GRADUAÇÃO E PESQUISA DE ENGENHARIA DA UNIVERSIDADE FEDERAL DO RIO DE JANEIRO COMO PARTE DOS REQUISITOS NECESSÁRIOS PARA A OBTENÇÃO DO GRAU DE DOUTOR EM CIÊNCIAS EM ENGENHARIA ELÉTRICA.

Orientador: Prof. Mauricio Aredes

Aprovada por: Prof. Luis Guilherme Barbosa Rolim
Prof. Edson Hirokazu Watanabe
Prof. Jorge Rodrigo Massing
Prof. Sergio Augusto Romana Ibarra
Prof. Samir Ahmad Mussa

RIO DE JANEIRO, RJ – BRASIL
MARÇO DE 2020

Caicedo Castaño, Jorge Eliécer

Analytical Harmonic Description of Dead-Time Effects
in Voltage Source Inverters/Jorge Eliécer Caicedo Castaño.
– Rio de Janeiro: UFRJ/COPPE, 2020.

XVII, 124 p.: il.; 29, 7cm.

Orientador: Mauricio Aredes

Tese (doutorado) – UFRJ/COPPE/Programa de
Engenharia Elétrica, 2020.

Referias Bibliográficas: p. 60 – 65.

1. harmonic analysis. 2. frequency analysis.
3. dead-time. 4. power electronics converter.
5. harmonic compensation. I. Aredes, Mauricio.
II. Universidade Federal do Rio de Janeiro, COPPE,
Programa de Engenharia Elétrica. III. Título.

*Este trabalho esta dedicado à
minha esposa, Joanna e à nossa
filha, Sara.*

Agradecimentos

À minha esposa, Joanna, pelo seu imenso apoio, amor e amizade, e especialmente pela sua infinita paciência.

À minha filha, Sara, pelo seu carinho e compreensão durante esta etapa.

Aos meus pais, Jorge e Miryam, pelos seus grandes sacrifícios e pelo apoio incondicional.

Ao meu orientador, Professor Mauricio Aredes, pelo seu grande apoio, amizade e confiança ao longo do tempo de meus estudos dentro de seu laboratório.

Aos colegas do laboratório LEMT: André Ramos De Castro, pelas inúmeras horas de discussões, pelo aprendizado e amizade, e especialmente pelo seu apoio fundamental na edição deste documento; Juliano Caldeira, pela grande amizade e confiança, pelo apoio e grande aprendizado para minha atuação como profissional; Bruno França e Leonardo Silva, pelo apoio e ensinamentos na minha adaptação no Brasil. Também agradeço de forma geral a todos os colegas do LEMT que criaram um ambiente rico para discussões técnicas, assim com também um espaço descontraído para o desenvolvimento desta tese.

Aos membros da banca pelas contribuições neste documento.

À Coordenação de Aperfeiçoamento de Pessoal de Nível Superior - Brasil (CAPES) pelo apoio financeiro.

Resumo da Tese apresentada à COPPE/UFRJ como parte dos requisitos necessários para a obtenção do grau de Doutor em Ciências (D.Sc.)

DESCRIÇÃO HARMÔNICA ANALÍTICA DOS EFEITOS DO TEMPO MORTO EM CONVERSORES ELETRÔNICOS DE ENERGIA

Jorge Eliécer Caicedo Castaño

Março/2020

Orientador: Mauricio Aredes

Programa: Engenharia Elétrica

Aplicações de eletrônica de potência usam esquemas de compensação harmônica para melhorar as distorções de baixa frequência, usualmente harmônicos da frequência fundamental menores ao vigésimo primeiro, causadas por cargas não lineares e tempo morto inserido no padrão de comutação. Poucos métodos analíticos foram propostos para entender os efeitos do tempo morto, e eles se concentraram principalmente em amplificadores de classe D, o que leva a expressões analíticas complexas. Este estudo propõe uma abordagem analítica que permite o entendimento dos principais componentes harmônicos da tensão de saída de inversores *PWM* com sinais moduladores de múltiplas frequências (fundamental e harmônicos). A abordagem analítica proposta é baseada em uma análise dupla da série de Fourier e focada no espectro das baixas frequências. Todas as premissas teóricas são validadas usando o simulador de transientes eletromagnéticos *PSCADTM/EMTDCTM*. Os resultados usando um inversor de fonte de tensão monofásico mostraram que é possível criar um modelo matemático eficiente com desempenho até cento e trinta vezes mais rápido que uma simulação tradicional de conversor eletrônico de potência. Além disso, usando a abordagem analítica proposta, é demonstrado que os efeitos do tempo morto são independentes da existência de harmônicos de frequência fundamental no sinal do modulador. No entanto, o tempo morto afeta um harmônico injetado se este for um harmônico de ordem inteira ímpar da frequência fundamental.

Abstract of Thesis presented to COPPE/UFRJ as a partial fulfillment of the requirements for the degree of Doctor of Science (D.Sc.)

ANALYTICAL HARMONIC DESCRIPTION OF DEAD TIME EFFECTS IN
POWER ELECTRONIC CONVERTERS

Jorge Eliécer Caicedo Castaño

March/2020

Advisor: Mauricio Aredes

Department: Electrical Engineering

Several power electronic applications use harmonic compensation schemes to improve the low-frequency distortions, usually fundamental-frequency harmonics smaller than twenty-first, caused by nonlinear loads and dead-time inserted into switching patterns. Few analytical methods have been proposed to understand the effects of dead-time, and they have focused mostly on Class-D power amplifiers, which leads to cumbersome analytical expressions. This study proposes an analytical approach that allows for the understanding of the principal harmonic components of the output voltage of *PWM* inverters with multiple-frequency modulator signals (fundamental and harmonics). The proposed analytical approach is based on a double Fourier-series analysis and focused on the low-frequency spectrum. All theoretical assumptions are validated by using *PSCADTM/EMTDCTM* electromagnetic transients simulator. Results using a single-phase voltage source inverter show that it is possible to create an efficient mathematical model with performance up to one hundred and thirty times faster than a traditional power electronic converter simulation. Additionally, using the proposed analytical approach, it is demonstrated that dead-time effects are independent of the existence of fundamental-frequency harmonics in the modulator signal. Nevertheless, dead-time affects an injected harmonic if this is an odd integer order harmonic of the fundamental frequency.

Contents

List of Figures	xi
List of Tables	xiv
List of Symbols	xv
List of Abbreviations	xvii
1 Introduction	1
1.1 Motivation and Research Scope	3
1.1.1 Research Question	4
1.1.2 Research Statement	4
1.2 Fundamental Concepts	5
1.2.1 Converter Topologies	5
1.2.2 Pulse Width Modulation Schemes	6
1.2.3 Dead Time in Voltage Source Inverters	8
1.3 Thesis Outline	10
1.4 Conclusions	10
2 Review of Previous Research	11
2.1 Dead-time Effects and Compensation Techniques in <i>PWM</i> Schemes .	12
2.2 Analytical Frequency Description of <i>PWM</i> Schemes	13
2.2.1 <i>Black's Method</i>	13
2.3 Analytical Frequency-Spectra of <i>PWM</i> with Dead Time	16
2.3.1 Dead-Time Spectra Calculation Using <i>Black's Method</i>	17
2.3.2 Dead-Time Spectra Calculation Using Song-Sarwate's Method	18
2.3.3 Dead-Time Spectra Calculation Using Poisson's Summation Method	20
2.4 State of the Art	23
2.4.1 State-of-the-Art Research Using <i>Black's Method</i>	23
2.4.2 State-of-the-Art Research Using <i>Song-Sarwate's Method</i>	23
2.4.3 State-of-the-Art Research Using <i>Poisson Summation Method</i> .	23

2.5	Conclusions	24
3	<i>PWM</i> Spectrum of One Inverter Phase Leg	25
3.1	Topology of One Inverter's Phase Leg	26
3.2	Ideal <i>PWM</i> with Multiple-Frequency Modulator	27
3.2.1	Ideal <i>PWM</i> Definition	27
3.2.2	Ideal Spectrum of a Naturally Sampled <i>PWM</i>	29
3.3	<i>PWM</i> with Multiple-Frequency Modulator and Dead-Time (<i>Original Contribution</i>)	32
3.3.1	<i>PWM</i> Definition Including Dead-Time Effects	32
3.3.2	Spectrum of a Naturally Sampled <i>PWM</i> Including Dead-Time	36
3.4	Conclusions	41
4	Single-Phase <i>PWM</i> Voltage Source Inverters	43
4.1	Topologies of a Single-Phase Inverter	44
4.2	Two-Level <i>PWM</i> Single-Phase Inverter	45
4.2.1	Low-Frequency Spectrum of a Two-Level Single-Phase Inverter	45
4.2.2	Simulation Results	46
4.3	Three-Level <i>PWM</i> Single-phase Inverter	50
4.3.1	Low-Frequency Spectrum	50
4.3.2	Simulation Results	51
4.4	Low-frequency model (<i>Original Contribution</i>)	53
4.5	Conclusions	57
5	Conclusion and Future Works	58
5.1	Contributions of this Thesis	59
5.2	Continuing Development	59
	Bibliography	60
A	3-D Geometrical Interpretation of the Carrier-Modulator Interaction in <i>Black's Method</i> (<i>Original Contribution</i>)	66
B	<i>Black's Method</i> (Equations Definition)	68
B.1	Trailing-Edge Naturally Sampled <i>PWM</i>	69
B.2	Double-Edge Naturally Sampled <i>PWM</i>	72
C	Analytical Low-Frequency Spectra (Equations Development)	74
C.1	<i>Maple</i> TM 2019 worksheet for Trailing-edge Naturally Sampled <i>PWM</i> .	75
C.2	<i>Maple</i> TM 2019 worksheet for Double-edge Naturally Sampled <i>PWM</i> .	93
D	<i>PSCAD</i>TM Simulation Diagrams	110

E	<i>PwmSpectra</i> Package	114
E.1	<i>PwmSpectra</i> Details	115
E.2	UML Diagram V1.0	116
E.3	<i>Wolfram Mathematica</i> [®] Notebook of a <i>PwmSpectra</i> Examples	117

List of Figures

1.1	Block diagram of a typical power electronic application.	2
1.2	Outline of frequency spectra in a power electronic application.	3
1.3	Converter topologies: a) Two-level single-phase; b) Three-level single-phase. The full-bridge topology in (b) can be used for two-level scheme by setting $s_3 = s_2$ and $s_4 = s_1$	5
1.4	Example of a <i>PWM</i> waveform formed by a multiple-frequency modulator signal.	6
1.5	Naturally sampled <i>PWM</i> schemes: a) Trailing-edge sawtooth carrier; b) Falling-edge sawtooth carrier; c) Triangular or double-edge carrier.	8
1.6	Regular sampling <i>PWM</i> : a) Sawtooth carrier; b) Symmetrical sampling with the triangular carrier (negative peak sampled); c) Asymmetrical sampling.	8
1.7	Creation of the <i>PWM</i> pattern with dead time.	9
1.8	Dead-time effects in the output voltage of a <i>VSI</i>	10
2.1	Example of a multiple-frequency-modulator <i>PWM</i> defined by <i>Black's method</i>	15
3.1	One inverter phase-leg topologies: a) phase-leg using ideal switches; b) phase-leg using power switches and its associated free-wheel diodes in an anti-parallel configuration.	26
3.2	Naturally sampled <i>PWM</i> definitions: A) and B) displays a classical <i>PWM</i> definition; C) and D) shown the 3D-model approach. Plot parameters: $V_{dc} = 1.0 \text{ p.u.}$, $M = 0.5$, $\omega_1 = 2\pi 60 \text{ rad/s}$, $\theta_1 = 0^\circ$, $h = 7$, $M_h = 0.1$, $\theta_h = 0^\circ$, $\theta_c = 0^\circ$, $M_f = 9$	28
3.3	Dead-time effects over the <i>PWM</i> signal.	33
3.4	Current boundaries definition. The angle φ is an approximation due to the multiple zero-crossing of the current ripple.	33
3.5	Details of dead-time effects on <i>PWM</i> signals.	34

3.6	Dead-time effects over the <i>PWM</i> 3D-model. Parameters used: $V_{dc} = 1.0$ p.u., $M = 0.6$, $\omega_o = 2\pi 60$ rad/s, $\theta_o = 30^\circ$, $h = 7$, $M_h = 0.1$, $\theta_h = 15^\circ$, $\theta_c = 45^\circ$, $M_f = 21$, $T_d = 100$ μ s, $\varphi = 30^\circ$	35
3.7	Components of the fundamental frequency. Parameters used: $M = 0.8$, $V_{dc} = 1.0$ p.u., $\varphi = 60^\circ$, $T_d = 20$ μ s, $\omega_1 = 2\pi 60$ rad/s, $\theta_1 = 0^\circ$, $M_f = 85$	38
3.8	Components of the injected-harmonic. Parameters used: $h = 3$, $M_h = 0.05$, $V_{dc} = 1.0$ p.u., $\varphi = 45^\circ$, $T_d = 20$ μ s, $\omega_o = 2\pi 60$ rad/s, $\theta_h = 0^\circ$, $M_f = 85$	39
3.9	Normalized low-frequency spectrum of a double-edge naturally sampled <i>PWM</i> signal considering dead-time effects and a multiple-frequency modulator. Parameters used: $M = 0.8$, $h = 5$, $M_h = 0.05$, $V_{dc} = 1.0$ p.u., $\varphi = 45^\circ$, $T_d = 5$ μ s, $\omega_o = 2\pi 60$ rad/s, $\theta_1 = \theta_h = 0^\circ$, $M_f = 85$	41
4.1	Two-level single-phase inverter topologies: a) Half-bridge single-phase inverter; b) Full-bridge single-phase inverter.	44
4.2	Three-level full-bridge single-phase inverter topology.	44
4.3	Analytical low-frequency spectra of a single-phase inverter. Parameters used: $M = 0.8871$; $\omega_1 = 376.9$ rad/s; $\theta_1 = \theta_h = 0^\circ$; $\varphi = 45^\circ$; $T_d = 5$ μ s; $M_f = 85$; $M_h = 0.05$; and $h = 5$	46
4.4	Block diagram and circuits of the proposed single-phase case scenarios. $S_a(t)$ represents the multi-frequency modulator signal and v'_{conv} represents the estimated voltage value of the converter using the proposed simplified model.	47
4.5	Voltage waveform before the output-filter. Dead-time effects can be seen in the highly nonlinear deformation of the model's waveform that occurs when the current changes its polarity.	49
4.6	Load's voltage-waveform comparison. Processing time step = 0.1μ s.	49
4.7	Output-voltage spectra comparison for two-level single-phase inverter.	50
4.8	Voltage waveform before the output filter for three-level single-phase inverter.	52
4.9	Load's voltage-waveform comparison for three-level single-phase inverter.	52
4.10	Output-voltage spectra comparison for three-level single-phase inverter.	53
4.11	Converter simulation behavior for different values of the simulation time step.	56
4.12	Output voltage comparison at different simulation step time: Analytical model using 100 μ s and converter simulation using 0.1 μ s.	56

A.1	2-Dimensional representation of a double-edge naturally sampled <i>PWM</i> .	66
A.2	3-Dimensional representation of $F_{gi}(x, y) = s_a(y) - c(x)$ for a double-edge naturally sampled <i>PWM</i> . This figure shows the iteration of two cycles of the modulating signal $s_a(y)$, and two periods of the carrier signal $c(x)$ in the 3-dimensional arrangement formed by the axes $x = \omega_c t$, $y = \omega_o t$, and $z = F_{gi}(x, y)$.	67
D.1	<i>PSCADTM</i> simulation of the two-levels single-phase <i>VSI</i> used in chapter 3.	111
D.2	<i>PSCADTM</i> simulation of the two levels single-phase full-bridge <i>VSI</i> used in chapter 3.	112
D.3	<i>PSCADTM</i> simulation of the three levels single-phase full-bridge <i>VSI</i> used in chapter 3.	113
E.1	<i>UML</i> diagram of <i>PwmSpectra</i> V1.0.	116

List of Tables

3.1	Boundary equations for a naturally sampled PWM scheme evaluated over the range $[-\pi, \pi]$	29
3.2	Boundary equations for a naturally sampled <i>PWM</i> scheme including dead time and evaluated over the range $[-\pi, \pi]$	34
4.1	Inverter parameters.	48
4.2	<i>PWM</i> model parameters.	48

List of Symbols

A_{mn}, B_{mn}	double-Fourier-series coefficients, p. 14
C_n	Fourier series coefficients of the periodic <i>PWM</i> signal, used in Song-Sarwate's Method, p. 20
C_{mn}	complex coefficient of the double Fourier-series, p. 14
$E(f)$	Fourier's transform of $e(t)$, used in Song-Sarwate's Method, p. 20
$F(x, y)$	multidimensional function of a <i>PWM</i> , p. 14
F_{1mn}, F_{2mn}	coefficient of the side-bands harmonics, used by Wu et al, p. 17
M_f	frequency ratio between the carrier and the fundamental frequency, p. 14
M_h	injected-harmonic amplitude, p. 27
P	plane that describes the relationship between axes x and y , p. 14
$P_c(f)$	Fourier's transform of $p_c(t)$, used in Song-Sarwate's Method, p. 20
$P_s(f)$	Fourier's transform of $p_s(t)$, used in Song-Sarwate's Method, p. 20
$P_{T_d}(f)$	Fourier's transform of $p_{T_d}(t)$, used in Song-Sarwate's Method, p. 20
T_c	period of the carrier signal, p. 20
$\delta(\cdot)$	<i>Dirac</i> delta function, used in Song-Sarwate's Method, p. 20
$\hat{v}_{conv}(t)$	Inverter's output voltage normalized by the magnitude of the fundamental-frequency, p. 44

ω_1	modulating angular-frequency, p. 14
ω_c	carrier angular frequency, p. 14
$\sigma(t)$	choice function, used time in Song-Sarwate's Method, p. 20
τ_k	pulse width for the k -th interval, used in Song-Sarwate's Method, p. 20
θ_1	arbitrary phase offset angle for the modulating waveform, p. 14
θ_c	arbitrary phase offset-angle for carrier waveform, p. 14
θ_h	injected-harmonic phase angle, p. 27
c	carrier signal, p. 27
$e(t)$	error introduced by dead time, used in Song-Sarwate's Method, p. 20
h	arbitrary harmonic of the fundamental-frequency, p. 26
$p_c(t)$	symmetrical square wave, used in Song-Sarwate's Method, p. 20
$p_s(t)$	bipolar pulse train, used in Song-Sarwate's Method, p. 20
$p_{T_d}(t)$	error introduced by dead time expressed as the convolution of a pulse, used in Song-Sarwate's Method, p. 20
s_a	modulator signal, p. 27
v_{a-}	output voltage of the phase a referenced to the negative rail of the DC link, p. 25
x	angular axis scale by ω_c , p. 14
$x'_f(y)$	falling function of the correction term, p. 33
$x_f(y)$	falling function, p. 14
$x'_r(y)$	rising function of the correction term, p. 33
$x_r(y)$	rising function, p. 14
y	angular axis scale by ω_1 , p. 14

List of Abbreviations

AC	Alternating Current, p. 5
DC	Direct Current, p. 5
DFT	Discrete Fourier Transform, p. 1
HC	Harmonic Compensation, p. 1
MMC	Modular Multi-level Converter, p. 15
PTM	Pulse-Time Modulation, p. 19
PWM	Pulse-Width Modulation, p. 1
SVM	Space Vector Modulation, p. 15
THD	Total Harmonic Distortion, p. 1
UPS	Uninterruptible Power Supply, p. 4
VSI	Voltage Source Inverters, p. 1

Chapter 1

Introduction

High power-quality applications using power electronic converters, such as high power-quality inverters and rectifiers, must deal with the presence of low-frequency distortions in voltage and current waveforms, usually fundamental-frequency harmonics. Some of these harmonic distortions are already present in the electrical network, especially in distribution levels, due to current disturbances created by non-linear loads. Hence, employing *Harmonic Compensation (HC)* systems or active filters is a common practice in these kinds of applications [1–4]. Moreover, the harmonics injected by the controller lead to multiple-frequency modulator signals for the *Pulse-Width Modulation (PWM)* technique. A typical power electronic inverter application using *PWM* is shown in Figure 1.1.

The term, *low-frequency*, will be used in this document as a reference of the fundamental-frequency harmonics lower than the switching-frequency. In practice the magnitude of the current and voltage harmonics greater than thirteen are usually neglected.

Low-frequency distortions also appear due to the dead time introduced in the switching pattern to avoid short-circuits in *Voltage Source Inverters (VSI)* [5–11]. This distortion can lead to instability issues in some power electronics applications [12], malfunction in sensitive equipment, over-sizing transformers, among other problems. Moreover, these low-frequency distortions are responsible for the power quality degradation of the converter and increases the *Total Harmonic Distortion (THD)*, which can lead to fines on industrial applications. Thus, several dead-time compensation techniques are proposed in the literature and implemented in industrial and commercial systems.

The standard approach for harmonic analysis in a power converter that implements *PWM* is to use a *Discrete Fourier Transform (DFT)* on measured signals, rather than an analytical solution to find the spectral components. The drawback of using *DFT* is that due to the usually large relationship between carrier and modulator frequency on power electronic applications, this approach requires an extensive

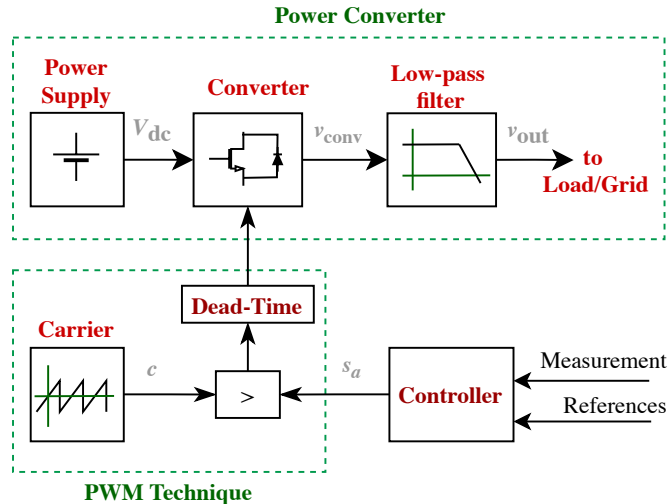


Figure 1.1 - Block diagram of a typical power electronic application.

sample-set to achieve good frequency resolution [7]. Hence, a small simulation time step should be used, causing high-computational cost simulations that limit the number of practical applications to study.

Few analytical methods have been proposed in the literature to understand the effects of dead time, and they have focused mostly on Class-D power amplifiers for radio and audio applications, where a full frequency-spectrum analysis is required. An extensive review of these techniques is presented in Chapter 2. Unlike *DFT*, an analytical solution provides a clear understanding of the influence of the system's parameters for each component of the frequency spectrum. Nevertheless, all of these methods provide analytical frequency spectra but lead to cumbersome expressions in order to describe the full frequency spectrum of the *PWM* signal with dead time.

In power electronics applications, the presence of low-pass output filters minimizes the contribution of high-frequency components on the output voltage of the power converter. Figure 1.2 depicts the outline of frequency spectra in different stages of a power electronic application. Considering the high-frequency attenuation of the output filter, it is possible to focus on the analytical low-frequency spectrum of power converter applications, including dead-time effects and a multiple-frequency modulator. This proposed study avoids the need for high computational-cost switched-simulations or cumbersome expressions for an analytical spectra.

This thesis proposes to use the double Fourier-series to develop the low-frequency spectra of *PWM* inverters with dead time and multiple-frequency modulator signals. This low-frequency approach successfully represents the principal dynamics of the output-voltage in the power converter. Additionally, this study shows how dead-time affects the frequency-components injected by multiple-frequency-modulator applications, e.g., harmonic compensation systems, active filter, multiple-frequency power

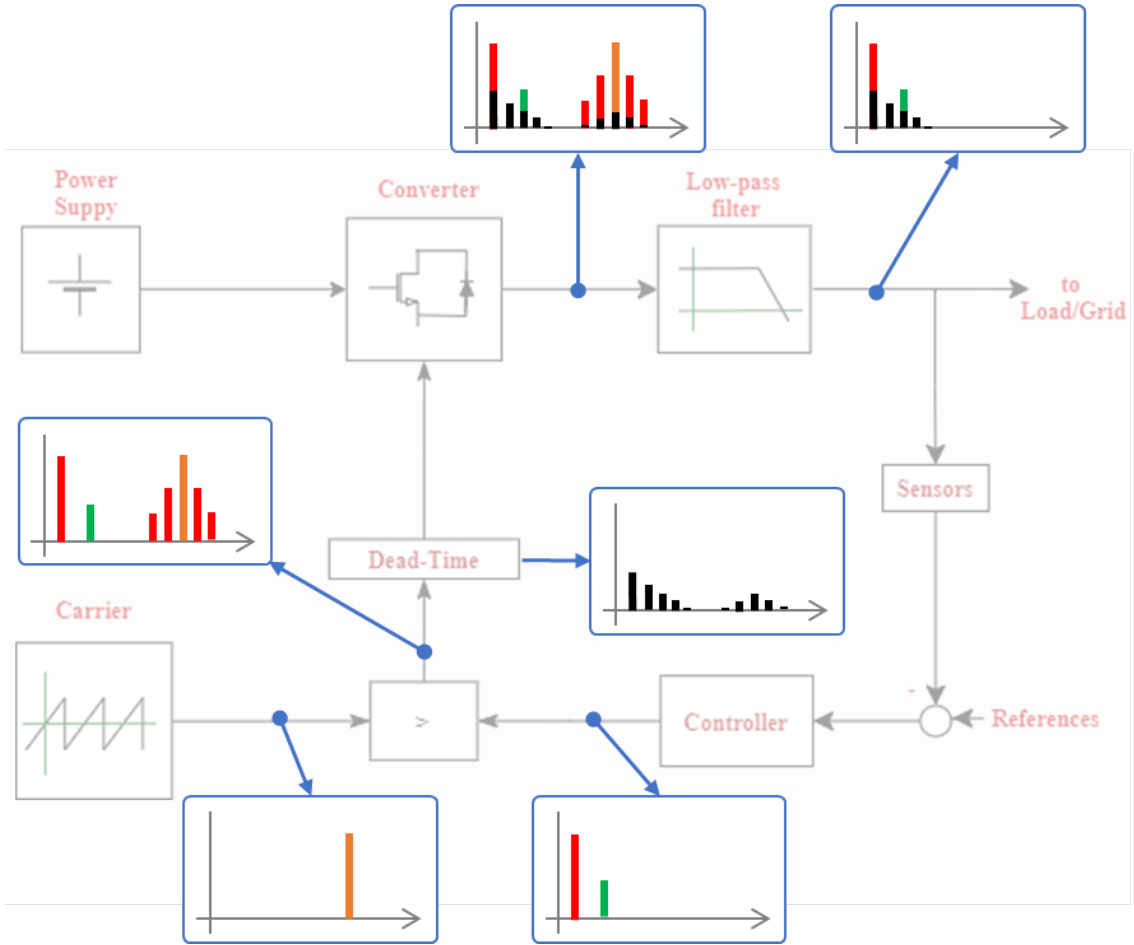


Figure 1.2 - Outline of frequency spectra in a power electronic application.

supplies, among others.

This introductory chapter aims to present some fundamental concepts before the development of the analytical frequency study. Nevertheless, it does not have the objective to provide a full understanding of these fundamental concepts. Instead, the main objective of this chapter is to establish the thesis scope, general aspects of the phenomena under study, and the terminology used in the following chapters.

The structure of this chapter is as follows: Section 1.1 explains the motivation and provides the research definition of this thesis. Section 1.2 explores the general aspects of the *PWM* schemes, inverter topologies, and the overall effects of dead time in *VSI*s. Finally, Section 1.3 provides the general outline of this document.

1.1 Motivation and Research Scope

Single-frequency power electronic applications present small low-frequency distortions in the output voltage waveform, and they are, in most cases, a consequence of dead-time effects. This distortion means that even when the controller tries to synthesize a pure single-frequency in the power inverter, due to the non-linear behavior

of dead time, the output voltage displays several odd harmonics of that fundamental frequency. Although small in magnitude, these harmonic components degrade the power quality of the equipment and can increase the *THD* above limits allowed by industrial standards.

Working with high-power-quality applications usually leads to elaborate control techniques in order to minimize *THD*. Some of these techniques involve voltage or current harmonic compensation and can be applied to islanded or grid-connected power converters. These control techniques deal with multiple-frequency in the control effort signals. In *PWM* converters, this means multiple-frequency modulator signals, e.g., a high-performance voltage controller for an *Uninterruptible Power Supply (UPS)* inverter [4], and a voltage harmonic compensation for a synchronverter that integrates wind and photovoltaic power [13], published by the author in 2015 and 2017, respectively.

Knowing that dead time creates harmonics of the fundamental-frequency in single-frequency applications, it is straightforward to ask, *what are the effects of dead time in PWM inverters with multiple-frequency modulator signals? And how can they be calculated?* The initial research in this topic led to a fascinating and extended research area, *the analytical description of PWM spectra in power converters*. Nevertheless, at the best of the author's knowledge, these specific questions have not been addressed yet. Thus, these were the questions that motivated this thesis and defined the associated research. The research is focused on half- and full-bridge converters with two- and three-level voltage topologies. As a summary of this research, the main question and the primary research statement are presented below.

1.1.1 Research Question

How to define a closed-form expression to determine the main effects of dead time in PWM inverters with multiple-frequency modulator signals?

1.1.2 Research Statement

The harmonic injected by the controller does not affect the frequency distortions already created by the dead time. Nevertheless, dead-time affects the injected harmonic if this is an odd integer order harmonic of the fundamental frequency. This effect has a non-linear relationship with the power factor of the load. Furthermore, it is inversely proportional to the harmonic order; and proportional to the DC voltage with a proportionality constant of four over pi squared.

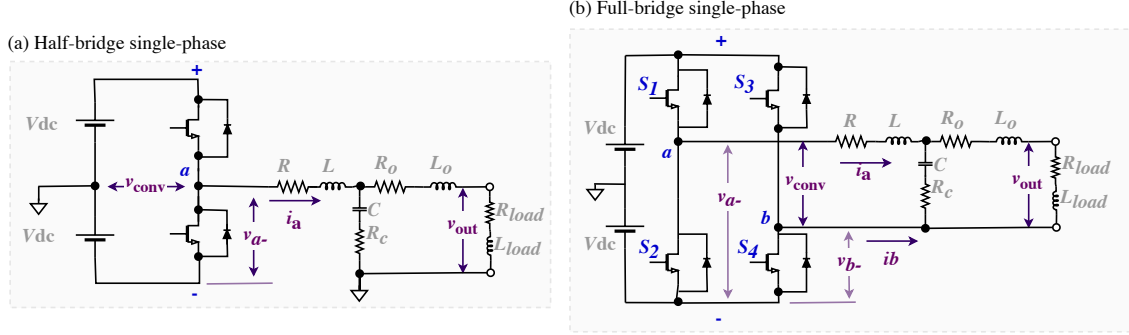


Figure 1.3 - Converter topologies: a) Two-level single-phase; b) Three-level single-phase. The full-bridge topology in (b) can be used for two-level scheme by setting $s_3 = s_2$ and $s_4 = s_1$.

This statement is mathematically demonstrated in the following chapters, and several partial conclusions are obtained during this mathematical procedure.

1.2 Fundamental Concepts

This section describes the inverter topologies used in this work, the modulation strategies, and the general description of the dead-time phenomenon. The main idea is to introduce the name of each topology and modulation technique, as well as the terminology of several parameters and variables that will be repeatedly mentioned in the following chapters.

1.2.1 Converter Topologies

Converter topologies that change energy from or into *Alternating Current (AC)*, normally involve more complex processes than those that solely involve *Direct Current (DC)* [12]. These topologies usually use high switching-frequencies modulated by low-frequency reference signals in order to achieve a high efficiency energy-conversion [14]. There are several inverter and rectifier topologies, and this thesis is focused on three of them, and they are listed below.

- Two-level single-phase.
 - Half-bridge.
 - Full-bridge.
- Three-level single-phase (full-bridge).

All converter topologies referred in this document are shown in Figure 1.3, and they are detailed in Chapters 3 and 4. The output-filter shown in this figure is an

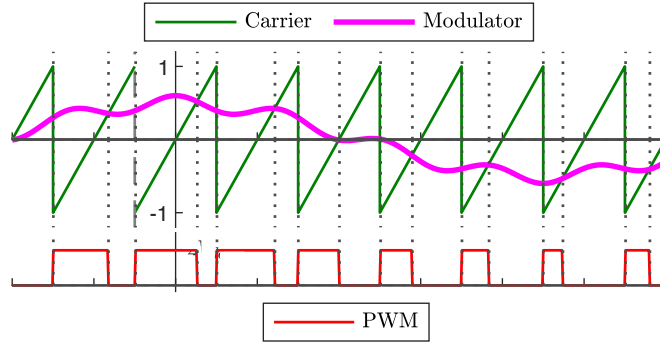


Figure 1.4 - Example of a *PWM* waveform formed by a multiple-frequency modulator signal.

LCL low-pass filter. This filter is typically used in grid-connected converter applications, but for the analytical study, it could be any other low-pass filter topology. Additionally, Figure 1.3 shows the main converter parameters, as well as the voltage and current measuring points. Those are key-elements to follow the mathematical expressions presented in the following chapters.

1.2.2 Pulse Width Modulation Schemes

The way that switches are operated in a power converter is known as a modulation strategy [12]. These strategies aim to generate an output signal that includes the information of the desired low-frequency waveform into a high-frequency signal. These low- and high-frequency signals are known as modulator and carrier, respectively [14]. This *PWM* waveform is generated by the interaction between the carrier and modulator. The comparison between these signals can be made by two conventional sampling methods, known as regular and natural sampling. Naturally-sampled *PWM* performs an analog comparison between the modulating and the carrier signals. Moreover, regular sampled *PWM* uses an ordinarily fixed-frequency rate to take a sample of the modulator-signal value and later perform the comparison of this sample with the carrier signal. *PWM* converters use both regular and natural sampling. Therefore, both modulation strategies are considered in this thesis.

As mentioned earlier, there are two primary signals in a *PWM* scheme. The first one is the carrier signal, which aims to transport the information presented in a modulation signal through a more favorable frequency rate. The other one is the modulator signal, which contains the desired waveform to be transported. This principle is used in communication systems to take advantage of different kinds of communication channels, such as air, wires, optical fiber, among others. In power converters, the same principle is used to reduce the power losses by using the power switches in the states where they are more efficient, i.e., on and off. Therefore,

a carrier signal commands the switching frequency of the power converter, and a modulator signal modulates the pulse width of the rectangular output-signal. Thus, this technique incorporates the desired waveform into a high-frequency switching pattern; see Figure 1.4 as an example of a *PWM* formed by a triangular carrier and a multiple-frequency modulator signal.

Despite the advantages of *PWM*, it generates a significant high-frequency distortion in the output voltage of *PWM* inverters [12]. This frequency distortion is also present in low-frequencies when dead-time effects are considered in the power converter [7, 10, 15]. These unwanted frequency-distortions depend on the selected modulation scheme, and they are discussed in the following chapters. Consequently, a general explanation of these modulation schemes is presented below to settle the basis of the terminology used in the following chapters.

Naturally Sampled *PWM*

The naturally sampled *PWM* scheme performs an analog comparison of a modulator and carrier signals to build the rectangular output waveform presented in Figure 1.5. It can be seen in this figure that the direct interaction between carrier and modulator signal commands the moments when the output waveform changes its state. This kind of modulation scheme is named depending on the carrier waveform. The most used carrier signals are trailing-edge sawtooth and triangular waveform. Each one of these carrier signals describes a different kind of frequency spectrum in the *PWM*, as shown in [12].

PWM waveform generated by natural sampling do not have any low-frequency distortion [12]. Thus, it makes natural sampling well suited to modern (class-D) audio amplifiers [15]. Nevertheless, this kind of system requires an analog implementation, which provides low flexibility.

Regularly Sampled *PWM*

One major limitation with naturally sampled *PWM* is the difficulty of its implementation in a digital modulation system because the intersection between modulator and carrier is defined by a transcendental equation and is complicated to calculate [12]. A popular alternative to overcome this limitation is to implement the modulation system using a *regularly sampled PWM* strategy, where the modulator signal is sampled and then held constant during each carrier period [12, 15]. These sampled values are compared to the carrier to create the *PWM* pattern, instead of the continuously varying modulator.

Usually, the samples of the modulator are taken at either positive or positive/negative peaks of the carrier waveform, depending on the sampling strategy. For a saw-

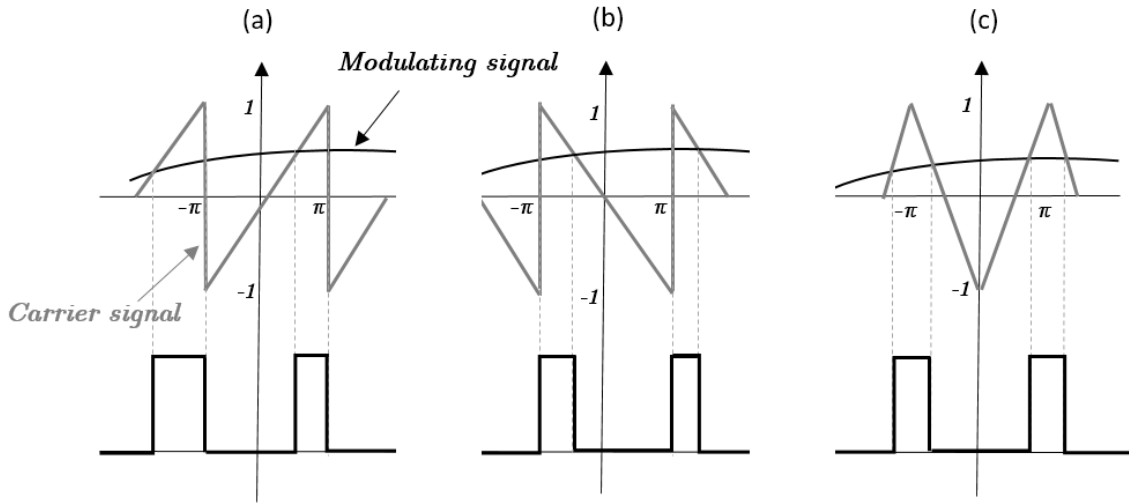


Figure 1.5 - Naturally sampled *PWM* schemes: a) Trailing-edge sawtooth carrier; b) Falling-edge sawtooth carrier; c) Triangular or double-edge carrier.

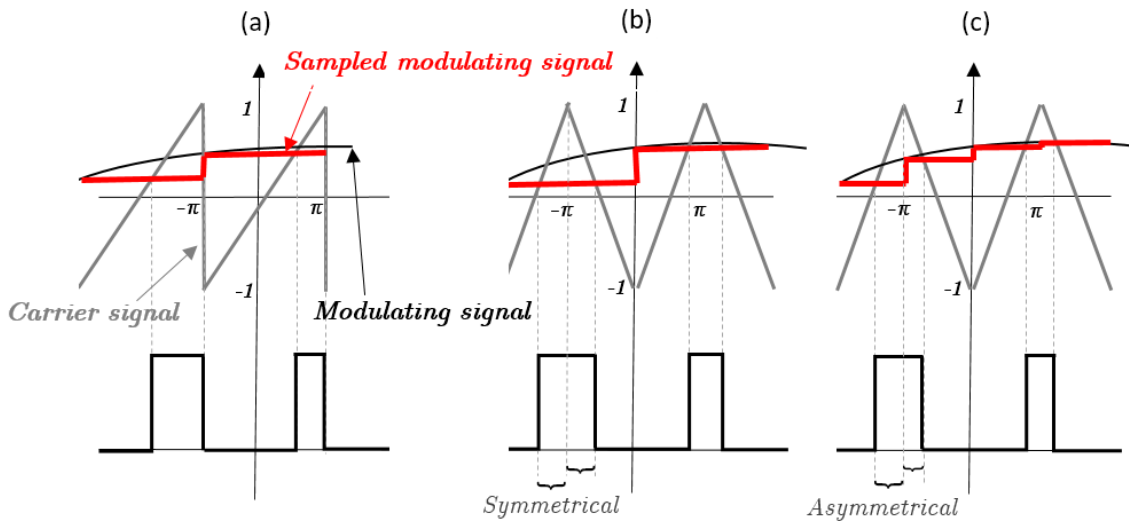


Figure 1.6 - Regular sampling *PWM*: a) Sawtooth carrier; b) Symmetrical sampling with the triangular carrier (negative peak sampled); c) Asymmetrical sampling.

tooth carrier, sampling occurs at the end of the ramping period. For a triangular carrier, sampling can be at either the positive or negative peak of the carrier and held constant for the entire carrier interval; this is known as symmetrical sampling. The other sampling strategy is to sample every half carrier interval at both positive and negative carrier peaks; this is known as asymmetrical sampling. These modulation strategies are shown in Figure 1.6.

1.2.3 Dead Time in Voltage Source Inverters

Dead-time is a technique that holds in an open state both active switches of one inverter-leg during a short interval to avoid short-circuiting the *DC* link of a *VSI*. This behavior introduces some distortions in the input and output voltage of the

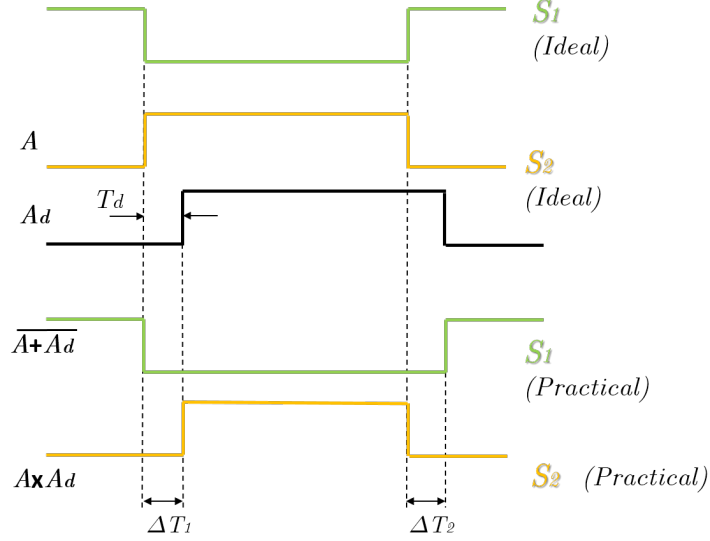


Figure 1.7 - Creation of the *PWM* pattern with dead time.

converter [5, 7, 8, 10, 11, 15, 16]. This technique is also referred in the literature as delay time, dead zone, dead band, blank time, or blanking-time. This thesis always refers to it as *dead time*. Additionally, there are some variations in the way to implement this technique. Figure 1.7 presents the dead-time strategy studied in this research. This figure shows a straightforward method to create the complementary signals in *PWM* schemes, including the dead time. First, let's rename for a moment the signal S_2 as A , then by using a register buffer, it is possible to create the delayed signal A_d . Now, by performing three simple Boolean operations, the complementary signals $S_{1(\text{practical})}$ and $S_{2(\text{practical})}$ can be calculated including secure dead-time zones ΔT_1 and ΔT_2 as shown in the bottom part of Figure 1.7.

In order to explain dead-time effects in the voltage waveform, it is useful to examine one phase-leg of a *PWM* inverter. Upper and lower switches in the phase-leg are arranged by a power switch and a diode in an anti-parallel configuration. Hence, when both power switches are open, the current has two possible paths to flow, and the actual path it takes will depend on its direction. Figure 1.8 shows the two possible commutations lead by the diodes during the dead time. It can be seen in this figure that due to the current direction, the diodes can conduct even if the power switch is open during the dead-time zones ΔT_1 and ΔT_2 . Furthermore, the output voltage v_{a-} in the practical scenario now shows some *gain* and *loss* effects, when comparing with the ideal output v_{a-} .

The main objective of this thesis is to incorporate these two phenomena, *gain* and *loss*, into analytical frequency-spectra that can describe the output voltage of the three *VSI* topologies presented earlier in section 1.2.1.

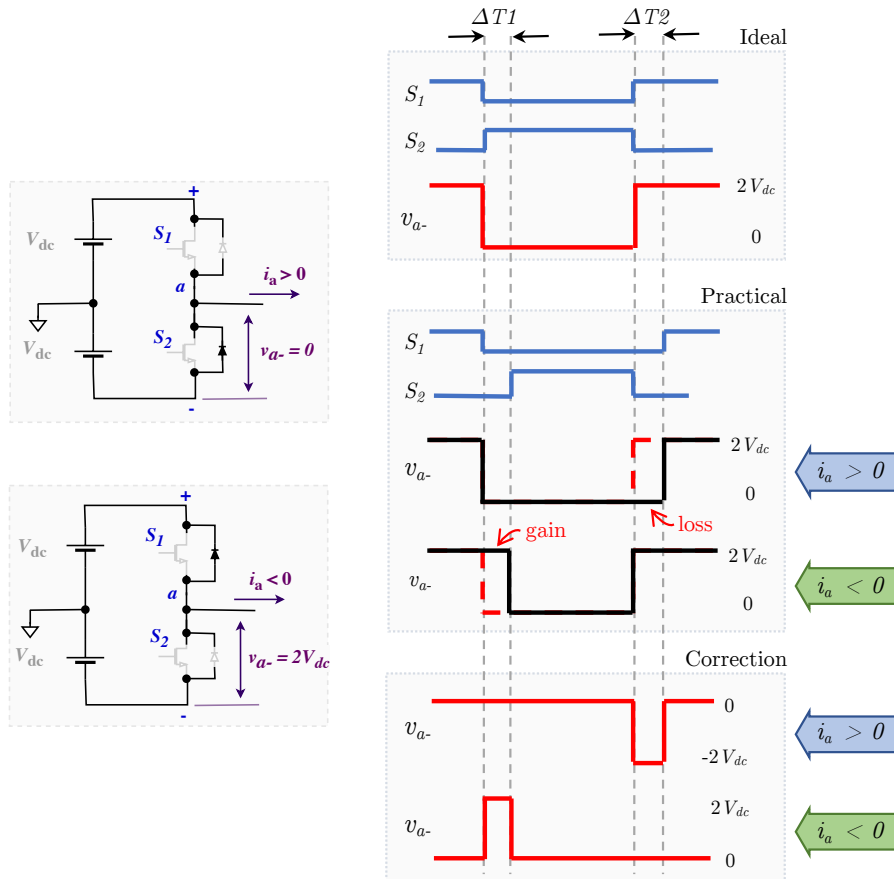


Figure 1.8 - Dead-time effects in the output voltage of a *VSI*.

1.3 Thesis Outline

The structure of this thesis is as follows: Chapter 2, investigate the most remarkable contributions in the research area. Later, Chapter 3 presents the development of the analytical low-frequency spectra for one phase of a power inverter; Chapter 4 extends the analytical spectra calculated in Chapter 3 to the single-phase inverter. Finally, Chapter 5 presents the general conclusions of this thesis and highlight interesting topics for future works in this area.

1.4 Conclusions

This chapter introduced the proposed study of the analytical low-frequency spectrum in voltage source inverters. It carried out the contextualization of the area where this thesis research takes place. Furthermore, the general description of the phenomenon under study, as well as the research question and the main research statement was presented.

Contributions of the author that motivated the research of this topic were presented in two conference papers [4, 13].

Chapter 2

Review of Previous Research

The primary objective of this chapter is to examine the most notable analytical techniques proposed by researchers to describe the frequency spectra in *VSI*s and its application to the description of dead-time effects with multiple-frequency modulator signals. The initial research covered the period from 1878, english publication of Fourier's book "*The Analytic Theory of Heat*", up to 2020 in several academic databases; and allows the identification of ten *key documents* in the field of study. All related documents cited in this chapter follow the numeric citation style used so far; nevertheless, the key-documents are highlighted in this chapter by citing the author's name together with the reference number. Once a key-document was identified, all the references to it were tracked up to 2020. This citation-tracking takes into consideration up to four thousand documents. These related citations were filtered by key-word searching and a final stage based on a detailed abstract-review. This two-stage-filtering methodology allowed to reduce from up to four thousand documents to nearly seven hundred, and finally up to one hundred and fifty related documents. Finally, the research reviewed in this chapter is based on thirty-eight of the most correlated documents and their contributions to the field of the analytical description of dead-time effects in multiple-frequency modulator applications.

This chapter is structured as follows: Section 2.1 focuses on dead-time effects and the techniques to compensate them; Section 2.2 reviews the most well-known analytical techniques to describe the *PWM* spectra; Section 2.3 explores the most significant proposed methodologies that incorporate dead-time effects into the spectra description; a summary of the state of the art is presented in Section 2.4; and finally, Section 2.5 summarizes the main contributions of this chapter.

2.1 Dead-time Effects and Compensation Techniques in *PWM* Schemes

Dead-time delays can generate different kinds of unwanted collateral effects in the voltage and consequently the current waveforms. The effects of dead time in the voltage waveform of *PWM VSI*s were first deeply detailed by GRANT and SEIDNER [16] in 1981 as part of their study on the modulation's frequency-ratio in *PWM* inverters. The most unwanted dead-time effect is the increase of harmonic distortion and losses in the fundamental voltage waveform, as documented in [5–11, 17]. In **1987**, EVANS and CLOSE [18] reported some significant qualitative conclusions on the dead-time effects in power converters. Using simulation and experimental results, they inferred generalized curves which they claim allowed the design engineer to estimate the amplitudes of harmonics generated by dead time.

One of the most significant concerns of researchers has been proposing methods to compensate dead-time effects in the output voltage of *VSI*s [5, 9, 11, 17]. Traditional compensation methods can be classified into two main categories depending on the way voltage error, due to dead time, is detected and compensated [11]. The categories are: *averaging theory* and *pulse-based compensation* methods. The first one compensates the voltage reference with the average voltage error over an entire cycle. The second one compensates the voltage error within each *PWM* pattern.

Several variations of dead-time minimization effects have been proposed over the years. The authors in [17] demonstrate that it is not necessary to insert dead time for every switching period in order to avoid unnecessary dead-time delays. Using this principle, some control algorithms were proposed to decide when to add dead time [5, 17]. Another essential aspect reported by the authors is the use of control algorithms to minimize dead-time effects. In [9], an output current feedback loop is discussed and shown to reduce dead-time effects. In [19, 20], harmonic-compensation schemes were implemented to minimize harmonics generated by dead time. In [21], a pulse-based compensation method is proposed. Finally, MUNOZ and LIPO [22] suggested one of the most common averaging compensation-method for a *PWM VSI*.

2.2 Analytical Frequency Description of *PWM* Schemes

This section presents a chronological description of the development of the most well-known technique to provide an analytical frequency description of the harmonic components in a *PWM* inverter. Although this is not the only technique reported in the literature, it is by far the oldest, most used and most documented method. It is also the theoretical basis used by Chapter 3 to define the low-frequency spectrum of a *VSI* with dead time and multiple-frequency modulator signal.

2.2.1 *Black's Method*

In 1933, BENNETT [23] introduced the double Fourier-series to solve the frequency spectrum of a half-wave diode-rectifier with a voltage input $e(t) = P \cos(pt + \theta_p) + Q \cos(qt + \theta_q)$. The output voltage in this case was formed by the positive lobes of the input voltage with the negative lobes replaced by a constant zero interval. *Bennet* shows that this kind of signal has the sufficient conditions to be represented as a double arrangement of the *Fourier* series, i.e., a *Fourier* series were the magnitude of the sine and cosine components are modulated by another periodic function. Thus, an analytical expression of the frequency-spectrum can be defined.

Later, in 1953, BLACK [24] extends *Bennet's* concept into communication systems in his book *Modulation theory*. It presents and evaluates the formal description of the spectrum for a pulse-amplitude-modulated system using the double *Fourier* integral-analysis. Using this concept, the most well-known analytical method for determining the harmonic components of a *PWM* inverter was first developed by BOWES and BIRD [25] in 1975. This method proposes the definition of a two-variable function, $F(x, y)$, that is able to represent the carrier-modulator interaction. Thus, a 3-D model can be studied using a double Fourier-series as demonstrated by BENNETT [23]. This two-variable function is defined using the angular frequencies ω_1 , and ω_c , of the modulator and carrier signal, respectively, i.e., $F(x, y)$ is defined by using the variable substitution $y \mapsto \omega_1 t$ in the modulator signal, and $x \mapsto \omega_c t$ in the carrier signal. This method is widely known in the literature as *Black's method*; and it establishes that the general spectrum of a *PWM* waveform can be represented

by

$$\begin{aligned}
F(x, y) = & \frac{1}{2}A_{00} \\
& + \sum_{n=1}^{\infty} \{A_{0n} \cos(ny) + B_{0n} \sin(ny)\} \\
& + \sum_{m=1}^{\infty} \{A_{m0} \cos(mx) + B_{m0} \sin(mx)\} \\
& + \sum_{m=1}^{\infty} \sum_{\substack{n=-\infty \\ n \neq 0}}^{\infty} \{A_{mn} \cos(mx + ny) + B_{mn} \sin(mx + ny)\}
\end{aligned} \tag{2.1}$$

where $\{m, n\} \in \mathbb{Z}^*$; $x = \omega_c t + \theta_c$; $y = \omega_1 t + \theta_1$; ω_c and θ_c are the carrier's angular-frequency and phase-angle, respectively; ω_1 and θ_1 are the modulator's angular-frequency and phase-angle, respectively.

The overall spectra of a *PWM* wave can be deduced directly from (2.1). The first term represents the mean value of the signal. The first summation term defines the fundamental and harmonic components of the modulating signal. The second summation term defines the fundamental and harmonic components of the carrier signal. And finally, the last summation term defines the sidebands around the carrier frequency and harmonics of the carrier frequency.

The *Fourier* coefficients in (2.1) are most conveniently represented by

$$C_{mn} = A_{mn} + jB_{mn} = \frac{1}{2\pi^2} \int_{-\pi}^{\pi} \int_{-\pi}^{\pi} F(x, y) e^{j(mx+ny)} dx dy \tag{2.2}$$

where $F(x, y)$ only takes one or zero values as a consequence of the interaction between the modulating and carrier signals.

The 3-D model proposed in *Black's method*, and the relationship between axes x and y define the *PWM* transitions. This relationship can be seen by letting $x_r(y)$, $x_f(y)$ be functions that define the rising and falling edges of the *PWM*, respectively. Also, let $M_f = \omega_c/\omega_1$ be the frequency ratio between the carrier and the fundamental frequency of the modulator signal. Then, there is a plane $P \in \mathbb{R}^2 : y = x/M_f$ that describes the relationship between axes x and y . Moreover, the projection of the intersection of P with $x_r(y)$ and $x_f(y)$ describes the moments when the *PWM* signal changes its voltage level. Figures 2.1 shows an example of a *PWM* defined by the 3-D model using a multiple-frequency modulator. Chapter 3 presents a detailed procedure to calculate the boundary functions for each *PWM* scheme.

A comprehensive compilation of several *PWM* schemes was presented by HOLMES and LIPO [12], in 2003, in their book *Pulse Width Modulation for Power Converters*. In that book, analog and digital implementations of *PWM* with single- and three-phase inverters are analytically studied using *Black's method* to investi-

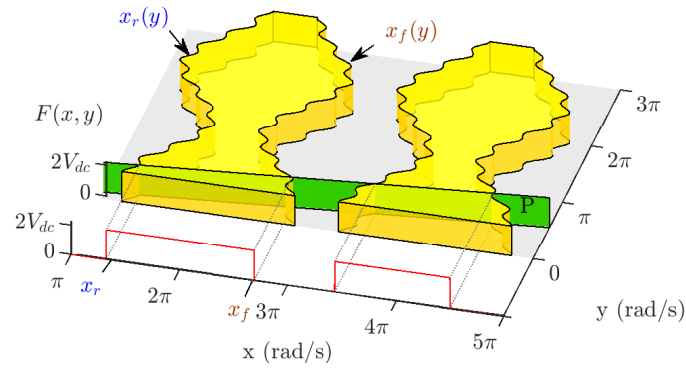


Figure 2.1 - Example of a multiple-frequency-modulator *PWM* defined by *Black's method*.

gate voltage and current spectra. Besides classical *PWM* schemes, they also included in their studies more complex and modern topologies like: multiple-frequency modulating signals (fundamental plus third-harmonic), multilevel inverters, and *Space Vector Modulation (SVM)*. Nevertheless, dead-time effects are not considered.

Using the well-established basis presented in [12] and [25], different authors extended the use of *Black's method* in more recent analytical studies in the *PWM* field. Suchlike: a general method for calculating inverter DC-link current harmonics [26], in **2009**; analytical expressions for the input current spectra for matrix power converters [27], in **2009**; analytical spectra for *PWM* inverters with multiple-frequency modulator signals (fundamental plus several harmonics) [28], in **2010**; voltage spectra of a four-switch three-phase *VSI* [29], in **2011**; unified analytical equation for determining the theoretical spectra components for all the carrier based *PWM* methods with redistributed zero space vector time-length [30], in **2011**; a generalized theory of phase-shifted carrier *PWM* for *Modular Multilevel Converters (MMC)* [31], in **2016**; among others. Also, [32, 33] showed the agreement between the analytical frequency spectrum generated using *Black's method* and experimental results.

2.3 Analytical Frequency-Spectra of *PWM* with Dead Time

This section evaluates converters that incorporate dead time in its switching patterns. So far, it was explored the most significant developments in the analytical spectra in *PWM* inverters using *Black's method*; nevertheless, only considering ideal conditions on the power converter switches. Dead-time effects in power converters have reached the attention of several authors over the years. They have mostly focused on understanding the impacts of this non-linearity and strategies to overcome its adverse effects in power converters applications. More recently, some authors have been working on the analytical description of *PWM* spectra when dead-time effects are incorporated. The following sections will show the most significant advances in this particular field.

The standard approach for harmonic analysis is to use the *DFT* on voltage measured signals, rather than an analytical solution to find the spectral components. The drawback of using DFT is that it is limited by its inputs: windowing will introduce side lobes in the frequency domain, and aliasing will introduce non-existing frequency components. Also, the magnitude of the measured signal will be influenced by the limits of the analog to digital conversion, the physical setup of the measurements, and external noise [30]. Another drawback of using *DFT* is that due to the usually large relationship between carrier and modulator frequency on power electronic applications, this approach requires an extensive sample set to achieve good frequency resolution [7]. Hence, a small simulation time step should be used, causing high-computational cost simulations that limit the number of practical applications to study.

The analytical solution, on the other hand, provides equations that define not only the behavior of *PWM* spectra but the magnitude of influence of each variable on each frequency component. To the best of the author's knowledge, the principal motivation of this analytical solution is: to identify the harmonic components caused by the dead time that require filtering; creation of more sophisticated compensation methods; and power losses calculation. These concerns have been shared in two principal areas: power electronics converters, and class-D amplifiers used for audio and radio applications. The latter one exhibits the most challenging scenarios because of the broad frequency-spectrum of the modulating signal in the *PWM* scheme.

The mathematical models required to determine frequency-spectra for inverters with dead time are more sophisticated than those described in section 2.2 and demands a considerable amount of additional algebra [8, 10, 12, 15]. Three principal methods have been proposed in the literature and will be presented in the following

sections. To simplify the comparison of the analytical expressions, they are modified to match the nomenclature adopted in this thesis.

2.3.1 Dead-Time Spectra Calculation Using *Black's Method*

The most notable attempt in the description of the analytical spectra of *PWM* inverters with dead time using *Black's method* was first presented by WU *et al.* [10] in **1999**. In this study, an analytical spectrum is determined for a single-phase inverter including dead time with both trailing- and double-edge, naturally sampled *PWM* schemes using a single-frequency modulator signal. The expression of the output voltage of a single-phase inverter with a double-edge naturally sampled *PWM* and dead time is found to be

$$\begin{aligned}
v_{conv}(t) = & \frac{2V_{dc}\Delta_x}{\pi^2} \sin(\omega_1 t - \varphi) + \frac{MV_{dc}}{4} (\sin(\omega_1 t) - \sin(\omega_1 t - \Delta_y)) \\
& + \frac{2V_{dc}\Delta_x}{\pi^2} \sum_{n=3,5,7,\dots}^{\infty} \frac{1}{n} \sin(n(\omega_1 t - \varphi)) \\
& + \frac{V_{dc}}{\pi^2} \sum_{m=1,3,5,\dots}^{\infty} \frac{-1^{m+3/2}}{m} \sum_{n=0,\pm 2,\pm 4,\dots}^{\pm\infty} \begin{bmatrix} F_{1mn} \cos(m\omega_c t + n\omega_1 t) \\ -F_{2mn} \sin(m\omega_c t + n\omega_1 t) \end{bmatrix} , \\
& + \frac{V_{dc}}{\pi^2} \sum_{m=2,4,6,\dots}^{\infty} \frac{-1^{m+2/2}}{m} \sum_{n=\pm 1,\pm 3,\pm 5,\dots}^{\pm\infty} \begin{bmatrix} F_{2mn} \cos(m\omega_c t + n\omega_1 t) \\ -F_{1mn} \sin(m\omega_c t + n\omega_1 t) \end{bmatrix}
\end{aligned} \tag{2.3}$$

where

$$\begin{aligned}
F_{1mn} = & \int_{\varphi}^{\pi+\varphi} \begin{bmatrix} \cos\left(\frac{\pi m M}{2} \sin(\omega_1 t - \Delta_y) - m\Delta_x - n\omega_1 t\right) \\ -\cos\left(\frac{\pi m M}{2} \sin(\omega_1 t) - ny\right) \end{bmatrix} dy \\
F_{2mn} = & \int_{\varphi}^{\pi+\varphi} \begin{bmatrix} \sin\left(\frac{\pi m M}{2} \sin(\omega_1 t - \Delta_y) - m\Delta_x - ny\right) \\ -\sin\left(\frac{\pi m M}{2} \sin(\omega_1 t) - ny\right) \end{bmatrix} dy
\end{aligned} \tag{2.4}$$

and $\Delta_x = \omega_c T_d$, $\Delta_y = \omega_1 T_d$, T_d is the dead-time duration, and φ is the angle between the output voltage and the load's current.

Wu *et al.* in [10] present the development of this equation through a geometrical interpretation. In said interpretation, Δ_x is the average voltage error due to the dead time, and Δ_y is a phase error introduced in the falling and rising functions that limit the contour regions.

Due to algebra presented in the integrals of (2.4), they were solved using numerical methods. That is the reason this is not a closed-form equation. Nevertheless, significant outcomes can be inferred from (2.3). These conclusions are expressed in

[10] as:

1. Dead time can generate a fundamental component which cannot be controlled by the reference magnitude M , which is the manipulated variable of *VSI*.
2. Dead time produces odd harmonics of the signal frequency which cannot be generated by an ideal natural sampling PWM process. The magnitudes of these harmonics are proportional to the dead time T_d and inversely proportional to the harmonic order n . Also, the lower order harmonics of this kind will degrade the performance of the inverters.
3. Dead time can produce carrier harmonics and cross-modulation harmonics which coincide with those generated by the ideal natural sampling PWM. From the approximation curves obtained by the numerical methods, one can infer that the magnitude of these harmonics is approximately proportional to the dead time T_d .

These conclusions were the first theoretical support for some of the observations reported by EVANS and CLOSE [18] in 1987.

To extend the work presented by WU *et al.* [10], [4] developed an analytical description of the low-frequency harmonics in a *PWM* with dead time, using a mathematical approach to describe Δ_x and Δ_y . Chapter 3 extends this work to create an analytical description of the low-frequency harmonics using multiple-frequency modulator signals.

Due to the sophisticated algebra involved in the double integrals, no analytical closed-form results have been presented in the literature when more complex modulating signals are investigated. In [34], a time-domain approach including circuitual effects is presented, and the analysis was extended to the frequency domain by [34] in **2010**. Later, in **2013**, [35] proposed the use of the nonlinear equations that govern the power switch into the limits of the double Fourier-series to include dead-time and turn-on/off delays effects. All these contributions were made by using the Black's method and solving, partially or totally, the integrals by numerical methods.

2.3.2 Dead-Time Spectra Calculation Using Song-Sarwate's Method

Besides the application in power electronic converters, *PWM* is a well-known member of the *Pulse Time Modulation (PTM)* family. This modulation is widely used in communication systems for the transmission of analog data such as TV, video and instrumentation signals over optical fibers [36]. It also has an essential role in the high-efficiency class-D amplifiers [8, 15, 37, 38]. And, it is in these two last

applications that the modulating signal is quite more complicated than in those used in power electronic applications. This complexity limits the implementation of *Black's method* for the analytical solution of multiple-frequency modulator signals and encourages the pursuit of new techniques to provide an analytical solution of *PWM* spectra.

In 1991, WILSON *et al.* [36] presented an analytical method to calculate the *PWM* spectrum of a two-frequency modulating signal in *PWM*. They proposed to view the modulated square wave as a waveform composed of positive and negative staircases and the interactions of their simple Fourier-transforms would describe the complete signal. Later, in 2003, SONG and SARWATE [38] proposed to define separate switching functions for a *PWM*. One of the switching-functions describes a fixed square wave of the carrier frequency and fifty-percent duty cycle, and the other one will define its width based on the modulating signal. Moreover, an approximation of the frequency spectrum of an ideal *PWM* signals for arbitrary, band-limited inputs can be calculated by using the Fourier-transform of these switching functions evaluated in one period. This general approach allows identifying the spectra of finite energy and periodic-modulating signal with a bounded frequency.

Using *Song-Sarwate's concept*, in **2010**, CHIERCHIE and PAOLINI [7] extend this approach into dead-time analysis by adding third switching-function that describes the voltage error due to dead-time delays. Additionally, in **2014**, they extend their work to arbitrary modulating signals including dead-time effects and develop a distortion index that they claim can be used as a measure of the dead-time effects.

Using this method, the output voltage of a *PWM* inverter can be described as $v_{a-}(t) = p_c(t) + p_s(t) - e(t)$, where $p_c(t)$ is a symmetrical square wave with an amplitude of ± 1 and a fixed duty cycle of fifty percent. $p_s(t)$ is a bipolar pulse train which depends on the modulation signal $s_a(t)$, $e(t)$ is the error signal defined by the difference between the ideal *PWM* and the actual one, and the coefficients of the Fourier-series of the periodic *PWM* signal $v_{a-}(t)$ are given by the evaluation over one period of each signal's Fourier's transform. This expression is given by

$$C_n = \frac{1}{T_c} [P_c(f) + P_s(f) - E(f)] \Big|_{f=\frac{n}{T_c}}, \quad (2.5)$$

where

$$\begin{aligned}
P_c(f) &= \sum_{k=-\infty}^{\infty} \frac{-2j}{2k+1} \delta\left(f - \frac{2k+1}{T_c}\right), \\
P_s(f) &= \frac{-j}{\pi f} \sum_{k=-\infty}^{\infty} e^{-j2\pi f(1+1/2)T_c} - e^{-j2\pi f(kT_c+\tau_k)T_c}, \\
E(f) &= P_{T_d}(f) \sum_{k=-\infty}^{\infty} e^{-j2\pi(kT_c+\tau_k)f} \begin{bmatrix} -1 \\ +\sigma(kT_c)e^{-j2\pi\tau_k f} \\ +\sigma(kT_c + \tau_k) \end{bmatrix}.
\end{aligned} \tag{2.6}$$

Moreover, τ_k is the pulse width for the k -th interval, $\delta(\cdot)$ is the *Dirac* delta function, $\sigma(t)$ is the choice function

$$\sigma(t) = \begin{cases} 1, & \text{if } i_a(t) > 0 \\ 0, & \text{otherwise} \end{cases},$$

and

$$P_{T_d}(f) = 2T_d \text{sinc}(T_d f) e^{-j\pi T_d f}, \tag{2.7}$$

where, for $k \in \mathbb{Z}$ and T_d is the dead-time duration.

The frequency spectrum calculated by this method is a quasi-analytical description, i.e., contains terms that involve the switching times and therefore give no immediate insight into the frequency spectrum [15]. Nevertheless, it presents a close agreement between theoretical and experimental results [37]. Furthermore, it allows one to identify which harmonics are introduced by dead time and their magnitudes.

2.3.3 Dead-Time Spectra Calculation Using Poisson's Summation Method

The first analytical closed-form method to describe the harmonic spectra of a *PWM* with dead time was proposed by MOORE *et al.* [8] in **2012**, and published in the *IMA Journal of Applied Mathematics* in **2014**. In this paper, the authors use Poisson's summation method to integrate the summation of the partial Fourier-transform of *PWM* switching-functions analytically. This technique does not use switching approximations as *Song-Sarwate's method* and, in some cases, is less algebraically cumbersome than *Black's method*.

This method is based on *Poisson's summation formula*, which establishes that the periodic summation of a function is completely defined by discrete samples of the original function's Fourier-transform. It is defined for a non-negative function f such that the integral $\int_{-\infty}^{\infty} f(t)dt$ exists as an improper Riemann integral [39]. This

principle is known as the Poisson's summation formula and is found to be

$$\sum_{m=-\infty}^{\infty} h(m) = \sum_{m=-\infty}^{\infty} \int_{-\infty}^{\infty} e^{j2\pi m\tau} h(\tau) d\tau . \quad (2.8)$$

The technique proposed by MOORE *et al.* [8] describes two key moments, A_m and B_m , as the moments when the rectangular pulse of a *PWM* changes its value. Hence, the discrete switching function of the output voltage for a single-leg inverter can be defined as

$$v_{a-}(t) = 1 - 2 \sum_{m=-\infty}^{\infty} \psi(t; A_m, B_m) , \quad (2.9)$$

where $\psi(t; t_1, t_2)$ is a *top-hat* function, given by

$$\psi(t; t_1, t_2) = \begin{cases} 1 & \text{if } t_1 < t < t_2, \\ 0 & \text{otherwise .} \end{cases} \quad (2.10)$$

Applying Fourier's transform into $v_{a-}(t)$, Poisson's summation formula, and the Jacobi-Anger identity (see [39]), the analytical description of the output voltage of a single-phase inverter with naturally sampled *PWM* is given by

$$\begin{aligned} v_{conv}(t) = & M \cos(\omega_1 t) - \frac{4\Delta_x}{\pi^2} \sum_{n=1,3,\dots}^{\infty} \frac{(-1)^{(1/2)(n-1)}}{n} \cos(n(\omega_1 t - \varphi)) \\ & + \sum_{m=-\infty}^{\infty} \sum_{n=-\infty}^{\infty} \frac{j^{m+n}}{(j\pi m)} e^{-jm\delta\Delta_x/2} e^{j(n\omega_1 + m\omega_c)t} \\ & \times \begin{bmatrix} \cos(m\Delta_x/2) J_n \left(\frac{1}{2} \pi m M \right) (1 - (-1)^{m+n}) \\ - \sin(m\Delta_x/2) \sum_{\substack{p=-\infty \\ p \neq n}}^{\infty} \frac{e^{j(p-n)\phi}}{\pi(p-n)} j_p \left(\frac{1}{2} \pi m M \right) E_{mnp} \end{bmatrix} , \end{aligned} \quad (2.11)$$

where

$$E_{mn} = ((-1)^{p-n} - 1)(1 + (-1)^{m+p}) . \quad (2.12)$$

Poisson's summation method can be extended to other *PWM* schemes. MOORE *et al.* [8] calculated the analytical spectra of the digital schemes, symmetrical and asymmetrical regular sampling *PWM* schemes. Based on this work, in **2013**, AINSLIE-MALIK [15] extended the use of *Poisson's summation method* into his Ph.D. thesis in applied mathematics. Here, the Poisson's method was used to describe single, and three-phase inverters. Calculating both, voltage and current spectra, for generalized load impedance. Furthermore, in this thesis is presented by the first time the analytical description of the harmonic content of the *DC* voltage in a

power electronics inverter including the dead-time effects.

2.4 State of the Art

This section explores the latest development in the field of analytical description of dead-time effects in *VSI* with multiple-frequency modulator signals. As mentioned in the last sections, there are three principal methodologies to define analytical frequency-spectra of *PWM* inverters; hence, this section presents the state of the art for each one of them.

2.4.1 State-of-the-Art Research Using *Black's Method*

In October of 2018, KUMAR [40] extended the work of WU *et al.* [10] by adding the sample-delay to describe regular sampled *PWM* schemes in a single-phase *VSI* with a single-frequency modulator. He also expressed the analytical spectra by using infinite summations of Bessel functions instead of the integrals expressed in [10].

More recently, in April of 2019, JIAO *et al.* [41] also extends the work of WU *et al.* [10] to the asymmetrical regular sampled *PWM* scheme with single-frequency modulator. Moreover, the authors proposed an alternative analytical method to avoid the unit-cell definition of *Black's method* and define a single Fourier-series analysis to avoid the cumbersome process of solving the double integral in *Black's method*.

To the best of the author's knowledge, An analytical study of dead-time effects in *PWM* with multiple-frequency modulator signals using *Black's method* have only been presented in this thesis, i.e., not using numerical methods to solve the double integral.

2.4.2 State-of-the-Art Research Using *Song-Sarwate's Method*

In March of 2019, JOHN [42] uses Song-Sarwate's method in his Ph.D. thesis to define frequency-domain modeling of *PWM* schemes applied to control of *VSI* drivers. This frequency model includes analog and digital *PWM* schemes using single- and multiple-frequency modulator signals. Using this approach, [42] also provides a closed-loop control analysis of a three-phase *VSI*.

2.4.3 State-of-the-Art Research Using *Poisson Summation Method*

The work of AINSLIE-MALIK [15] and MOORE *et al.* [8], in 2013 and 2014, still represent the state-of-the-art research for the *Poisson Summation Method*. The

analytical spectra of analog and digital *PWM* schemes are covered in [8] for single-frequency modulator signals. Moreover, [15] used this method to describe single- and three-phase inverters.

According to the authors of [8, 15], this method could be extended for multiple-frequency modulator signals with relatively minor modifications but a considerable amount of additional algebra. Nevertheless, to the best of the author's knowledge, this has not been addressed yet.

2.5 Conclusions

An extensive review of previous research was presented in this chapter. It was possible to identify three of the most advanced methods to study the analytical frequency-spectrum of dead-time effects. These methods have been used to define the harmonic content of dead-time effects for analog and digital *PWM* schemes, and the effects of multiple-frequency modulator signals. Nevertheless, only one document was found addressing both topics at the same time, i.e., dead-time effects and multiple-frequency modulator signal. However, the frequency-spectrum is not a closed-form expression, i.e., it contains terms that involve the switching times and therefore give no immediate insight into the frequency spectrum.

After the review presented in this chapter, the most suitable techniques to develop the proposed research of this thesis are *Black's* and *Poisson summation* methods. Nevertheless, the research in this thesis is performed using *Black's method* due to the reduced documentation and lack of development of the *Poisson summation method* in *PWM* with multiple-frequency modulator signals.

Chapter 3

PWM Spectrum of One Inverter Phase Leg

This chapter explores the use of double Fourier-series analysis to develop an analytical expression of the low-frequency spectrum of a *PWM* scheme; including dead-time effects and multiple-frequency modulators. Commonly, power electronics applications include a low-pass output filter, which minimizes the contribution of high-frequency components on the output voltage in a power converter. Thus, this study proposes to focus on the analytical expression of the low-frequency spectrum without the typical cumbersome expressions involved in describing carrier and side-bands components.

The proposed low-frequency approach describes the principal frequency-components that are responsible for degradation in the output voltage of a power converter. Moreover, this chapter shows that harmonics created by dead time do not depend on the frequency-components injected by harmonic compensation systems or other multiple-frequency control techniques.

The outline of this chapter is as follows: the first section details the topology of the inverter studied in this chapter; section two develops the analytical output-voltage spectrum for an ideal *PWM* scheme, i.e., considering ideal switches in the power converter; section three includes the effects of dead time into the analytical spectrum. Moreover, section four summarizes the partial conclusions and contributions in this chapter.

Development of the equations used in this chapter are presented in Appendices B and C.

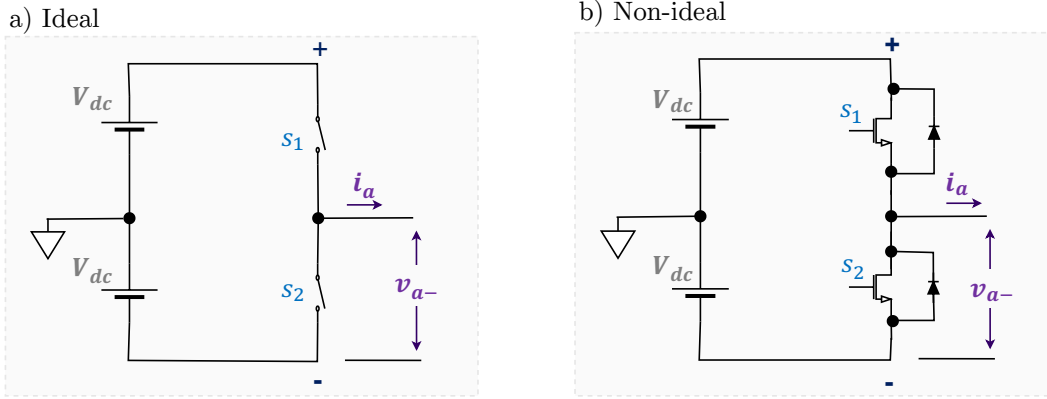


Figure 3.1 - One inverter phase-leg topologies: a) phase-leg using ideal switches; b) phase-leg using power switches and its associated free-wheel diodes in an anti-parallel configuration.

3.1 Topology of One Inverter's Phase Leg

Conventional power converter applications have separated *PWM* signals for each inverter phase-leg. Therefore, the calculated voltage spectrum in one phase can be extended to define the spectrum between different phases, such as full-bridge single-phase and three-phase converters [12, 15]. Two cases of one-phase-leg topology are presented in Figure 3.1, where, the main difference is the use of ideal and non-ideal switches. This figure also displays signal notations and some converter parameters that will be used by the analytical expression developed throughout this chapter.

The studied waveform is the output voltage of the phase leg referenced to the negative rail of the *DC* link, v_{a-} henceforth. The reference point of the voltage measurement was selected to be the negative rail of the *DC* link in order to create a common reference to facilitate the analysis of multiple-phase converters, as will be shown in Chapter 4.

3.2 Ideal *PWM* with Multiple-Frequency Modulator

This section uses *Black's method* to obtain the analytical low-frequency spectra of analog *PWM* schemes using ideal switches. Although *Black's method* in ideal *PWM* inverter topologies is a topic widely covered in literature, this section details the specific case when a modulator signal has a major fundamental component and a set of small fundamental-frequency harmonics. This multiple-frequency modulator signal is commonly produced by the control law of high-power-quality applications, where the primary objective is to reduce the fundamental-frequency harmonics that distort the output-voltage waveform.

Additionally, a power electronic converter usually has a low-pass filter at the output stage. This filter attenuates nearly all of the high-frequency components introduced by the *PWM* switching pattern. Therefore, the combined actions of the output filter and the control law allow us to propose focusing only on the low-frequency spectrum, i.e., *DC* and fundamental-frequency components.

Furthermore, a set of harmonic components injected by the control law can be studied by letting $h \in \mathbb{Z}^*$ be an index that represents any harmonic of this set. Thus, it is possible to extend the conclusions of harmonic h to any other harmonic-component in the set. This assumption is conceivable due to the linear behavior of the double-Fourier-series analysis [39]. This approach simplifies the analytical expression of the *PWM* spectrum and allows further analysis that is presented in the following sections.

3.2.1 Ideal *PWM* Definition

The *PWM* is defined by the interaction between a low-frequency modulator signal, $s_a(y)$, and a high-frequency carrier signal, $c(x)$. This *PWM* signal has only two voltage levels, and the changes between them are defined by the moments where both signals, modulator and carrier, have the same value. For the proposed study of multiple input frequencies, the modulator signal is given by

$$s_a(y) = M \cos(y + \theta_1) + M_h \cos(hy + \theta_h) \quad , \quad (3.1)$$

where M_h and θ_h are the amplitude and phase of the harmonic h injected by the control law, respectively. Moreover, the carrier signal can be defined by either

$$c(x) = \left\{ \begin{array}{l} \frac{(x+\theta_c)}{\pi}, \quad -\pi \leq x < \pi \end{array} \right. \quad (3.2)$$

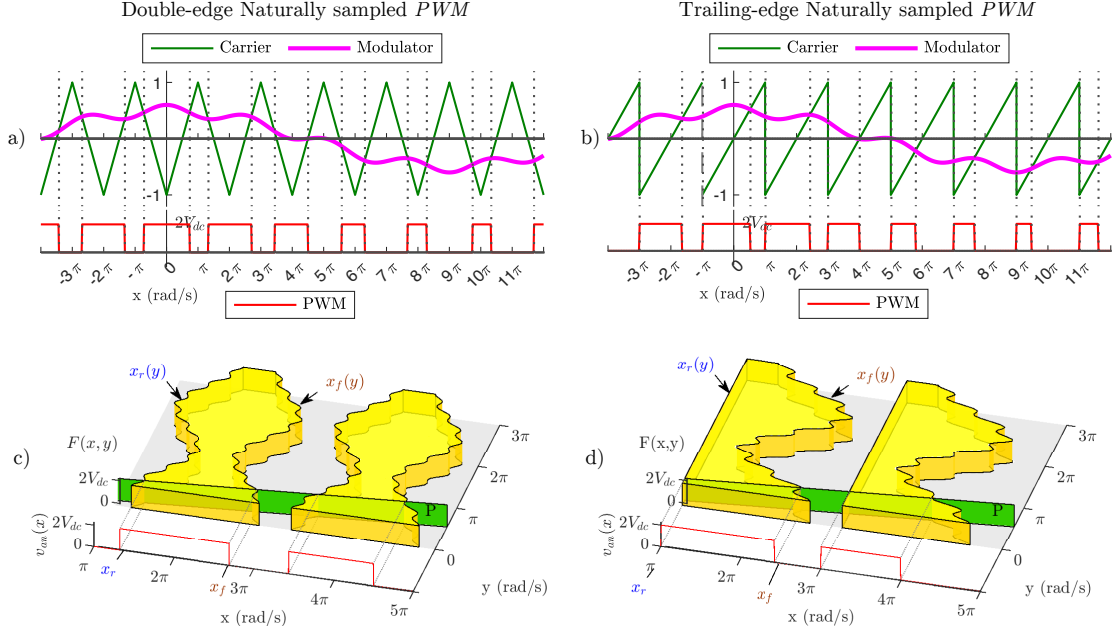


Figure 3.2 - Naturally sampled PWM definitions: A) and B) displays a classical PWM definition; C) and D) show the 3D-model approach. Plot parameters: $V_{dc} = 1.0 \text{ p.u.}$, $M = 0.5$, $\omega_1 = 2\pi 60 \text{ rad/s}$, $\theta_1 = 0^\circ$, $h = 7$, $M_h = 0.1$, $\theta_h = 0^\circ$, $\theta_c = 0^\circ$, $M_f = 9$.

or

$$c(x) = \begin{cases} c_n(x) = -\frac{2(x+\theta_c)}{\pi} - 1, & -\pi \leq x < 0 \\ c_p(x) = \frac{2(x+\theta_c)}{\pi} - 1, & 0 \leq x < \pi \end{cases}, \quad (3.3)$$

depending on the selected modulation scheme. Equation (3.2) defines a saw-tooth or trailing-edge carrier signal, and (3.3) defines a triangular or double-edge carrier signal. The over-modulation condition is out of the scope of this study, therefore, $|s_a(y)| \leq 1$.

Ideal boundary functions and 3-D model

Recalling from section 2.2.1, the 3-D model proposed by [25] in *Black's method*, and the relationship between axes x and y define the PWM transitions. To show this fact, let $x_r(y)$ and $x_f(y)$ be the functions that define the rising and falling edges, respectively, of the 3-D model. Also, let $M_f = \omega_c/\omega_1$ be the frequency ratio between the carrier and the fundamental frequency of the modulator signal. Finally, let $P \in \mathbb{R}^2 : y = x/M_f$ be the plane that describes the relationship between axes x and y . Then, the intersection of P with $x_r(y)$ and $x_f(y)$ describes the moments when the PWM signal changes its voltage level, as shown in Figures 3.2-c and 3.2-d.

The boundary functions $x_r(y)$ and $x_f(y)$ can be defined by finding the moment x when the modulator signal equals the carrier signal, e.g., as shown in the double-edge naturally sampled case in Figure 3.2-b. The rising edge of the PWM signal

Table 3.1 - Boundary equations for a naturally sampled PWM scheme evaluated over the range $[-\pi, \pi]$.

Carrier	Parameter	Expression
Trailing-edge	$x_r(y)$	$-\theta_c - \pi$
	$x_f(y)$	$-\theta_c + \pi [M \cos(y + \theta_1) + M_h \cos(hy + \theta_h)]$
Double-edge	$x_r(y)$	$-\theta_c - \frac{\pi}{2} [M \cos(y + \theta_1) + M_h \cos(hy + \theta_h) + 1]$
	$x_f(y)$	$-\theta_c + \frac{\pi}{2} [M \cos(y + \theta_1) + M_h \cos(hy + \theta_h) + 1]$

occurs when the negative slope of the triangular equals the modulator signal. Then, the expression for the rising function is found to be

$$\begin{aligned}
 c_n(x_r(y)) &= s_a(y) \\
 -\frac{2(x_r(y) + \theta_c)}{\pi} - 1 &= M \cos(y + \theta_1) + M_h \cos(hy + \theta_h) \\
 x_r(y) &= -\theta_c - \frac{\pi}{2} [M \cos(y + \theta_1) + M_h \cos(hy + \theta_h) + 1] .
 \end{aligned} \tag{3.4}$$

Similarly, this process can be used to find the falling-edge, as well as the boundary functions for the saw-tooth signal. Table 3.1 shows all the definitions for the boundary functions and the development of these expressions is presented in Appendix B. Using these functions, the voltage waveform in one leg of the ideal power electronic converter is given by

$$v_{a-}(t) = F(x, y) = \begin{cases} 2V_{dc}, & x_r(y) \leq x \leq x_f(y) \\ 0, & \textit{Otherwise} \end{cases} . \tag{3.5}$$

A complementary procedure to define a *PWM* scheme is presented in Appendix A. Although the mathematical approach to calculate the boundary functions $x_r(y)$ and $x_f(y)$ is the appropriate way to define the 3-D model in *Black's method*, the proposed geometrical approach, shown in Appendix A, aids to capture the fundamental interaction between carrier and modulator signals in *Black's method*.

3.2.2 Ideal Spectrum of a Naturally Sampled *PWM*

Due to the periodicity of function $F(x, y)$ in both axes, it is possible to calculate the analytical expression of the *PWM* spectrum using a double Fourier-series [12, 23–25, 43, 44]. The main idea is to express the function $F(x, y)$ as an infinite addition of harmonic components of the modulator and carrier signals. Recalling from Section

2.2.1, a double Fourier-series is defined by

$$\begin{aligned}
F(x, y) &= \frac{1}{2}A_{00} \\
&+ \sum_{n=1}^{\infty} \{A_{0n} \cos(ny) + B_{0n} \sin(ny)\} \\
&+ \sum_{m=1}^{\infty} \{A_{m0} \cos(mx) + B_{m0} \sin(mx)\} \\
&+ \sum_{m=1}^{\infty} \sum_{\substack{n=-\infty \\ n \neq 0}}^{\infty} [A_{mn} \cos(mx + ny) + B_{mn} \sin(mx + ny)]
\end{aligned} \tag{3.6}$$

and the general expression to calculate each coefficient is given by

$$\begin{aligned}
C_{mn} &= A_{mn} + jB_{mn} \\
&= \frac{1}{2\pi^2} \int_{-\pi}^{\pi} \int_{-\pi}^{\pi} F(x, y) e^{j(mx+ny)} dx dy
\end{aligned} \tag{3.7}$$

Using the complex representation of the coefficients and evaluating them over the range of $[-\pi, \pi]$ simplifies the development of the analytical expressions [12].

Low-frequency components of an ideal naturally-sampled *PWM*

The main idea of this study is to focus only on the low-frequency components of the analytical expression, i.e, harmonics components of the fundamental frequency. As shown in chapter 1, a typical power electronics application has a low-pass filter after the converter stage. This filter is designed to reduce the switching-frequency components. Thus, it is possible to neglect all the high-frequency terms of the Fourier analysis, i.e., all harmonic components of the carrier signal and their side-bands. This assumption is valid for M_f values that does not overlap the side bands of the first carrier component with the most significant fundamental-frequency harmonics. Therefore, let $F'(x, y)$ define the low-frequency approximation of the *PWM* signal as

$$\begin{aligned}
F'(x, y) &= \frac{1}{2}A_{00} \\
&+ \sum_{n=1}^{\infty} \{A_{0n} \cos(ny) + B_{0n} \sin(ny)\}
\end{aligned} \tag{3.8}$$

where the first term represents the DC component of the Fourier series, and the second term is the infinite addition of fundamental-frequency harmonics (or so-called base-band harmonics). The coefficients A_{0n} and B_{0n} , $\forall n \in \mathbb{Z}^*$, can be defined by using the output-voltage definition presented in (3.5), and the general Fourier's

integral given by (3.7). These coefficients can be calculated as

$$\begin{aligned} C_{0n} &= A_{0n} + jB_{0n} \\ &= \frac{V_{dc}}{\pi^2} \int_{-\pi}^{\pi} \int_{x_r(y)}^{x_f(y)} e^{jny} dx dy \quad . \end{aligned} \quad (3.9)$$

Equation (3.9) represents the magnitude and phase of each harmonic in the double Fourier-series. Moreover, using the boundary functions shown in Table 3.1, and solving (3.9) for $n = \{0, 1, h, n > 1 \wedge n \neq h\}$, it is possible to define the analytical expression of the low-frequency spectrum for an ideal analog *PWM* scheme as

$$C_{0n_{(ideal)}} = \begin{cases} 2V_{dc}, & n = 0 \\ MV_{dc}e^{-j\theta_1}, & n = 1 \\ M_h V_{dc}e^{-j\theta_h}, & n = h \\ 0, & \textit{Otherwise} \end{cases} \quad . \quad (3.10)$$

This expression defines the low-frequency spectrum of both naturally sampled *PWM* schemes, trailing- and double-edge. As shown in [12] and demonstrated in Appendix C, naturally-sampled *PWM* schemes differ only in the carrier and side-band harmonics, which are out of the scope in this study.

The coefficients in (3.10) show that:

- fundamental-frequency and harmonic components depend only on their terms of the modulator signal, i.e., M and θ_1 for the fundamental frequency, and M_h and θ_h for the injected harmonic h ;
- the *DC* voltage V_{dc} affects all frequency components;
- and, *the injected harmonic at order h does not affect the ideal fundamental-frequency component, and vice versa.*

Low-frequency time definition of an ideal naturally-sampled *PWM*

The low-frequency approximation of the output voltage can be defined by using the reduced double Fourier-series shown in (3.8) and the coefficients shown in (3.10). This low-frequency approximation is found to be

$$\begin{aligned} v_{a-(ideal)}(t) &= F'(\omega_c t, \omega_1 t) \\ &= V_{dc} + MV_{dc} \cos(\omega_1 t + \theta_1) + M_h V_{dc} \cos(h\omega_1 t + \theta_h) \quad . \end{aligned} \quad (3.11)$$

3.3 *PWM* with Multiple-Frequency Modulator and Dead Time

This section evaluates converters that incorporate the dead-time effects in their switching patterns. When using non-ideal switches, voltage transitions are not instantaneous. Thus, as presented in Section 1.2.3, a small gap or dead time is inserted into the complementary switching pattern to avoid short-circuiting the *DC* rail through the converter leg. Nevertheless, when a load or low-pass filter is connected to a converter, the output voltage waveform is distorted by the uncontrolled conduction of the free-wheel diodes (see Figure 3.1). This distortion is commonly known as *gain* and *loss*, and its effects depend on the actual polarity of the current waveform [12, 18].

In [10], the authors proposed to create a correction function, $F_{corr}(x, y)$, which could incorporate *gain* and *loss* effects into the ideal function $F(x, y)$ of a two-level single-phase inverter with a single-frequency modulator signal. This new correction function takes into consideration the current polarity and defines a pulse that adds to or subtracts from the original 3D-model. This section extends the technique presented by [10] to study the dead-time effects with a more elaborate modulator signal.

3.3.1 *PWM* Definition Including Dead-Time Effects

Dead time modifies the duty cycle of the *PWM* signal. In the positive part of the current waveform, it delays the rising-edge. Moreover, in the negative part of the current waveform, it delays the falling-edge [7, 8, 10, 12, 15, 35, 43]. These effects are shown in Figure 3.3 when a resistive load is connected. Nevertheless, when a low-pass filter or an inductive load is connected to the converter, a shift angle φ must be considered. Figure 3.4 uses the fundamental-frequency component of the output voltage as a reference to define the shift angle φ of the current waveform of a partially inductive load. This study is focused on modulator signals that do not create more than two changes of polarity over one fundamental-frequency period.

Time Substitution Concept

To incorporate dead-time effects into a *PWM*, let t be the time when rising or falling edges occur in the ideal *PWM*. Also, let $t' = t + T_d$ be the time when rising or falling edges occur in the *PWM* with dead time, where T_d is the dead-time duration (see Fig. 3.5). Consequently, the time substitution, $t \mapsto t' - T_d$, allows us to incorporate the dead-time effects into the modulator and carrier expressions, i.e., the boundary functions presented in the previous section can now be calculated using the carrier

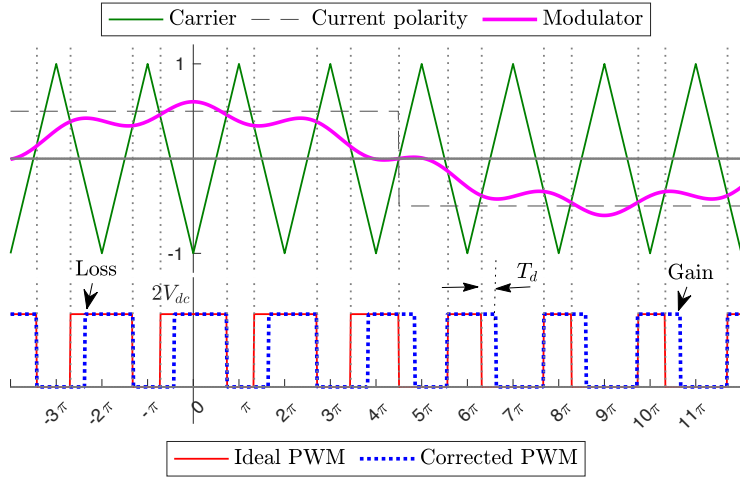


Figure 3.3 - Dead-time effects over the PWM signal.

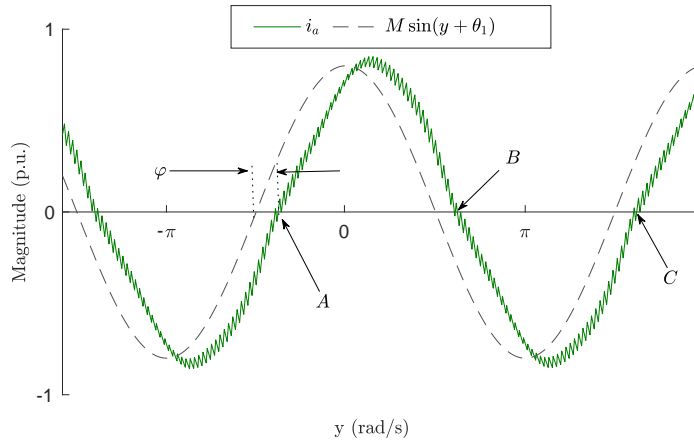


Figure 3.4 - Current boundaries definition. The angle φ is an approximation due to the multiple zero-crossing of the current ripple.

and modulator expression with this time substitution. Hence,

$$t \mapsto t' - T_d \implies \begin{cases} x_r \mapsto x'_r - \Delta_x \\ x_f \mapsto x'_f - \Delta_x \\ y \mapsto y - \Delta_y \end{cases}$$

where $\Delta_x = \omega_c T_d$ and $\Delta_y = \omega_1 T_d$. Note that y' was not used in the third implication in order to maintain the nomenclature in Fourier's equations.

The proposed mathematical approach, $t \mapsto t' - T_d$, produces the same results presented geometrically by [10]. However, it extends dead-time effects analysis more efficiently to more elaborate modulator signals, such as the one defined in Equation (3.1). Certainly, the proposed time substitution represents the fundamental theoretical concept that allows modifying Black's method to perform all dead-time studies presented in this thesis.

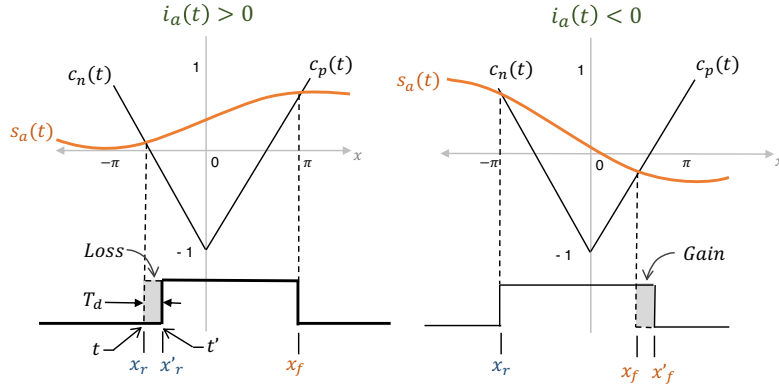


Figure 3.5 - Details of dead-time effects on PWM signals.

Table 3.2 - Boundary equations for a naturally sampled PWM scheme including dead time and evaluated over the range $[-\pi, \pi]$.

Carrier	Parameter	Expression
Trailing-edge	$x'_r(y)$	$-\theta_c - \pi + \Delta_x$
	$x'_f(y)$	$\left[\begin{array}{l} \pi \left(\begin{array}{l} M \cos(y + \theta_o - \Delta_y) \\ + M_h \cos(hy + \theta_h - h\Delta_y) \end{array} \right) \\ + \Delta_x - \theta_c \end{array} \right]$
Double-edge	$x'_r(y)$	$\left[\begin{array}{l} -\frac{\pi}{2} \left(\begin{array}{l} M \cos(y + \theta_o - \Delta_y) \\ + M_h \cos(hy + \theta_h - h\Delta_y) + 1 \end{array} \right) \\ + \Delta_x - \theta_c \end{array} \right]$
	$x'_f(y)$	$\left[\begin{array}{l} \frac{\pi}{2} \left(\begin{array}{l} M \cos(y + \theta_o - \Delta_y) \\ + M_h \cos(hy + \theta_h - h\Delta_y) + 1 \end{array} \right) \\ + \Delta_x - \theta_c \end{array} \right]$

Correction boundary functions

Using the time-substitution concept, the new boundary functions of the correction term $x'_r(y)$ and $x'_f(y)$ can be found in a similar way as presented in Section 3.2.1. Table 3.2 resumes all boundary-functions for both analog PWM schemes.

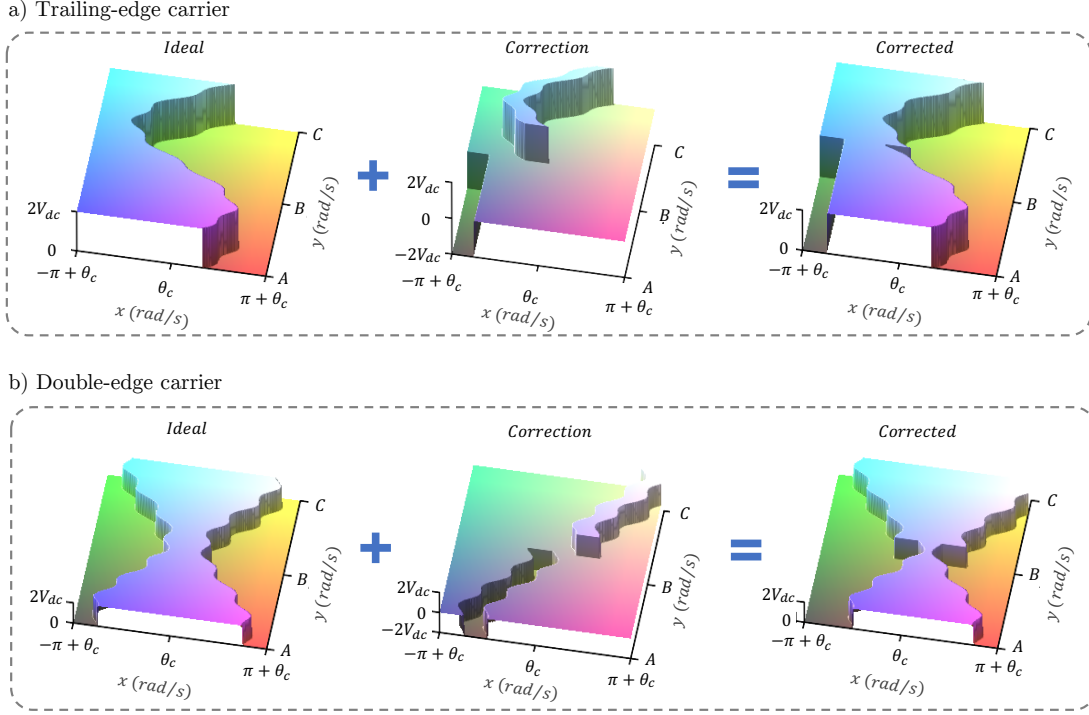


Figure 3.6 - Dead-time effects over the PWM 3D-model. Parameters used: $V_{dc} = 1.0$ p.u., $M = 0.6$, $\omega_o = 2\pi 60$ rad/s, $\theta_o = 30^\circ$, $h = 7$, $M_h = 0.1$, $\theta_h = 15^\circ$, $\theta_c = 45^\circ$, $M_f = 21$, $T_d = 100$ μs , $\varphi = 30^\circ$.

3D-Model Including Dead-Time Effects

Dead-time effects can be defined using the shift-angle between voltage and current waveforms, and the correction boundary-functions as follow

$$F_{(corr)}(x, y) = \begin{cases} -2V_{dc}, & x_r(y) \leq x \leq x'_r(y) \wedge A \leq y < B \\ 2V_{dc}, & x_f(y) \leq x \leq x'_f(y) \wedge B \leq y < C \\ 0, & \text{Otherwise} \end{cases} \quad (3.12)$$

Where $A = -\pi/2 + \varphi + \theta_1$, $B = \pi/2 + \varphi + \theta_1$, and $C = -3\pi/2 + \varphi + \theta_1$ (see figure 3.4).

Figure 3.6 shows the correction 3D-model and the effects over the ideal one. As can be seen in this figure, the effects of the correction function are to decrease the volume of the 3D-model during the positive part of the current signal (from A to B) and increase it during the negative part (from B to C). This is consistent with the effects reported in Figure 3.3, i.e., *loss* effects during the positive semi-cycle of the modulator signal and *gain* effects during the negative semi-cycle.

3.3.2 Spectrum of a Naturally Sampled *PWM* Including Dead Time

To incorporate the effects of dead time into the calculations of the double Fourier-coefficients, it is necessary to modify the double integral that defines the complex coefficients C_{0n} . As shown in Figure 3.6, the volume of the correction 3D-model is defined in two separate regions, which affects the outer Fourier-integral. Nevertheless, this discontinuity does not affect the convergence of the double Fourier-series [44]. Moreover, using the boundary functions presented in Table 3.2, the correction function $F_{corr}(x, y)$, and the shift-angle φ , the complex coefficients of the double Fourier-series are given by

$$C_{0n_{(corr)}} = \frac{V_{dc}}{\pi^2} \left[- \int_{-\frac{\pi}{2} + \varphi + \theta_1}^{\frac{\pi}{2} + \varphi + \theta_1} \int_{x_r}^{x'_r} e^{jny} dx dy + \int_{\frac{\pi}{2} + \varphi + \theta_1}^{\frac{3\pi}{2} + \varphi + \theta_1} \int_{x_f}^{x'_f} e^{jny} dx dy \right] . \quad (3.13)$$

These complex coefficients represent the magnitude and phase of each harmonic in the double Fourier-series of the correction term and will be discussed below.

***DC* Component**

The analytical expression for the *DC* component is calculated by setting $n = 0$, using the boundary functions presented in Table 3.1 and 3.2, and solving the ideal and correction integrals of the Fourier coefficients, (3.10) and (3.13) respectively. After algebraic manipulations, the expression of the *DC* component for the ideal term is given by

$$\frac{C_{00_{(ideal)}}}{2} = \begin{cases} V_{dc} & \text{trailing-edge naturally sampled} \\ V_{dc} & \text{double-edge naturally sampled} \end{cases} \quad (3.14)$$

and the correction term is given by

$$\frac{C_{00(\text{corr})}}{2} = \begin{cases} \frac{V_{dc}M_h}{2\pi h} \begin{bmatrix} 2 \cos(\varphi + \theta_1) \\ -2 \cos(\varphi + \theta_1 - \Delta_y) \\ -\sin\left(\left(\varphi - \frac{\pi}{2}\right)h + \theta_h\right) \\ +\sin\left(\left(\varphi - \frac{\pi}{2} - \Delta_y\right)h + \theta_h\right) \\ +\sin\left(\left(\frac{\pi}{2} + \varphi\right)h + \theta_h\right) \\ -\sin\left(\left(\frac{\pi}{2} + \varphi - \Delta_y\right)h + \theta_h\right) \end{bmatrix} & \begin{array}{l} \text{trailing-edge} \\ \text{naturally sampled} \\ \text{double-edge} \\ \text{naturally sampled} \end{array} \\ 0 & \end{cases} \quad (3.15)$$

Recalling that $\Delta_y = \omega_1 T_d$ and T_d is normally a very small value due to the high switching-frequency in practical applications. Then, to build a general approximated model, the DC component in the correction term for the trailing-edge natural sample can be neglected. Hence, both analog PWM schemes can be described by the same analytical expression. Additionally, the corrected DC component is given by the sum of the ideal and correction term as

$$\frac{C_{00}}{2} = V_{dc} \quad (3.16)$$

Fundamental-frequency

The analytical expression for the fundamental frequency is defined by the sum of the ideal and correction terms of the complex coefficients of the Fourier series

$$C_{01(\text{ideal})} = MV_{dc}e^{-j\theta_1} \quad (3.17)$$

and

$$C_{01(\text{corr})} = 2MV_{dc}e^{-j\theta_1} (e^{j\Delta_y} - 1) - 4 \frac{e^{j\varphi} \Delta_x V_{dc}}{\pi^2} \quad (3.18)$$

As mentioned in [10], considering that $\Delta_y \ll 1$, then the first term of (3.18) can be neglected, and the complete fundamental component is found to be

$$C_{01} = MV_{dc}e^{-j\theta_1} - \frac{4\Delta_x V_{dc}}{\pi^2} e^{j\varphi} \quad (3.19)$$

The analytical expression of the fundamental component shown in (3.19) is the same expression reported by [10] for the single-frequency input case. Hence, *the harmonic at order h introduced in the modulator does not affect the value of the fundamental component.*

Figure 3.7 shows the effect of dead time over the fundamental component. Recall-

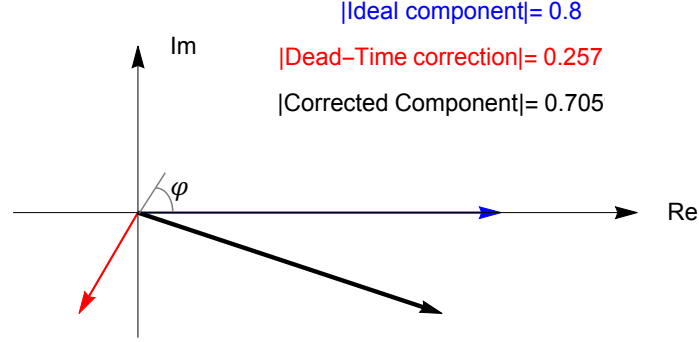


Figure 3.7 - Components of the fundamental frequency. Parameters used: $M = 0.8$, $V_{dc} = 1.0 \text{ p.u.}$, $\varphi = 60^\circ$, $T_d = 20 \mu s$, $\omega_1 = 2\pi 60 \text{ rad/s}$, $\theta_1 = 0^\circ$, $M_f = 85$.

ing that $\Delta_x = \omega_c T_d$, it is possible to see from (3.19) that the corrected component, C_{01} , is proportional to the dead-time duration, the switching frequency, and the *DC* voltage. Furthermore, the magnitude and phase of the corrected component are affected by the angle (φ) between the fundamental-frequency of the voltage and the output current. Thus, the power factor of the load affects the corrected fundamental-component.

The results shown in this section extend the same conclusions presented experimentally by [18], and analytically by [7, 8, 15, 43], to the actual case of a single-phase converter with multiple-frequency modulator and dead time. These conclusions are:

- the correction component has the opposite direction of the output current;
- the fundamental component introduced by dead time is proportional to T_d , ω_c , and V_{dc} ;
- and the proportionality constant equals to four over the square of π .

Furthermore, the *PWM* definition presented in this section takes into consideration the arbitrary initial phase of the injected harmonics θ_h , likewise the carrier signal θ_c . Nevertheless, (3.19) shows that the fundamental component is only affected by the initial phase of the fundamental-frequency θ_1 . Hence, *the phase of the injected harmonic h , and the phase of the carrier signal do not affect the corrected fundamental-component.*

Base-band and injected harmonics

Recalling that the base-band harmonics are the result of the sum of ideal and correction terms, then, this section analyzes Fourier-coefficients for all harmonics of the

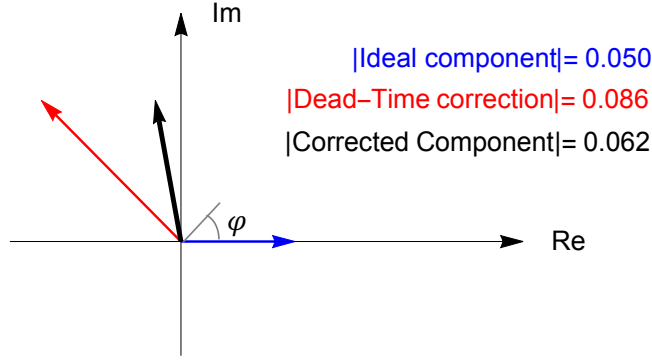


Figure 3.8 - Components of the injected-harmonic. Parameters used: $h = 3$, $M_h = 0.05$, $V_{dc} = 1.0 \text{ p.u.}$, $\varphi = 45^\circ$, $T_d = 20 \mu\text{s}$, $\omega_o = 2\pi 60 \text{ rad/s}$, $\theta_h = 0^\circ$, $M_f = 85$.

fundamental-frequency. The base-band harmonics of the ideal term are defined by

$$C_{0n_{(ideal)}} = \begin{cases} 2V_{dc}, & n = 0 \\ MV_{dc}e^{-j\theta_1}, & n = 1 \\ M_h V_{dc}e^{-j\theta_h}, & n = h \\ 0, & \textit{Otherwise} \end{cases} . \quad (3.20)$$

and the correction terms are defined by

$$C_{0n_{(corr)}} = \begin{cases} j \frac{4\Delta_x V_{dc}}{n\pi^2} e^{j(\frac{\pi}{2}n+n\varphi)}, & n = [1, 3, 5, \dots] , \\ 0, & n = [0, 2, 4, \dots] . \end{cases} \quad (3.21)$$

The above expression shows that the injected harmonic h is only affected by dead time for odd values of h . As shown in (3.21), dead time only introduces odd harmonics. Hence, for even values of h , the corrected harmonic component depends only on the harmonic information in the modulator signal, M_h and θ_h , and the voltage of the DC link V_{dc} , (see case $n = h$ in (3.20)). For odd values of the harmonic h in the modulator signal, the output voltage is affected by the dead-time harmonics, as shown in the vector diagram in Figure 3.8. In this case, the corrected component is given by

$$C_{0h_{(odd)}} = M_h V_{dc}e^{-j\theta_h} + j \frac{4\Delta_x V_{dc}}{h\pi^2} e^{j(\frac{\pi}{2}h+h\varphi)} . \quad (3.22)$$

Moreover, the analysis over (3.21), and recalling that $\Delta_x = \omega_c T_d$, then it can be seen that:

- neither the arbitrary phase of the fundamental-frequency nor the carrier's in-

fluence the base-band components of the dead time;

- the harmonics of the correction term are proportional to dead time and V_{dc} , with a proportionality constant of four over the square value of π ;
- the base-band harmonics of the correction part decays rapidly, inversely proportional to the harmonic order;
- and, the injected harmonic h does not affect other base-band harmonics introduced by the dead time.

Low-frequency time definition of *PWM* scheme including dead time

The correction term of the voltage in one arm of the power converter is found by using the reduced double Fourier-series shown in (3.8) and the coefficient computed with (3.13). The low-frequency approximation of the correction voltage waveform is found to be

$$v_{a-(corr)}(t) = V_{dc} \left[\begin{aligned} & \frac{1}{2}M \cos(\omega_1 t + \theta_1) + \frac{1}{2}M \cos(\omega_1 t + \theta_1 - \Delta_y) \\ & + \sum_{n=3}^{\infty} 4 \frac{\Delta_x \sin\left(-\frac{n\pi}{2} - n\varphi + n\omega_1 t\right)}{n\pi^2} \end{aligned} \right], \quad (3.23)$$

where $n = [1, 3, 5, 7, 9, \dots]$.

Finally, neglecting the effect of the parameter Δ_y in (3.23), then the complete corrected term of the voltage in one arm of the power converter is given by

$$\begin{aligned} v_{a-}(t) &= v_{a-(ideal)}(t) + v_{a-(corr)}(t) \\ &= V_{dc} + MV_{dc} \cos(\omega_1 t + \theta_1) + M_h V_{dc} \cos(h\omega_1 t + \theta_h) \\ & \quad + \sum_{n=3}^{\infty} 4V_{dc} \frac{\Delta_x \sin\left(-\frac{n\pi}{2} - n\varphi + n\omega_1 t\right)}{n\pi^2}, \end{aligned} \quad (3.24)$$

where $n = [1, 3, 5, 7, 9, \dots]$.

Figure 3.9 shows an example of a low-frequency spectrum calculated using (3.24) and normalized by the magnitude of the fundamental frequency.

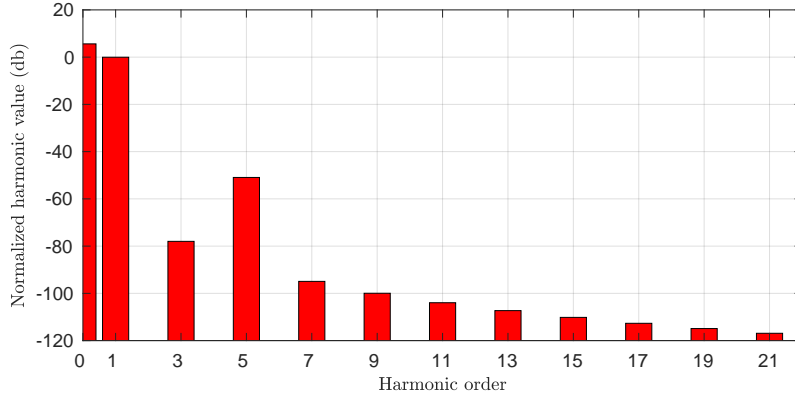


Figure 3.9 - Normalized low-frequency spectrum of a double-edge naturally sampled *PWM* signal considering dead-time effects and a multiple-frequency modulator. Parameters used: $M = 0.8$, $h = 5$, $M_h = 0.05$, $V_{dc} = 1.0 \text{ p.u.}$, $\varphi = 45^\circ$, $T_d = 5 \mu\text{s}$, $\omega_o = 2\pi 60 \text{ rad/s}$, $\theta_1 = \theta_h = 0^\circ$, $M_f = 85$.

3.4 Conclusions

This chapter performed a detailed analysis of the effects of dead time in one inverter phase-leg using naturally sampled *PWM* schemes with multiple-frequency modulators. The principal outcomes are highlighted below.

- The proposed *time substitution concept* produces the same results as those presented geometrically in the bibliography. Moreover, it allows a straightforward method to include dead-time effects in elaborate modulator signals.
- Dead time introduces a small DC component in *PWM* with a trailing-edge carrier. In order to build a general model, this small DC component was neglected. Nevertheless, this DC component should be considered for any power electronics application that use a transformer in the output stage. In these application even a small *DC* voltage component can produce a significant *DC* current due to the low impedance value of the transformer at zero Hz.
- The base-band harmonics introduced by dead time do not depend on injected harmonics introduced by the control law.
- The injected harmonic h does not affect the ideal fundamental-frequency component, and *vice versa*.
- The arbitrary phase of the injected harmonic and the carrier signal do not affect the *PWM* spectrum. Nevertheless, the power factor of the load does.

The theoretical development presented in this chapter was used as the basis to build a *Wolfram Mathematica*[®] package application called *PwmSpectra*. This application provides simple functions to facilitate the study of digital and analog

PWM schemes, e.g., Figures 3.7 and 3.8 were calculated and plotted using the *PlotComponentVectors* function offered by the application. Details of *PwmSpectra* are shown in Appendix E.

Chapter 4

Single-Phase *PWM* Voltage Source Inverters

Once the low-frequency spectra in one phase-leg have been determined in Chapter 3, the next step is to consider the interaction between phase-legs that are grouped to make a complete inverter system [12]. This chapter analyses the overall low-frequency performance of three different single-phase inverter topologies and proposes a simplified model that allows understanding of the principal harmonic components that are responsible for the power quality degradation in these power electronic converters.

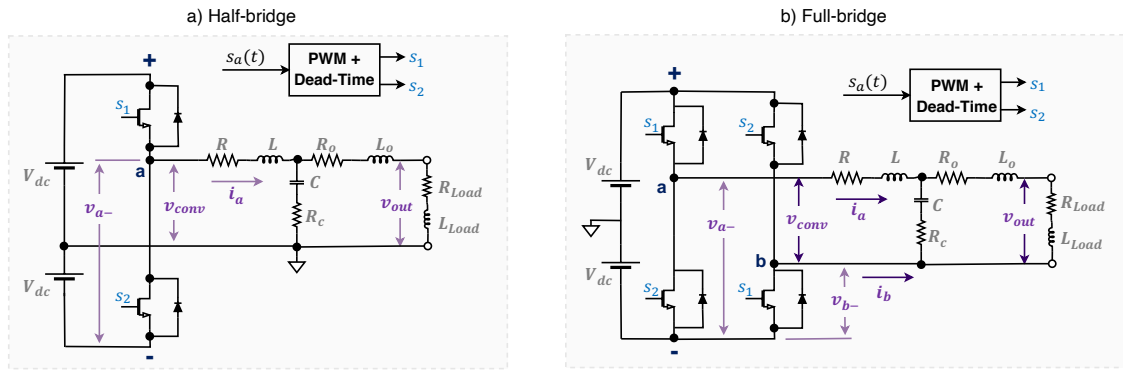


Figure 4.1 - Two-level single-phase inverter topologies: a) Half-bridge single-phase inverter; b) Full-bridge single-phase inverter.

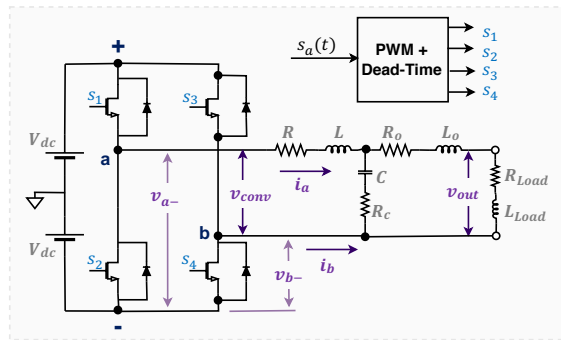


Figure 4.2 - Three-level full-bridge single-phase inverter topology.

4.1 Topologies of a Single-Phase Inverter

Figure 4.1 presents two topologies for a two levels single-phase inverter. The first one is a half-bridge inverter built from a split DC link and a phase-leg equal to the one described in Chapter 3. The second two-level topology is a full-bridge inverter made up of two phase-legs connected to a common DC bus and modulated by a bipolar PWM scheme. Furthermore, Figure 4.2 presents a three-level single-phase inverter. This topology is made by a full-bridge single-phase inverter modulated by a unipolar PWM scheme. An LCL low-pass filter forms the output filter stage for all topologies. Additionally, an RL branch was used as a load. The following sections explore the low-frequency spectra of PWM with a multiple-frequency modulator signal and dead-time effects over all these single-phase topologies.

4.2 Two-Level *PWM* Single-Phase Inverter

Using the topology description presented Figures 4.1 and 4.2, and the analytical expression for one phase leg of a voltage source inverter developed in Chapter 3, it is possible to build the analytical frequency spectra of interaction between different phases in a power inverter [12, 15]. The analytical *PWM* spectra presented in Chapter 3 describes the low-frequency components in each phase leg of a power electronic converter referred to the negative pole of the *DC* link (v_{a-} in Figures 4.1 and 4.2). The following sections extend these analytical spectra to describe the output voltages of a two-level single-phase inverter, i.e., the voltage waveform applied to the filter stage or v_{conv} in Figure 4.1.

4.2.1 Low-Frequency Spectrum of a Two-Level Single-Phase Inverter

As presented in [12], the voltage waveform v_{conv} can be defined by the analytical time definition of v_{a-} and the voltage analysis of the inverter topology shown in Figure 4.1. For a half-bridge inverter, it is straightforward to see from Figure 4.1-a that the output voltage is given by

$$v_{conv(half)} = v_{a-} - V_{dc} \quad . \quad (4.1)$$

Moreover, in a two-level full-bridge topology, the control signals S_1 and S_2 are diagonally opposite, see Figure 4.1-b. This *PWM* technique is known as bipolar voltage switching [45]. Recalling from Section 1.2.3, dead-time effects depend on the output-current polarity, and, for a single-phase inverter, current in leg b is inverse to the current in leg a . Thus, the dead-time effects in the output voltage of each phase are opposite, i.e., *loss* effect in one phase means *gain* effect in the other phase, and *vice versa*. This situation means that the *PWM* pulse v_{b-} is a complementary waveform of v_{a-} and it can be found as $v_{b-} = 2V_{dc} - v_{a-}$. Therefore, the output voltage for the two-level full-bridge topology is given by

$$\begin{aligned} v_{conv(full)} &= v_{ab} \\ &= v_{a-} - v_{b-} \quad . \\ &= 2(v_{a-} - V_{dc}) \end{aligned} \quad (4.2)$$

Equations (4.1) and (4.2) show how output voltage for the topologies shown in Figure 4.1 can be defined by using the analytical expression developed in Chapter 3. Furthermore, the output voltages for both two-level topologies only differ by a factor of two. Nevertheless, when analyzing low-frequency harmonic com-

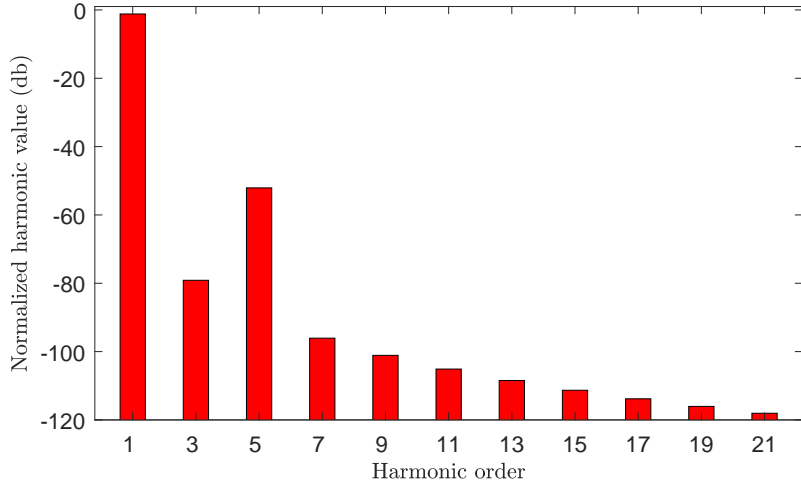


Figure 4.3 - Analytical low-frequency spectra of a single-phase inverter. Parameters used: $M = 0.8871$; $\omega_1 = 376.9$ rad/s; $\theta_1 = \theta_h = 0^\circ$; $\varphi = 45^\circ$; $T_d = 5 \mu\text{s}$; $M_f = 85$; $M_h = 0.05$; and $h = 5$.

ponents, it is a common practice to normalize the spectrum by the magnitude of the fundamental-frequency component; therefore, both topologies displays the same harmonic components, and they are defined by

$$\hat{v}_{conv}(t) = \cos(\omega_1 t + \theta_1) + \frac{M_h}{M} \cos(h\omega_1 t + \theta_h) + \sum_{n=1}^{\infty} 4 \frac{\Delta_x \sin\left(-\frac{n\pi}{2} - n\varphi + n\omega_1 t\right)}{nM\pi^2}, \quad (4.3)$$

where $n = [1, 3, 5, 7, 9, \dots]$ and $\hat{v}_{conv}(t)$ stands for the output voltage of the inverter normalized by the magnitude of the fundamental-frequency. Figure 4.3 shows the analytical low-frequency spectrum calculated by (4.3).

4.2.2 Simulation Results

The electromagnetic transients simulation software *PSCADTM/EMTDCTM* was used to create two different simulation scenarios. The basic schematic diagram is shown in Figure 4.4 and the implementations using *PSCADTM* blocks are presented in Appendix D. Dead time is not a native feature of *PSCADTM* thus a combinational logic was implemented as described in Figure 1.7. The first case scenario presented in Figure 4.4-a simulates the switching patterns of a single-phase *PWM* inverter. The second case scenario is shown in Figure 4.4-b, where a voltage source is controlled by a mathematical model based on the analytical low-frequency spectrum defined in the last section. Details of this mathematical model are presented in section 4.4. Both scenarios use the same multiple-frequency modulator signal defined by (3.1). Also, they both use the same parameter values for the output-filter and load stages.

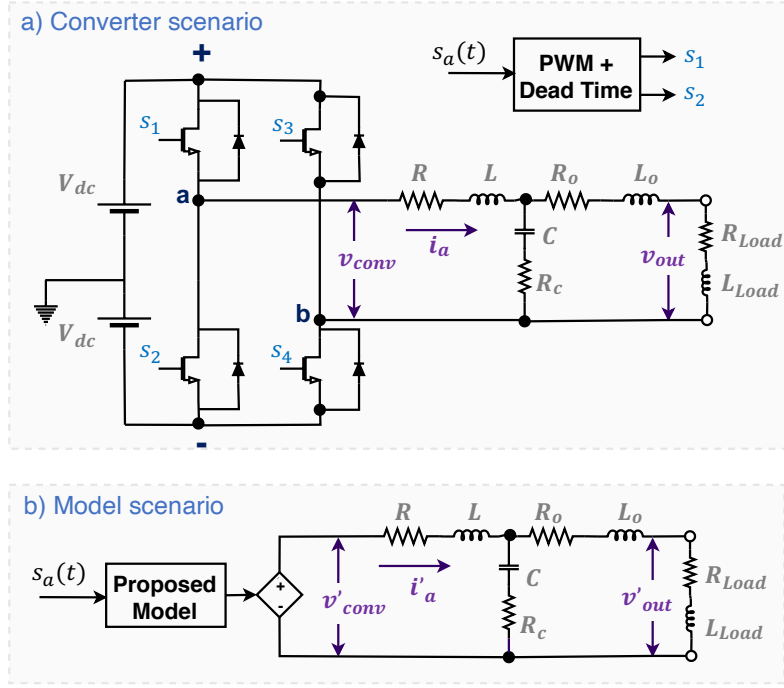


Figure 4.4 - Block diagram and circuits of the proposed single-phase case scenarios. $S_a(t)$ represents the multi-frequency modulator signal and v'_{conv} represents the estimated voltage value of the converter using the proposed simplified model.

Case study: 10 kVA single-phase inverter

The selected case study is the inverter stage of an industrial *UPS*, typically used in oil and gas offshore platforms. The parameters used are summarized in Tables 4.1, and 4.2. Moreover, parameters used for the modulator signal are: $M = 0.8871$; $\omega_1 = 376.9$ rad/s; $\theta_1 = \theta_h = 0^\circ$; $M_h = 0.05$; And $h = 5$. The parameters of the modulator signal were calculated to synthesize a nominal-value component in the fundamental-frequency and injection of 5.6% of 5th harmonic, i.e., these values are equivalent to those presented by [19] for the voltage controller of a *UPS* inverter when it is compensating distortions of a nonlinear load. The proposed scenarios and study cases are sufficient to perform time, frequency, and performance studies, and the results are discussed in the following sections.

Time- and frequency-domain comparison

The primary hypothesis presented in this thesis is that due to the low-pass filter of the power converter, the frequency analysis should only take into consideration the harmonics of the fundamental frequency. To prove this hypothesis, a time-domain comparison was performed in the two different scenarios described earlier.

The input and output voltages for the two scenarios are shown in Figures 4.5 and 4.6, respectively. It can be seen that a high-frequency *PWM* defines the input

Table 4.1 - Inverter parameters.

Parameter	Value
Power	10 kVA
$2V_{dc}$	405 V
V_{out}	220 V_{rms}
f_1	60 Hz
f_c	5100 Hz
T_d	5 μs
L	1.8 mH
R	1.85 $m\Omega$
C	90 μF
R_C	10 $\mu\Omega$
L_o	170 μH
R_o	1.85 $m\Omega$
R_{load}	1.45 Ω
L_{load}	427.9 μH

Table 4.2 - *PWM* model parameters.

Parameter	Value
Δ_x	0.321 rad
ω_1	376.991 rad/s
φ	0.414 rad
Number of fundamental-frequency harmonics	13

voltage synthesized by the converter. However, the proposed model only synthesizes the first six odd-harmonics of the fundamental-frequency, i.e., $h = [3, 5, 7, 9, 11, 13]$. Nevertheless, as shown in Figure 4.6, the output-voltages at the end of the filter stage for both case scenarios (v_{out} and v'_{out}) are extremely close. As expected, the low-pass characteristic of the output filter of the power inverter successfully reduces all high-frequencies introduced by the switching pattern of the inverter. Therefore, the analytical model successfully follows the output voltage waveform of the simulated power converter.

Additionally, the spectra comparison of the output voltage is depicted in Figure 4.7. It is shown that the modulator components and the low order harmonics introduced by the dead time are comparable for both scenarios. These results validate the assumption and demonstrate that the proposed analytical approximation successfully achieves the dominant dynamics of the equipment when a signal with

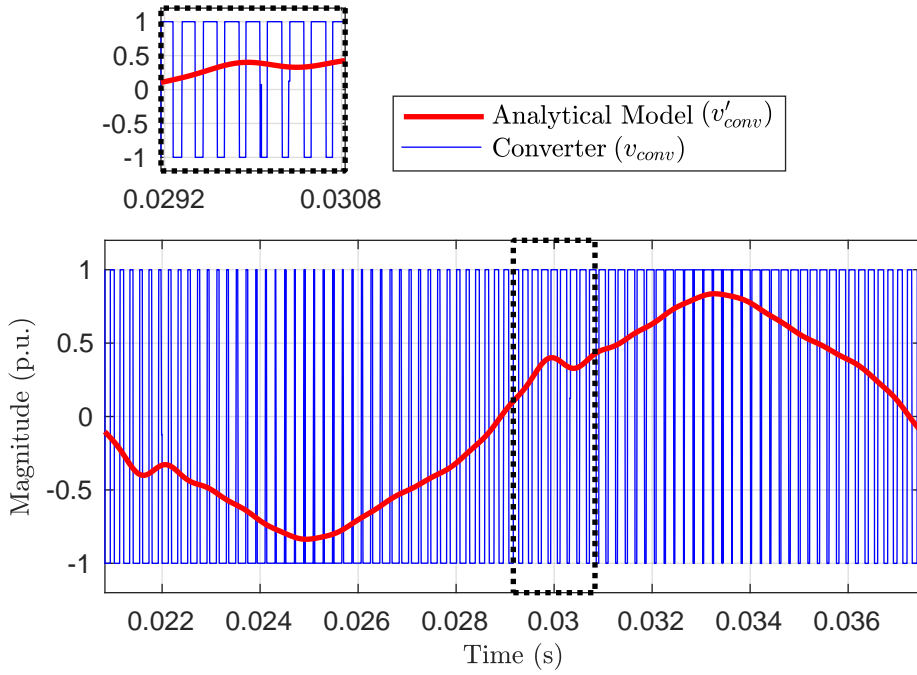


Figure 4.5 - Voltage waveform before the output-filter. Dead-time effects can be seen in the highly nonlinear deformation of the model's waveform that occurs when the current changes its polarity.

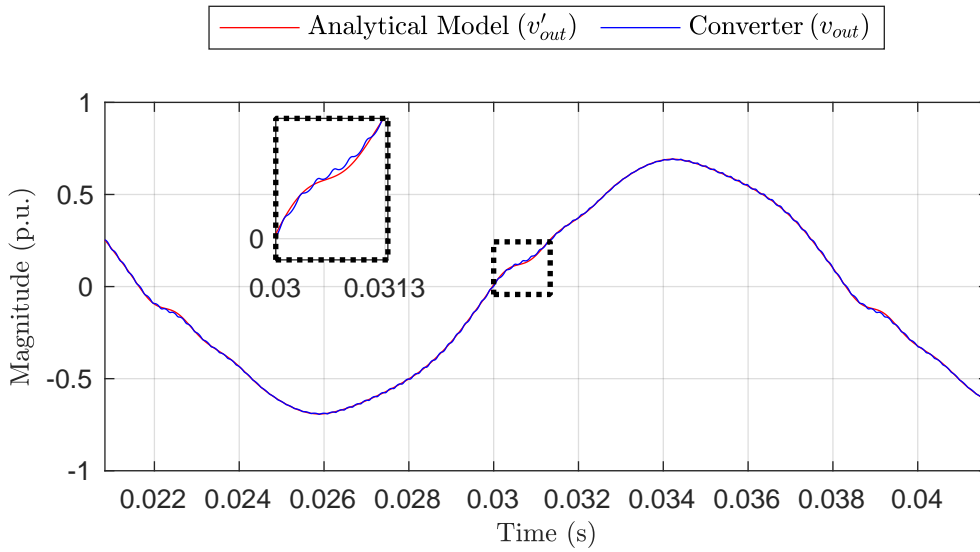


Figure 4.6 - Load's voltage-waveform comparison. Processing time step = $0.1\mu s$.

multiple frequencies is used as a modulator, i.e., fundamental-frequency plus 5.6% of 5th harmonic. Also, the proposed model can reproduce the most significant dynamics of the dead-time effects. The zoomed area in Figure 4.6, and high-frequency components in Figure 4.7 show that the two scenarios predominantly differ in a small high-frequency ripple of the converter simulation, but this value is negligible.

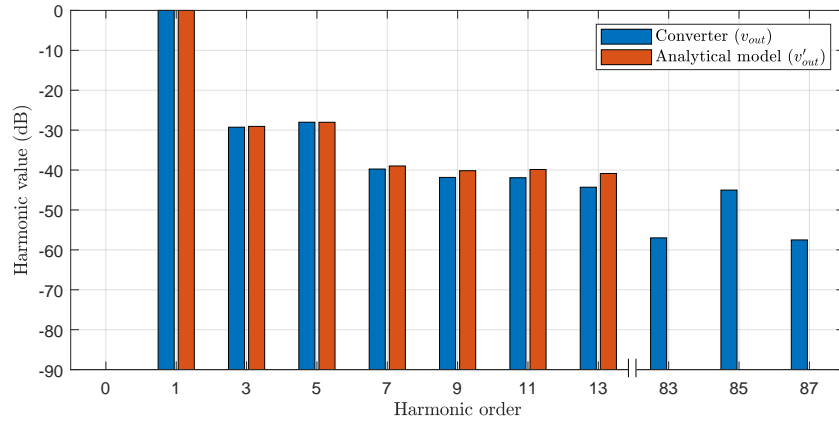


Figure 4.7 - Output-voltage spectra comparison for two-level single-phase inverter.

4.3 Three-Level *PWM* Single-phase Inverter

Three level single-phase *PWM* inverter can be achieved by using the same carrier and a shifted modulator signal for each phase-leg of a *VSI*. This technique is commonly know as a *unipolar PWM* [12, 45]. This topology depicts some advantages, such as: it applies a smaller dV/dt to the switching devices when compared with bipolar *PWM* technique; allows some high-frequency harmonic cancellations between the inverter-legs as presented in [12]; moreover, a smaller output-filter stage can be designed due to lower high-frequency components in the output voltage of a power converter. These advantages make this modulation technique a popular choice in single-phase *PWM* inverters. Therefore, this section uses the analytical low-frequency spectrum developed in Chapter 3 to explore dead-time effects into the unipolar *PWM* single-phase inverter.

4.3.1 Low-Frequency Spectrum

The analytical spectrum of the output voltage waveform for a unipolar *PWM* technique can be achieved by using the analytical expression of v_{a-} and introducing a shift-phase of π radians to create v_{b-} [12, 15]. Thus, using (3.24), the analytical

expression of output-voltage in phase b is found to be

$$\begin{aligned}
v_{b-}(y) &= V_{dc} \left[1 + M \cos(y + \theta_1 + \pi) + M_h \cos(hy + \theta_h + \pi) \right. \\
&\quad \left. + \sum_{n=1}^{\infty} \frac{4\Delta_x}{n\pi^2} \sin\left(ny - n\varphi - \frac{\pi}{2}n + \pi\right) \right] \\
&= V_{dc} \left[1 - M \cos(y + \theta_1) - M_h \cos(hy + \theta_h) \right. \\
&\quad \left. - \sum_{n=1}^{\infty} \frac{4\Delta_x}{n\pi^2} \sin\left(ny - n\varphi - \frac{\pi}{2}n\right) \right] \quad , \quad (4.4) \\
&= 2V_{dc} - v_{a-}
\end{aligned}$$

where $n = [1, 3, 5, 7, 9, \dots]$.

In (4.4) is showed that the output voltage of phase b is equal to the case of a full-bridge two level single phase presented in Section 4.2.1. Therefore, the low-frequency spectrum of the three-level single-phase inverter is equal to the full-bridge two-level single-phase inverter defined in (4.3), even considering the harmonic components introduced by the dead time and a multiple-frequency modulator signal.

4.3.2 Simulation Results

This section uses the same concept of using the proposed scenarios in Section 4.2.2 to compare the analytical low-frequency spectrum and the voltage output waveforms of a simulated three-level single-phase converter. The implementations using *PSCADTM* blocks are presented in Appendix D, and the principal results are discussed in the following sections.

Time- and frequency-domain comparison

The input and output voltages for both scenarios are shown in Figures 4.8 and 4.9, respectively. Moreover, The frequency-spectra comparison of the output voltage is shown in Figure 4.10.

It can be seen that even when the model uses only the first six odd harmonics of the fundamental frequency, the output voltages of the inverter and the analytical model are extremely close. As can be seen in the zoomed area of Figure 4.9, the high-frequency ripple of the converter voltage is smaller due to the smaller dV/dt of the topology. This difference is also shown in Figure 4.10, where it can be seen that the first group of high-frequency components are side-bands of the second carrier-harmonic, where the attenuation of the LCL low-pass filter is more prominent.

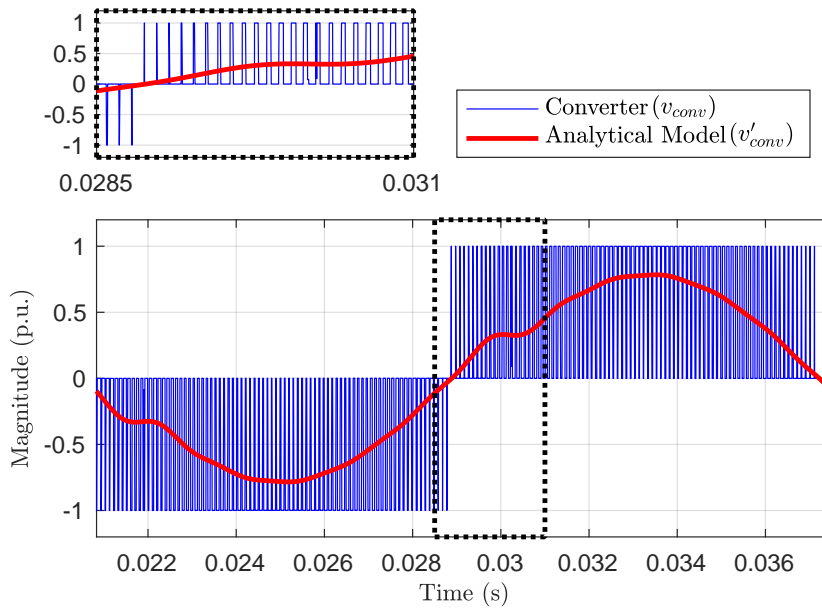


Figure 4.8 - Voltage waveform before the output filter for three-level single-phase inverter.

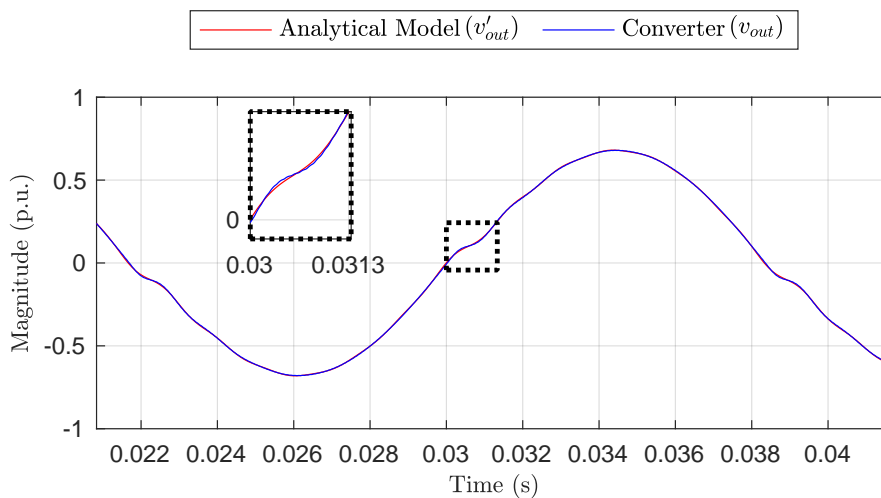


Figure 4.9 - Load's voltage-waveform comparison for three-level single-phase inverter.

Similarly to the results in the last section, differences for both case scenarios are minimal. Therefore, these results validate the assumption and demonstrate that the proposed analytical approximation successfully achieves the dominant dynamics of the single-phase equipment with dead time and a multiple-frequencies modulator signal.

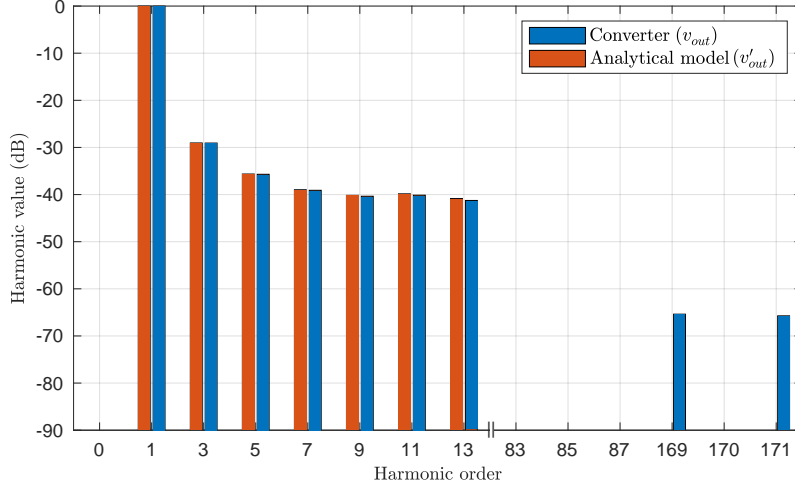


Figure 4.10 - Output-voltage spectra comparison for three-level single-phase inverter.

4.4 Low-frequency model (*Original Contribution*)

This section presents the detailed description of the proposed simplified model based on the analytical spectra described in Chapter 3, and used in simulations presented by previous sections. The proposed simplified model is given by the sum of the ideal and correction parts studied in Sections 3.2.2 and 3.3.2, respectively. Hence, a time-function of the output voltage in one arm of the converter can be described as

$$v_{a-}(y) = V_{dc} \left[1 + M \cos(y + \theta_1) + M_h \cos(hy + \theta_h) + \sum_{n=1}^{\infty} \frac{4\Delta_x}{n\pi^2} \sin\left(ny - n\varphi - \frac{\pi}{2}n\right) \right] \quad (4.5)$$

$$= V_{dc} \left[1 + s_a(y) + \sum_{n=1}^{\infty} \frac{4\Delta_x}{n\pi^2} \sin\left(ny - n\varphi - \frac{\pi}{2}n\right) \right],$$

where $n = [1, 3, 5, 7, 9, \dots]$.

Finally, according to (4.1), the low-frequency output-voltage model for a half-bridge single-phase inverter is given by

$$v_{conv}(t) = V_{dc} \left[s_a(t) + \sum_{n=1}^{\infty} \frac{4\Delta_x}{n\pi^2} \sin\left(n\omega_1 t - n\varphi - \frac{\pi}{2}n\right) \right], \quad (4.6)$$

where $n = [1, 3, 5, 7, 9, \dots]$.

As shown in (4.2), the output-voltage model for a full-bridge single-phase inverter can be define multiplying (4.6) by a factor of two.

Proposed Model Constraints

The proposed simplified model achieves high performance, and high accuracy under some operational constraints listed below.

- The current waveform and its high-frequency ripple should not create more than two changes of the current polarity over one cycle of the fundamental frequency [10] (see figure 3.4).
- The modulator signal should not over-modulate the *PWM*, i.e., the magnitude of the modulator signal should be lower than the maximum value of the carrier signal.
- The magnitude ratio of the fundamental component and the injected harmonic should not create a modulator signal with more than two zero-crossings over one cycle of the fundamental-frequency signal.
- The switching frequency of the power converter should be high enough to avoid overlapping between side-band and base-band harmonics.

In practice, low-power converter applications with high power quality satisfy these conditions, e.g., active filters and voltage source converters with harmonic-compensation schemes.

Mathematical model implementation

The proposed mathematical model defined by (4.6) can be implemented using a small functional code. This thesis implements the previously mentioned model using a C-code function, as presented in Listing 4.4. *C* language was selected due to the integration capability to *PSCADTM*.

Listing 4.1 - C-code implementation of the proposed model

```

float pwmModel (float modulator_t, float Delta_X, float Vdc, float
    omega_1, float Varphi, int nMax)
{
    /*----- local variables -----*/
    float ideal;
    float B0n;
    float correction=0.0;
    float pi=3.14159235659;
    int i;

    /*----- Mathematical model described by equation (4.6) -----*/
    ideal=Vdc*modulator_t;
    for (i=1; i<=nMax; i=i+2)
    {
        n=(float) i;
        B0n=4*Delta_X*Vdc/(n*pi*pi);
        correction=correction+B0n*sin (n*omega_1*t-n*Varphi-n*pi/2.0);
    }
    return ideal+correction;
}

```

Performance comparison

High switching-frequency equipment demands small simulation time steps, and in consequence, long simulation times, i.e., the switching frequency is normally in the kHz order which demands simulation steps in the order of micro-seconds that leads to an overall simulation time of several seconds for each mili-second simulated. In practice, this fact limits the number of applications, such as a large number of power converter connected in micro-grid systems, or slow dynamics studies in high-frequency power converters. Thus, knowing that the proposed mathematical model achieved equivalent results when compared with classical switching simulation, then it is interesting to compare the performance of these two approaches.

Figure 4.11 shows the behavior of both simulation scenarios for multiple values of the simulation time step. It can be seen from this figure that the difference between converter simulation and the proposed model is proportional to the simulation time step. Moreover, only full converter model results change, and they tend to converge to the mathematical model results. Variations on the converter results are expected due to the calculation error produced by the differences between processing sampling-frequency and the switching-frequency of the converter. Figure 4.11 shows that both cases fit when a simulation time step less than one-tenth microsecond is

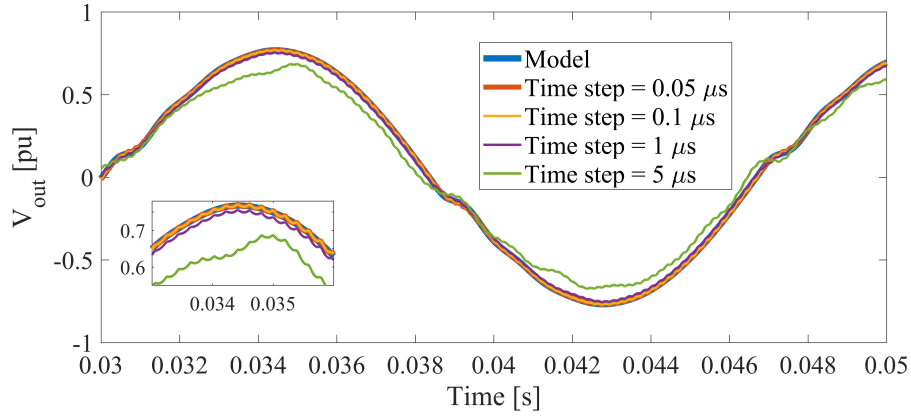


Figure 4.11 - Converter simulation behavior for different values of the simulation time step.

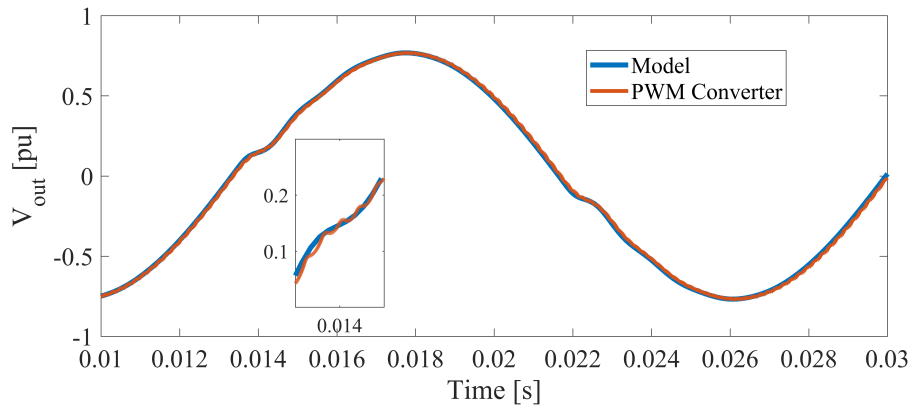


Figure 4.12 - Output voltage comparison at different simulation step time: Analytical model using $100 \mu s$ and converter simulation using $0.1 \mu s$.

used.

The maximum value of the simulation time step is related to the maximum frequency of interest in the analysis, e.g., if the objective of the study is focused on the fifth harmonic. Then, the maximum simulation time step should be set to guarantee proper sampling for that frequency. A simulation time step of one hundred microseconds was selected in this work. The time-domain behavior with the selected time step is presented in Figure 4.12, which shows that the proposed mathematical model can achieve an equivalent result by using this larger simulation time step.

The selected simulation time step decreases the number of evaluation points of the simulation by a factor of one thousand, which allows for a faster overall simulation time. An illustrative example of this difference was developed by simulating three seconds for both case scenarios, and the results have shown that the proposed model was up to one hundred thirty times faster when compared with the traditional simulation of a switching converter.

4.5 Conclusions

A low-frequency spectrum for two- and three-level single-phase inverters considering dead-time effects and a multiple-frequency input was proposed in this chapter. Simulation results showed that it is possible to create an efficient mathematical model that can recreate the output voltage of a single-phase inverter using the first six odd harmonics of the fundamental frequency.

The proposed simplified model achieves high performance, and high accuracy under some operational constraints listed below.

- The load's current and the modulator signal cannot have more than two changes of polarity in one fundamental-frequency period.
- The switching frequency of the power converter should be high enough to avoid overlapping between side-band and base-band harmonics.

Additionally, this chapter proposed a case study of a *ten kVA* industrial *UPS*. The results showed that the proposed model needs one thousand times fewer simulation points, and its performance is up to one hundred thirty times faster than a traditional power electronics simulation. Hence, the proposed simplified model gives an analytical understanding of the principal harmonics that are responsible for the degradation of power quality and provides an option to study the harmonic distortion of a power electronic converter with low computational-cost for the simulation tool. Furthermore, the simulation results presented in this chapter confirm the theoretical assumption introduced in Chapter 3.

Chapter 5

Conclusion and Future Works

The analytical approach developed in this thesis allows the understanding of the effects of dead time in *PWM* inverters with multiple-frequency modulator signals. All studies proposed in this thesis were based on two fundamental concepts.

1. It is possible to simplify the analytical development by restricting the scope to the low-frequency spectra, i.e., fundamental-frequency harmonics lower than switching-frequency components.
2. The *time substitution concept*, $t \mapsto t - T_d$, allows to extend the state-of-the-art dead-time analysis using *Black's method* to the case of multiple-frequency modulator signals.

Using these two fundamental concepts, this thesis developed a mathematical approach to understand the phenomenon under study. Several specific conclusions were presented at the end of each chapter as a result of this analytical approach. Moreover, recalling the question that motivates this thesis, "*what are the effects of dead time in PWM inverters with multiple-frequency modulator signals?*", and considering the insights shown in previous chapters, the following statement can be made.

Dead-time effects are independent of the existence of fundamental-frequency harmonics in the modulator signal. Nevertheless, dead-time affects an injected harmonic if this is an odd integer order harmonic of the fundamental frequency. This effect has a nonlinear relationship with the power factor of the load. Furthermore, it is inversely proportional to the harmonic number; and proportional to the DC voltage with a proportionality constant of four over the square value of pi.

The primary constraint for said statement is that the load's current and modulator signals cannot have more than two changes of polarity in one fundamental-frequency period. Nevertheless, several high-power-quality power electronics appli-

cations satisfy this constraint, e.g., voltage harmonic compensation systems, which is the kind of application that motivates this thesis.

Results using single-phase *VSI*s validate the theoretical assumptions and demonstrate that the proposed analytical approximation successfully achieves the dominant dynamics of the power electronic converter when a signal with multiple frequencies is used as a modulator. Furthermore, it was shown that, using the first six odd harmonics of the fundamental frequency, it is possible to create an efficient mathematical model that can recreate the output voltage of a single-phase inverter. This proposed simplified model gives an analytical understanding of the principal harmonics that are responsible for the degradation of power quality and provides an option to study the harmonic distortion of a power electronic converter with low computational cost for the simulation tool.

5.1 Contributions of this Thesis

- Two power-quality control schemes using multiple-frequency modulators were presented at conference papers [4, 13].
- The theoretical development presented in this thesis was used as the basis to build a *Wolfram Mathematica*[®] package application called *PwmSpectra*. This application provides simple analytical and numerical functions to facilitate the study of digital and analog *PWM* schemes. *PwmSpectra* is published as an open software project available to download and develop under the *Academic Free License v3.0 (AFL3)* [46].

5.2 Continuing Development

This thesis has primarily focused on analog *PWM* inverters using multiple-frequency modulators and restricted to a load current with no more than two changes of polarity over one fundamental-frequency period. However, there are other important concerns associated with the frequency-spectra of power electronic inverters. From the author's point of view, one natural step forward in this particular field is to use the *time substitution concept* to extend the more recent advances in the study of dead-time effects in regular-sampled *PWM*, see Section 2.4, and incorporate the analysis of multiple-frequency modulator signals. Additionally, another important aspect of the analytical frequency spectra is to include the effects of multiple zero-crossings of non-negligible high-frequency components of the output current. This is a common scenario in low-power-quality applications and motor drives.

Bibliography

- [1] AKAGI, H., WATANABE, E. H., AREDES, M. *Instantaneous power theory and applications to power conditioning*. John Wiley & Sons, 2017.
- [2] LISERRE, M., TEODORESCU, R., BLAABJERG, F. “Multiple harmonics control for three-phase grid converter systems with the use of PI-RES current controller in a rotating frame”, *Power Electronics, IEEE Transactions on*, v. 21, n. 3, pp. 836–841, 2006. ISSN: 0885-8993.
- [3] TEODORESCU, R., BLAABJERG, F., LISERRE, M., et al. “Proportional-resonant controllers and filters for grid-connected voltage-source converters”, *Electric Power Applications, IEE Proceedings*, v. 153, n. 5, pp. 750–762, 2006. ISSN: 1350-2352.
- [4] CAICEDO, J., AREDES, M. “Voltage control for three-phase ups inverter using P+resonant controllers”. In: *2015 IEEE 13th Brazilian Power Electronics Conference and 1st Southern Power Electronics Conference (COBEP/SPEC)*, pp. 1–6, nov. 2015. doi: 10.1109/COBEP.2015.7420285. ISSN: null.
- [5] CHEN, L., PENG, F. Z. “Dead-Time Elimination for Voltage Source Inverters”, *IEEE Transactions on Power Electronics*, v. 23, n. 2, pp. 574–580, mar. 2008. ISSN: 0885-8993. doi: 10.1109/TPEL.2007.915766.
- [6] MURAI, Y., WATANABE, T., IWASAKI, H. “Waveform Distortion and Correction Circuit for PWM Inverters with Switching Lag-Times”, *IEEE Transactions on Industry Applications*, v. IA-23, n. 5, pp. 881–886, set. 1987. ISSN: 0093-9994. doi: 10.1109/TIA.1987.4504998.
- [7] CHIERCHIE, F., PAOLINI, E. E. “Analytical and numerical analysis of dead-time distortion in power inverters”. In: *2010 Argentine School of Micro-Nanoelectronics, Technology and Applications (EAMTA)*, pp. 6–11, out. 2010. ISSN: null.
- [8] MOORE, D. C., ODAVIC, M., COX, S. M. “Dead-time effects on the voltage spectrum of a PWM inverter”, *IMA Journal of Applied Mathematics*,

v. 79, n. 6, pp. 1061–1076, 2014. doi: 10.1093/imamat/hxt006. Available at: <[+http://dx.doi.org/10.1093/imamat/hxt006](http://dx.doi.org/10.1093/imamat/hxt006)>.

- [9] LIN, J.-L. “A new approach of dead-time compensation for PWM voltage inverters”, *Circuits and Systems I: Fundamental Theory and Applications, IEEE Transactions on*, v. 49, n. 4, pp. 476–483, 2002. ISSN: 1057-7122.
- [10] WU, C., LAU, W.-H., CHUNG, H.-H. “Analytical Technique for Calculating the Output Harmonics of an H-Bridge Inverter with Dead Time”, *Circuits and Systems I: Fundamental Theory and Applications, IEEE Transactions on*, v. 46, n. 5, pp. 617–627, 1999. ISSN: 1057-7122.
- [11] D’ARPINO, M. *Multi-Inverter Architectures for High Efficiency Power Conversion*. PhD Thesis, SCUOLA DI DOTTORATO IN INGEGNERIA, UNIVERSIT A DEGLI STUDI DI CASSINO E DEL LAZIO MERIDIONALE, 2014.
- [12] HOLMES, D. G., LIPO, T. A. *Pulse width modulation for power converters: principles and practice*, v. 18. John Wiley & Sons, 2003.
- [13] CAICEDO, J., DE CASTRO, A. R., FRANÇA, B., et al. “Resonant harmonic compensation for synchronverter, integrating wind and photovoltaic power generation into an electrical grid, case study: Nonlinear and unbalanced load”. In: *2017 Brazilian Power Electronics Conference (COBEP)*, pp. 1–6. IEEE, 2017.
- [14] MOHAN, N., UNDELAND, T. M., ROBBINS, W. P. *Power electronics*. Wiley New York, 2011.
- [15] AINSLIE-MALIK, G. R. *Mathematical analysis of PWM processes*. PhD Thesis, University of Nottingham, 2013.
- [16] GRANT, D., SEIDNER, R. “Ratio changing in pulse-width-modulated inverters”. In: *IEE Proceedings B (Electric Power Applications)*, v. 128, pp. 243–248. IET, 1981.
- [17] CHOI, J.-S., YOO, J.-Y., LIM, S.-W., et al. “A novel dead time minimization algorithm of the PWM inverter”. In: *Conference Record of the 1999 IEEE Industry Applications Conference. Thirty-Forth IAS Annual Meeting (Cat. No.99CH36370)*, v. 4, pp. 2188–2193 vol.4, 1999. doi: 10.1109/IAS.1999.798757.

- [18] EVANS, P. D., CLOSE, P. R. “Harmonic distortion in PWM inverter output waveforms”, *IEE Proceedings B - Electric Power Applications*, v. 134, n. 4, pp. 224–232, jul. 1987. ISSN: 0143-7038. doi: 10.1049/ip-b:19870038.
- [19] CAICEDO, J. *HIGH PERFORMANCE VOLTAGE CONTROL FOR THREE-PHASE UPS INVERTER*. Masters Thesis, Universidade Federal do Rio de Janeiro, 2014.
- [20] GARCIA-CERRADA, A., RONCERO-SANCHEZ, P., GARCIA-GONZALEZ, P., et al. “Detailed analysis of closed-loop control of output-voltage harmonics in voltage-source inverters”, *Electric Power Applications, IEE Proceedings -*, v. 151, n. 6, pp. 734–743, 2004. ISSN: 1350-2352.
- [21] CHOI, J.-W., SUL, S.-K. “Inverter output voltage synthesis using novel dead time compensation”, *IEEE Transactions on Power Electronics*, v. 11, n. 2, pp. 221–227, mar. 1996. ISSN: 0885-8993. doi: 10.1109/63.486169.
- [22] MUNOZ, A. R., LIPO, T. A. “On-line dead-time compensation technique for open-loop PWM-VSI drives”, *IEEE Transactions on Power Electronics*, v. 14, n. 4, pp. 683–689, jul. 1999. ISSN: 0885-8993. doi: 10.1109/63.774205.
- [23] BENNETT, W. “New results in the calculation of modulation products”, *Bell Labs Technical Journal*, v. 12, n. 2, pp. 228–243, 1933.
- [24] BLACK, H. S. *Modulation theory*. van Nostrand, 1953.
- [25] BOWES, S., BIRD, B. “Novel approach to the analysis and synthesis of modulation processes in power convertors”. In: *Proceedings of the Institution of Electrical Engineers*, v. 122, pp. 507–513. IET, 1975.
- [26] MCGRATH, B. P., HOLMES, D. G. “A General Analytical Method for Calculating Inverter DC-Link Current Harmonics”, *IEEE Transactions on Industry Applications*, v. 45, n. 5, pp. 1851–1859, set. 2009. ISSN: 0093-9994. doi: 10.1109/TIA.2009.2027556.
- [27] COX, S. M., CREAGH, S. C. “Voltage and current spectra for matrix power converters”, *SIAM Journal on Applied Mathematics*, v. 69, n. 5, pp. 1415–1437, 2009.
- [28] ODAVIC, M., SUMNER, M., ZANCHETTA, P., et al. “A Theoretical Analysis of the Harmonic Content of PWM Waveforms for Multiple-Frequency Modulators”, *IEEE Transactions on Power Electronics*, v. 25, n. 1,

pp. 131–141, jan. 2010. ISSN: 0885-8993. doi: 10.1109/TPEL.2009.2026751.

- [29] WANG, X., ZHANG, C., LI, X., et al. “Weighted control research on seamless transfer for dual-mode three phase inverter in micro-grid”. In: *2011 International Conference on Electrical Machines and Systems*, pp. 1–5, Beijing, China, ago. 2011. IEEE. ISBN: 978-1-4577-1044-5. doi: 10.1109/ICEMS.2011.6073978. Available at: <<http://ieeexplore.ieee.org/document/6073978/>>.
- [30] MATHE, L., CORNEAN, H., SERA, D., et al. “Unified analytical equation for theoretical determination of the harmonic components of modern PWM strategies”. In: *IECON 2011 - 37th Annual Conference of the IEEE Industrial Electronics Society*, pp. 1648–1653, nov. 2011. doi: 10.1109/IECON.2011.6119554.
- [31] LI, Y., WANG, Y., LI, B. Q. “Generalized Theory of Phase-Shifted Carrier PWM for Cascaded H-Bridge Converters and Modular Multilevel Converters”, *IEEE Journal of Emerging and Selected Topics in Power Electronics*, v. 4, n. 2, pp. 589–605, jun. 2016. ISSN: 2168-6777. doi: 10.1109/JESTPE.2015.2476699.
- [32] GUINEE, R., LYDEN, C. “A single Fourier series technique for the simulation and analysis of asynchronous pulse width modulation in motor drive systems”. In: *Circuits and Systems, 1998. ISCAS’98. Proceedings of the 1998 IEEE International Symposium on*, v. 6, pp. 653–656. IEEE, 1998.
- [33] BOYS, J., HANDLEY, P. “Harmonic analysis of space vector modulated PWM waveforms”. In: *IEE Proceedings B (Electric Power Applications)*, v. 137, pp. 197–204. IET, 1990.
- [34] BERKHOUT, M. “An integrated 200-W class-D audio amplifier”, *IEEE Journal of Solid-State Circuits*, v. 38, n. 7, pp. 1198–1206, jul. 2003. ISSN: 0018-9200. doi: 10.1109/JSSC.2003.813238.
- [35] KOESLAG, F., MOUTON, H. D., BEUKES, J. “Analytical Modeling of the Effect of Nonlinear Switching Transition Curves on Harmonic Distortion in Class D Audio Amplifiers”, *IEEE Transactions on Power Electronics*, v. 28, n. 1, pp. 380–389, jan. 2013. ISSN: 0885-8993. doi: 10.1109/TPEL.2012.2200264.

- [36] WILSON, B., GHASSEMLOOY, Z., LOK, A. “Spectral structure of multitone pulse width modulation”, *Electronics Letters*, v. 27, n. 9, pp. 702–704, abr. 1991. ISSN: 0013-5194. doi: 10.1049/el:19910437.
- [37] CHIERCHIE, F., PAOLINI, E. E., STEFANAZZI, L., et al. “Simple real-time digital PWM implementation for class-D amplifiers with distortion-free baseband”, *IEEE Transactions on Industrial Electronics*, v. 61, n. 10, pp. 5472–5479, 2014.
- [38] SONG, Z., SARWATE, D. V. “The frequency spectrum of pulse width modulated signals”, *Signal Processing*, v. 83, n. 10, pp. 2227–2258, 2003.
- [39] APOSTOL, T. M. *Mathematical Analysis*. Addison Wesley Publishing Company, 1974.
- [40] KUMAR, M. “Time -Domain Characterization of Digitized PWM Inverter With Dead-Time Effect”, *IEEE Transactions on Circuits and Systems I: Regular Papers*, v. 65, n. 10, pp. 3592–3601, out. 2018. ISSN: 1558-0806. doi: 10.1109/TCSI.2018.2827950. Conference Name: IEEE Transactions on Circuits and Systems I: Regular Papers.
- [41] JIAO, N., WANG, S., LIU, T., et al. “Harmonic Quantitative Analysis for Dead-Time Effects in SPWM Inverters”, *IEEE Access*, v. 7, pp. 43143–43152, 2019. ISSN: 2169-3536. doi: 10.1109/ACCESS.2019.2907176. Conference Name: IEEE Access.
- [42] JOHN, M. *Frequency domain modeling of harmonic interactions in pulse-width modulated voltage-source inverter drives*. Ph.D. thesis, Leibniz University Hannover, 2019. Available at: <https://pdfs.semanticscholar.org/4e91/9ff9d68932e3ccaef9e77ddb2b09d4856b66.pdf?_ga=2.219961563.379295614.1580838571-434799140.1580838571>.
- [43] WU, C. M., LAU, W. H., CHANG, H. “Analytical solution to harmonic characteristics of PWM H-bridge converters with dead time”. In: *Circuits and Systems, 1998. ISCAS '98. Proceedings of the 1998 IEEE International Symposium on*, v. 6, pp. 462–465 vol.6, 1998. doi: 10.1109/ISCAS.1998.705311.
- [44] TITCHMARSH, E. C. “The Double Fourier Series of a Discontinuous Function”, *Proceedings of the Royal Society of London. Series A, Containing Papers of a Mathematical and Physical Character*, v. 106, n. 737, pp. 299–314, 1924. ISSN: 0950-1207. Available at: <<https://www.jstor.org/stable/94384>>.

- [45] NED, M., ULLMANN, F., ROBBINS, W. *Power electronics*. Wiley India, 2003. ISBN: 978-81-265-1090-0. Available at: <<http://aiktc.space.org:8080/jspui/handle/123456789/660>>.
- [46] CAICEDO, J. “PwmSpectra”. 2020. Available at: <<https://github.com/jrgcaicedo/PwmSpectra>>. Library Catalog: github.com.
- [47] KOESLAG, F. *A detailed analysis of the imperfections of pulsewidth modulated waveforms on the output stage of a class D audio amplifier*. PhD Thesis, Stellenbosch: University of Stellenbosch, 2009.

Appendix A

3-D Geometrical Interpretation of the Carrier-Modulator Interaction in *Black's Method* (*Original Contribution*)

This section proposes a geometrical interpretation of the interaction between carrier and modulator signal in *Black's method*. This interaction is straightforward in the conventional 2-D representation of a *PWM*, as shown in figure A.1. Nevertheless, in *Black's method*, carrier-modulator interaction is defined mathematically by the boundaries functions, and its interaction becomes implicit in the 2-D unit-cell diagrams shown in the literature [12]. The proposed geometrical representation is a didactic way to understand the origin of those 2-D unit-cell diagrams used in *Black's method*.

As shown in figure A.1, changes in the voltage level of a *PWM* are defined by the moment where carrier and modulator signals are equal. This also can be represented as a 3-D model by letting $F_{gi}(x, y) = s_a(y) - c(x)$ be the two variable function that takes the shape of the modulating signal $s_a(y)$ and extends it in the path formed by the carrier signal $c(x)$, as shown in figure A.2-a.

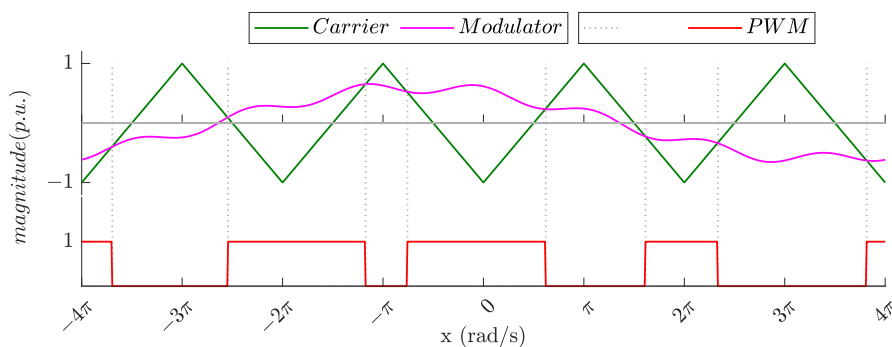


Figure A.1 - 2-Dimensional representation of a double-edge naturally sampled *PWM*.

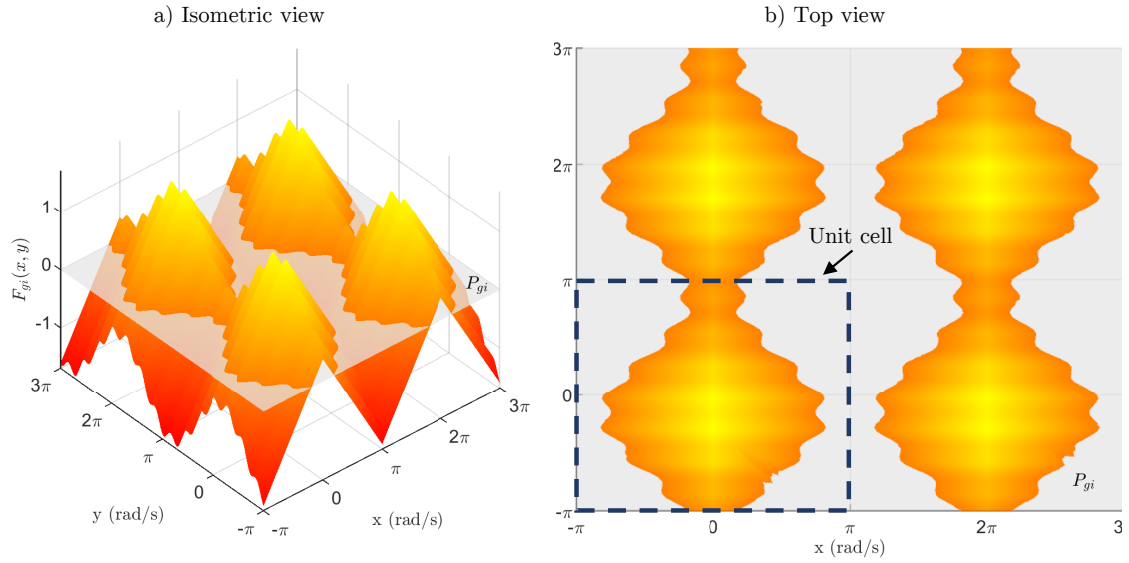


Figure A.2 - 3-Dimensional representation of $F_{gi}(x, y) = s_a(y) - c(x)$ for a double-edge naturally sampled *PWM*. This figure shows the iteration of two cycles of the modulating signal $s_a(y)$, and two periods of the carrier signal $c(x)$ in the 3-dimensional arrangement formed by the axes $x = \omega_c t$, $y = \omega_o t$, and $z = F_{gi}(x, y)$.

It is straightforward to see that $F_{gi}(x, y) = 0 \implies s_a(y) = c(x)$, i.e., the points of the surface created by $F_{gi}(x, y)$ at a high of $z = 0$ represent the moments were modulator and carrier signals have the same value. Hence, let $P_{gi} \in \mathbb{R}^2 : P = 0$ be a xy plane at z equals zero. Then, the cutting edges of the cross-section between P_{gi} and F_{gi} describe the boundaries of voltage level change in the *PWM* signal, as shown in figure A.2-a. The top-view of this 3-D arrangement agrees with the 2-D unit-cells diagram shown in the literature [12, 28, 47].

Appendix B

Black's Method (Equations Definition)

This appendix defines all integrals of the double Fourier-series for each *PWM* scheme presented in former chapters. Moreover, it is developed the analytical expression of the boundary functions evaluating one cycle in the range of $[-\pi, \pi]$. These boundary functions are developed for both cases, ideal and dead-time correction.

B.1 Trailing-Edge Naturally Sampled *PWM*

This section will summarize the development of the principal equations of *Black's method* for an analog *PWM* using a saw-tooth carrier signal and a multiple-frequency modulator. Recalling from section 3.2, the saw-tooth carrier function is defined by

$$c(x) = \left\{ \frac{(x+\theta_c)}{\pi}, \quad -\pi \leq x < \pi \quad , \quad (B.1) \right.$$

and the multiple-frequency modulator signal is given by

$$s_a(y) = M_1 \cos(y + \theta_1) + M_h \cos(hy + \theta_h) \quad . \quad (B.2)$$

Using the comparison of these two functions and the *PWM* time definition presented in Sections 3.2.1 and 3.3.1, it is possible to define the analytical expression of the Fourier's coefficient and the boundary functions that allows the double Fourier-series described by *Black's method*.

Integral definition of Fourier's coefficient for analog *PWM* schemes

As presented in [12], the general expression to calculate the complex coefficient of a double Fourier-series is given by

$$C_{mn(\text{ideal})} = \frac{1}{2\pi^2} \int_{-\pi}^{\pi} \int_{-\pi}^{\pi} F(x, y) e^{j(mx+ny)} dx dy \quad , \quad (B.3)$$

where m and n are indices of the carrier and base-band harmonics, respectively.

Additionally, recalling from section 3.2, the output voltage is found to be

$$v_{a-}(t) = F(x, y) = \begin{cases} 2V_{dc}, & x_r(y) \leq x \leq x_f(y) \\ 0, & \text{Otherwise} \end{cases} \quad . \quad (B.4)$$

Therefore, for a naturally sampled *PWM* scheme the complex coefficients of a double Fourier-series are given by

$$C_{mn(\text{ideal})} = \frac{V_{dc}}{\pi^2} \int_{-\pi}^{\pi} \int_{x_r(y)}^{x_f(y)} e^{j(mx+ny)} dx dy \quad . \quad (B.5)$$

Nevertheless, considering only low-frequencies, i.e., only DC and base-band harmon-

ics. Then, it is possible to simplify (B.5) as

$$C_{0n_{(ideal)}} = \frac{V_{dc}}{\pi^2} \int_{-\pi}^{\pi} \int_{x_r(y)}^{x_f(y)} e^{j(ny)} dx dy \quad . \quad (B.6)$$

Equation (B.6) represents the magnitude and phase of the low-frequency harmonics for both carrier types in the naturally sampled *PWM* schemes. This equation is used in section 3.2 to study each component of the ideal low-frequency spectrum.

Boundary functions for trailing-edge naturally sampled *PWM*

In trailing-edge naturally sampled *PWM* scheme, the rising edge of the *PWM* does not depend on the modulator signal. It occurs at the discontinuity of the saw-tooth waveform. Therefore, the rising function is found to be

$$x_r(y) = -\pi + \theta_c \quad . \quad (B.7)$$

Moreover, the falling function depends on the carrier-modulator interaction and can be found as

$$\begin{aligned} c(x_f) &= s_a(y) \\ \frac{1}{\pi}(x_f + \theta_c) &= M_1 \cos(y + \theta_1) + M_h \cos(hy + \theta_h) \\ x_f(y) &= -\theta_c + \pi (M_1 \cos(y + \theta_1) + M_h \cos(hy + \theta_h)) \end{aligned} \quad (B.8)$$

Integral definition of Fourier's coefficient for analog *PWM* schemes including dead time

The effects of dead time can be included using the integral definition presented in [10] and adapting it to match the terminology of this thesis as follow.

$$C_{mn} = C_{0n_{(ideal)}} + C_{mn_{(corr)}} \quad , \quad (B.9)$$

where $C_{mn_{(corr)}}$ represents the correction in the rising and falling edges of *PWM* signals due to the load current polarity.

Recalling from section 3.3, the output voltage of the correction term is found to be

$$F_{(corr)}(x, y) = \begin{cases} -2V_{dc}, & x_r(y) \leq x \leq x'_r(y) \wedge A \leq y < B \\ 2V_{dc}, & x_f(y) \leq x \leq x'_f(y) \wedge B \leq y < C \\ 0, & \text{Otherwise} \end{cases} \quad , \quad (B.10)$$

where $A = -\pi/2 + \varphi + \theta_1$, $B = \pi/2 + \varphi + \theta_1$, $C = 3\pi/2 + \varphi + \theta_1$, and φ is the phase dif-

ference between voltage's fundamental-frequency and the current wave-forms. The terms x'_r and x'_f are the correction of the boundaries in the inner integral due to dead-time effects. Therefore, substituting (B.10) in (B.6), the complex coefficients of the low-frequency correction term for a naturally sampled *PWM* scheme are given by

$$C_{0n_{(corr)}} = \frac{V_{dc}}{\pi^2} \left[- \int_A^B \int_{x_r}^{x'_r} e^{j(ny)} dx dy + \int_B^C \int_{x_f}^{x'_f} e^{j(ny)} dx dy \right] . \quad (\text{B.11})$$

Equation (B.11) represents the magnitude and phase of the low-frequency harmonics for both carrier types in the naturally sampled *PWM* schemes. This equation is used in section 3.3 to study each component of the low-frequency spectrum of the correction term.

Boundary functions for trailing-edge naturally sampled *PWM* with dead-time

Using the *time substitution* concept presented in section 3.3.1, $t \mapsto t' - T_d \implies x_r \mapsto x'_r - \Delta_x$. Thus, the rising function can be defined as

$$x'_r(y) = -\pi + \theta_c + \Delta_x . \quad (\text{B.12})$$

Moreover, $t \mapsto t' - T_d \implies x_f \mapsto x'_f - \Delta_x \wedge y \mapsto y - \Delta_y$. Hence, the falling function of the correction term is given by

$$\begin{aligned} c(x'_f - \Delta_x) &= s_a(y - \Delta_y) \\ \frac{1}{\pi}(x'_f + \theta_c - \Delta_x) &= M_1 \cos(y - \Delta_y + \theta_1) + M_h \cos(h(y - \Delta_y) + \theta_h) \\ x'_f(y) &= \pi \left[\begin{array}{l} M \cos(y + \theta_o - \Delta_y) \\ + M_h \cos(hy + \theta_h - h\Delta_y) \end{array} \right] + \Delta_x - \theta_c \end{aligned} \quad (\text{B.13})$$

B.2 Double-Edge Naturally Sampled *PWM*

This section summarizes the development of the principal equations of *Black's method* for an analog *PWM* using a triangular carrier signal and a multiple-frequency modulator. Recalling from section 3.2, the triangular carrier function is defined by

$$c(x) = \begin{cases} c_n(x) = -\frac{2}{\pi}x - 1, & -\pi \leq x \leq 0 \\ c_p(x) = \frac{2}{\pi}x - 1, & 0 \leq x \leq \pi \end{cases}. \quad (\text{B.14})$$

Using this expression and a similar procedure to that showed in Section B.1, it is possible to define the boundary functions for the double-edge naturally sampled case.

Boundary functions for double-edge naturally sampled *PWM*

Using the triangular carrier signal $c(x)$ and the multiple-frequency modulator signal $s_a(y)$; the rising function is found to be

$$\begin{aligned} c_n(x_r) &= s_a(y) \\ -\frac{2}{\pi}x_r - 1 &= M_1 \cos(y + \theta_1) + M_h \cos(hy + \theta_h) \\ x_r(y) &= -\frac{\pi}{2}(M_1 \cos(y + \theta_1) + M_h \cos(hy + \theta_h) + 1) \end{aligned}, \quad (\text{B.15})$$

and the falling function is defined by

$$\begin{aligned} c_p(x_f) &= s_a(y) \\ \frac{2}{\pi}x_f - 1 &= M_1 \cos(y + \theta_1) + M_h \cos(hy + \theta_h) \\ x_f(y) &= \frac{\pi}{2}(M_1 \cos(y + \theta_1) + M_h \cos(hy + \theta_h) + 1) \end{aligned}. \quad (\text{B.16})$$

Boundary functions for double-edge naturally sampled *PWM* with dead-time

Using the *time substitution* concept presented in section 3.3.1, $t \mapsto t' - T_d \implies x_r \mapsto x'_r - \Delta_x$. Thus, the rising function can be defined as

$$\begin{aligned} c_n(x'_r - \Delta_x) &= s_a(y - \Delta_y) \\ -\frac{2}{\pi}(x'_r - \Delta_x) - 1 &= M_1 \cos(y - \Delta_y + \theta_1) + M_h \cos(h(y - \Delta_y) + \theta_h) \\ x'_r(y) &= -\frac{\pi}{2}[M_1 \cos(y - \Delta_y + \theta_1) + M_h \cos(h(y - \Delta_y) + \theta_h) + 1] + \Delta_x \end{aligned}, \quad (\text{B.17})$$

and the correction falling function is defined by

$$\begin{aligned}
c_p(x'_f - \Delta_x) &= s_a(y - \Delta_y) \\
\frac{2}{\pi}(x'_f - \Delta_x) - 1 &= M_1 \cos(y - \Delta_y + \theta_1) + M_h \cos(h(y - \Delta_y) + \theta_h) \\
x'_f(y) &= \frac{\pi}{2} [M_1 \cos(y - \Delta_y + \theta_1) + M_h \cos(h(y - \Delta_y) + \theta_h) + 1] + \Delta_x
\end{aligned} \tag{B.18}$$

Appendix C

Analytical Low-Frequency Spectra (Equations Development)

This appendix presents the equation development of the Low-frequency spectra shown in Chapter 3. These equations were developed using *MapleTM2019* and the step-by-step worksheet for each *PWM* scheme is shown.

Due to some compatibility issues between the terminology used in this thesis and *MapleTM2019* some symbols in the worksheet were changed. Those symbols are: $\omega_1 = \omega_o$, $\theta_1 = \theta_o$, $\Delta_x = \Delta_X$, and $\Delta_y = \Delta_Y$.

This appendix is divided in two main sections. Section C.1 shows the equation development for the trailing-edge naturally sampled *PWM* scheme, and section C.2 develops the equations for the double-edge naturally sampled *PWM*.

C.1 MapleTM2019 worksheet for Trailing-edge Naturally Sampled PWM

[trailingEdgeNaturallySampledPwm.mw](#)

Trailing-edge Naturally Sampled PWM

restart :

(Ideal Part)

Parameters

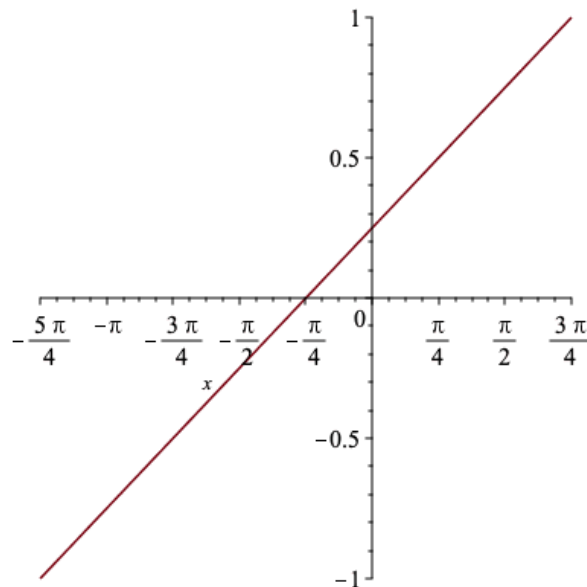
with(plots) :
testParameters := $\left[M = 0.6, \theta_o = \frac{30 \cdot \text{Pi}}{180}, \theta_c = \frac{45 \cdot \text{Pi}}{180}, M_h = 0.05, \theta_h = \frac{0 \cdot 15 \cdot \text{Pi}}{180}, h = 7, V[dc] = 1, M[f] = 21, \omega_o = \right.$
 $\left. \text{Pi} \cdot 60, \omega_c = \omega_o \cdot M[f], T_d = 0.0001, \text{varphi} = \frac{30 \cdot \text{Pi}}{180}, \Delta[X] = 2 \cdot \text{Pi} \cdot 60 \cdot 21 \cdot 0.0001, \Delta[Y] = 2 \cdot \text{Pi} \cdot 60 \cdot 0.0001 \right]$

Carrier waveform

$$c(x) := \frac{1}{\pi} \cdot (x + \theta_c)$$

$$c := x \mapsto \frac{x + \theta_c}{\pi} \quad (1)$$

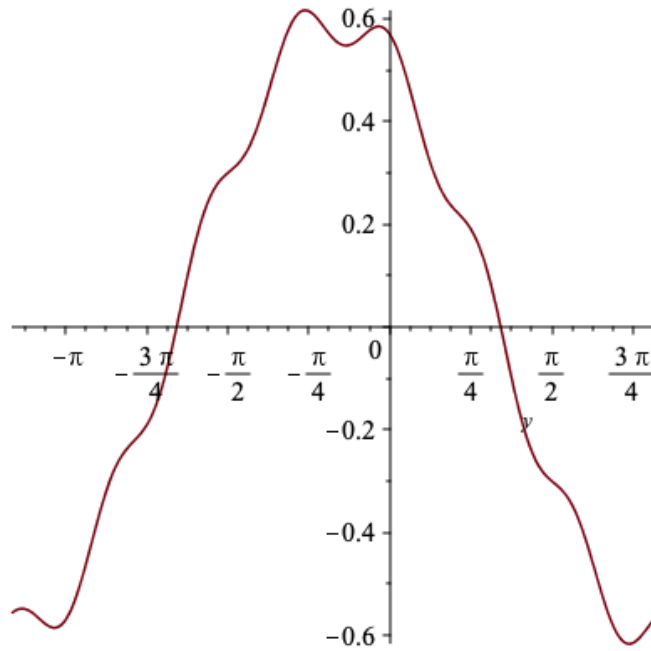
plot(eval(c(x), testParameters), x = eval(-Pi - \theta_c..Pi - \theta_c, testParameters))



Modulator waveform $v_o(y) := M \cos(y + \theta_o) + M_h \cos(h \cdot y + \theta_h)$;

$$v_o := y \mapsto M \cos(y + \theta_o) + M_h \cos(h y + \theta_h) \quad (2)$$

`plot(eval(v[o])(y), testParameters), eval(y=-Pi-θo..Pi-θo, testParameters))`



PWM Definition

The rising function can be found by $x[r](y) := -\pi - \theta_c : \text{factor}(x[r](y))$

$$-\pi - \theta_c \quad (3)$$

and the falling function $x[f](y) := \text{solve}(c(x) = v[o](y), x) : \text{factor}(x[f](y))$

$$M \cos(y + \theta_o) \pi + M_h \cos(h y + \theta_h) \pi - \theta_c \quad (4)$$

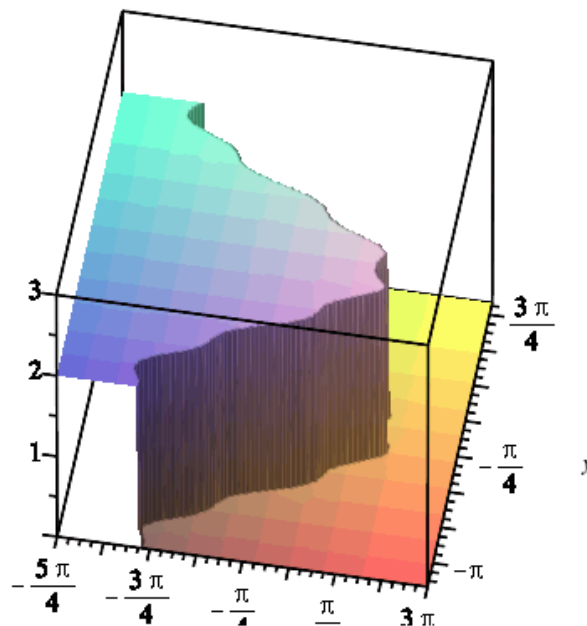
$F(x, y) := \text{piecewise}(x[r](y) \leq x \leq x[f](y), 2 V[dc], 0)$

$$F := (x, y) \mapsto \begin{cases} 2 V_{dc} & x_r(y) \leq x \leq x_f(y) \\ 0 & \text{otherwise} \end{cases} \quad (5)$$

3-D Model of the Ideal Term $numContours := 2$:

```
limits := [eval(-pi - 2c..pi - 2c, testParameters), eval(-pi - 2o..pi - 2o, testParameters), 0..3]:
numOfpoints := 150:
gridPoints := [numOfpoints, numOfpoints]:
initialOrientation := [280, 40, 0]:
```

```
plot3d(eval(F(x, y), testParameters), eval(x=-pi-2c..pi-2c, testParameters), eval(y=-pi-2o..pi-2o,
testParameters),
contours = numContours,
orientation = initialOrientation,
view = limits,
style = surface,
grid = gridPoints);
```



Low Frequency Spectrum of the Ideal Term

DC component

```
Integrand :=  $\frac{v[dc]}{\pi^2}$ :
A00 := int(int(Integrand, x=x[r](y)..x[f](y)), y=-Pi..Pi):
idealA00 := eval(A00) assuming h::posint:
idealOffset :=  $\frac{idealA00}{2}$ 
```

$$idealOffset := v_{dc} \quad (6)$$

Conclusions:

- The DC component only depends of the Vdc

Fundamental component

$$Integrand := \frac{v[dc]}{\pi^2} \cdot \exp(I \cdot y) : C01 := \text{int}(\text{int}(Integrand, x = x[r](y) .. x[f](y)), y = -\pi .. \pi);$$

$$C01 := -\frac{1}{\pi(h^2 - 1)} (v_{dc} (IM \pi \sin(\theta_0) h^2 - M \pi \cos(\theta_0) h^2 - IM \pi \sin(\theta_0) - 2 IM_h \sin(\pi h) \sin(\theta h) + 2 M_h h \sin(\pi h) \cos(\theta h) + M \pi \cos(\theta_0))) \quad (7)$$

$$idealA01 := \text{evalc}(\text{Re}(C01));$$

$$idealB01 := \text{evalc}(\text{Im}(C01));$$

$$idealFundamental := \text{combine}(idealA01 \cdot \cos(\omega[o] t) + idealB01 \cdot \sin(\omega[o] t)) \text{ assuming } h :: \text{posint}$$

$$idealA01 := -\frac{v_{dc} (-M \pi \cos(\theta_0) h^2 + 2 M_h h \sin(\pi h) \cos(\theta h) + M \pi \cos(\theta_0))}{\pi (h^2 - 1)}$$

$$idealB01 := -\frac{v_{dc} (M \pi \sin(\theta_0) h^2 - M \pi \sin(\theta_0) - 2 M_h h \sin(\pi h) \sin(\theta h))}{\pi (h^2 - 1)}$$

$$idealFundamental := M v_{dc} \cos(\omega_o t + \theta_0) \quad (8)$$

Conclusions:

- The fundamental component only depends of the fundamental component of the modulator signal and it is proportional to Vdc

Base-band harmonics (n≠h)

$$Integrand := \frac{v[dc]}{\pi^2} \cdot \exp(I \cdot n \cdot y) : C0n := \text{int}(\text{int}(Integrand, x = x[r](y) .. x[f](y)), y = -\pi .. \pi);$$

$$C0n := -\frac{2 (I \sin(\theta h) n - \cos(\theta h) h) \sin(\pi h) M_h (-1)^n v_{dc}}{(h^2 - n^2) \pi} \quad (9)$$

$$idealA0n := \text{evalc}(\text{Re}(C0n));$$

$$idealB0n := \text{evalc}(\text{Im}(C0n));$$

$$idealBasebandHarmonics := \text{combine}(idealA0n \cdot \cos(n \cdot \omega[o] t) + idealB0n \cdot \sin(n \cdot \omega[o] t)) \text{ assuming } h :: \text{posint}$$

$$idealBasebandHarmonics := 0 \quad (10)$$

Conclusions:

- The ideal case has not baseband harmonics for the frequencies different of the h harmonic.

Base-band harmonics (n=h)

$$\begin{aligned}
 \text{Integrand} &:= \frac{v[dc]}{D_1 \cdot \omega} \cdot \exp(I \cdot h \cdot y) : \text{COh} := \text{int}(\text{int}(\text{Integrand}, x = x[r](y) \dots x[f](y)), y = -1 \\
 \text{COh} &:= \frac{1}{\pi h (h^2 - 1)} \left(v_{dc} (1M_h \sin(\pi h) \cos(\pi h) \sin(\theta h) e^{1h\pi h^2} - I e^{21\pi h} h^2 - 1M_h \pi \sin(\theta h) e^{1h\pi h^3} \right. \\
 &+ M_h \pi \cos(\theta h) e^{1h\pi h^3} + M_h \sin(\pi h) \cos(\theta h) \cos(\pi h) e^{1h\pi h^2} - 1M_h \sin(\pi h) \cos(\pi h) \sin(\theta h) e^{1h\pi} \\
 &+ 1M_h \pi \sin(\theta h) e^{1h\pi h} + I e^{21\pi h} + M \sin(\theta \omega) e^{21\pi h} h - M_h \pi \cos(\theta h) e^{1h\pi h} \\
 &\left. - M_h \sin(\pi h) \cos(\theta h) \cos(\pi h) e^{1h\pi} + I h^2 - M \sin(\theta \omega) h + 1M \cos(\theta \omega) e^{21\pi h} h^2 - 1M \cos(\theta \omega) h^2 - 1 \right) \\
 &e^{-1\pi h}
 \end{aligned} \tag{11}$$

$$\begin{aligned}
 \text{idealAOh} &:= \text{evalc}(\text{Re}(\text{COh})) : \\
 \text{idealBOh} &:= \text{evalc}(\text{Im}(\text{COh})) :
 \end{aligned}$$

$$\text{idealBaseband_h} := \text{combine}(\text{idealAOh} \cos(h \cdot \omega_o [o] \cdot t) + \text{idealBOh} \sin(h \cdot \omega_o [o] \cdot t)) \text{ assuming } h :: \text{posint}$$

$$\text{idealBaseband_h} := \cos(h \omega_o t + \Theta) (-1)^{2h} v_{dc} M_h \tag{12}$$

$$\text{idealBaseband_h} := \text{eval}(\text{idealBaseband_h}, (-1)^{2h} = 1)$$

$$\text{idealBaseband_h} := \cos(h \omega_o t + \Theta) v_{dc} M_h \tag{13}$$

Conclusions:

- the h harmonic only depends of the h component of the modulator and it is proportional to Vdc

(Correction Part)

PWM Defintion

The rising function can be found by $x[rp](y) := x[r](y) + \text{Delta}[X] : \text{factor}(x[rp](y))$

$$-\pi - \theta c + \Delta_X \tag{14}$$

and the falling function

$x[fp](y) := \text{solve}(c(x - \text{Delta}[X]) = v[o](y - \text{Delta}[Y]), x) : \text{factor}(x[fp](y))$

$$M \cos(y - \Delta_Y + \theta \omega) \pi + M_h \cos(h y - h \Delta_Y + \theta h) \pi - \theta c + \Delta_X \tag{15}$$

$$\text{Fcor}(x, y) := \text{piecewise} \left(x[r](y) \leq x \leq x[rp](y) \wedge -\frac{\text{Pi}}{2} + \varphi + \theta \omega \leq y < \frac{\text{Pi}}{2} + \varphi + \theta \omega, -2 V[dc], \right.$$

$$\begin{aligned}
& x[f](y) \leq x \leq x[fp](y) \wedge \frac{\pi}{2} + \varphi + \vartheta_0 \leq y < \frac{3 \cdot \pi}{2} + \varphi + \vartheta_0, 2 V[dc], \\
& 0) \\
& Fcor := (x, y) \mapsto \begin{cases} -2 V_{dc} & x_r(y) \leq x \leq x_{rp}(y) \text{ and } -\frac{\pi}{2} + \varphi + \vartheta_0 \leq y \text{ and } y < \frac{\pi}{2} + \varphi + \vartheta_0 \\ 2 V_{dc} & x_f(y) \leq x \leq x_{fp}(y) \text{ and } \frac{\pi}{2} + \varphi + \vartheta_0 \leq y \text{ and } y < \frac{3 \pi}{2} + \varphi + \vartheta_0 \\ 0 & \text{otherwise} \end{cases} \quad (16)
\end{aligned}$$

3-D Model of the Corrected Term

```

numOfpoints := 250 :

xRange := eval(-pi - theta..pi - theta, testParameters) :
yRange := eval(-pi/2 + phi + theta + 0.001..3*pi/2 + phi + theta, testParameters) :
# xTick := [eval(-pi - theta, testParameters) = typeset(-pi - theta | c)], eval(-theta, testParameters) = typeset(-theta | c)], eval(pi - theta, testParameters) = typeset(pi - theta | c)] :
# yTick := [eval(-pi/2 + phi + theta + 0.001, testParameters) = typeset(A), eval(pi/2 + phi + theta, testParameters) = typeset(B), eval(3*pi/2 + phi + theta, testParameters) = typeset(C)] :
xTick := [eval(-pi - theta, testParameters) = typeset( ), eval(-theta, testParameters) = typeset( ), eval(pi - theta, testParameters) = typeset( )] :
yTick := [eval(-pi/2 + phi + theta + 0.001, testParameters) = typeset( ), eval(pi/2 + phi + theta, testParameters) = typeset( ), eval(3*pi/2 + phi + theta, testParameters) = typeset( )] :

plotOptions :=
contours = 2,
orientation = [280, 40, 0],
style = surface,
grid = [numOfpoints, numOfpoints],
axes = framed,
scaling = constrained,
labels = [x, y, Vdc],
font = [Helvetica, italic, 16],
labelFont = [Helvetica, italic, 16] :

#plotsetup(wmf, plotoutput = `ideal3D.wmf`, plotoptions = `portrait, noborder, width=2.33in, height=2.33in`) :
plotsetup(bmp, plotoutput = `ideal3D.bmp`, plotoptions = `portrait, noborder, width=4.66in, height=4.66in`) :
plotIdeal := plot3d(eval(F(x, y), testParameters), x = xRange, y = yRange, plotOptions, tickmarks = [xTick, yTick 2], view = [xRange, yRange, 0..2], title = "Ideal Part");

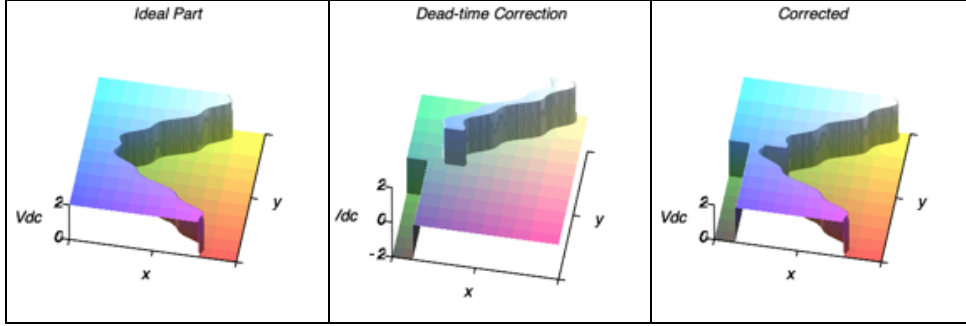
plotsetup(bmp, plotoutput = `correction3D.bmp`, plotoptions = `portrait, noborder, width=4.66in, height=4.66in`) :
plotCorrection := plot3d(eval(Fcor(x, y), testParameters), x = xRange, y = yRange, plotOptions, tickmarks = [xTick, yTick 3], view = [xRange, yRange, -2..2], title = "Dead-time Correction");

plotsetup(bmp, plotoutput = `corrected3D.bmp`, plotoptions = `portrait, noborder, width=4.66in, height=4.66in`) :
plotCorrected := plot3d(eval(F(x, y) + Fcor(x, y), testParameters), x = xRange, y = yRange, plotOptions, tickmarks = [xTick, yTick 2], view = [xRange, yRange, 0..2], title = "Corrected");

plotsetup(default) :
Arr := Array(1..3) :
Arr[1] := plotIdeal :
Arr[2] := plotCorrection :
Arr[3] := plotCorrected :

```

display(Arr);



Low Frequency Spectrum of the Correction Term

DC component

$$\text{Integrand} := \frac{v[dc]}{\text{Pi}^2};$$

A00 :=

$$\begin{aligned} & -\text{int}\left(\text{int}(\text{Integrand}, x = x[r](y) \dots x[rf](y)), y = -\frac{\text{Pi}}{2} + \text{varphi} \dots \frac{\text{Pi}}{2} + \text{varphi}\right) \\ & + \text{int}\left(\text{int}(\text{Integrand}, x = x[f](y) \dots x[fp](y)), y = \frac{\text{Pi}}{2} + \text{varphi} \dots \frac{3\text{Pi}}{2} + \text{varphi}\right) \text{ assuming } h :: \text{posint}, h > 2: \end{aligned}$$

A00 := (expand(convert(A00, exp)))

$$\begin{aligned} A00 := & -\frac{Iv_{dc} M_h e^{Ih \Delta_Y} e^{-\frac{1}{2} \pi h}}{2 \pi h e^{Ih \varphi} e^{I \theta h}} + \frac{Iv_{dc} M_h e^{\frac{1}{2} \pi h} e^{I \theta h} e^{Ih \varphi}}{2 \pi h e^{Ih \Delta_Y}} - \frac{Iv_{dc} M_h e^{I \theta h} e^{\frac{31}{2} \pi h} e^{Ih \varphi}}{2 \pi h e^{Ih \Delta_Y}} \\ & + \frac{Iv_{dc} M_h e^{Ih \Delta_Y} e^{-\frac{31}{2} \pi h}}{2 \pi h e^{Ih \varphi} e^{I \theta h}} - \frac{v_{dc} M e^{I \Delta_Y}}{\pi e^{I \theta h} e^{I \varphi}} - \frac{v_{dc} M e^{I \theta h} e^{I \varphi}}{\pi e^{I \Delta_Y}} - \frac{Iv_{dc} M_h e^{\frac{1}{2} \pi h} e^{I \theta h} e^{Ih \varphi}}{2 \pi h} + \frac{Iv_{dc} M_h e^{-\frac{1}{2} \pi h}}{2 \pi h e^{Ih \varphi} e^{I \theta h}} \\ & - \frac{Iv_{dc} M_h e^{-\frac{31}{2} \pi h}}{2 \pi h e^{Ih \varphi} e^{I \theta h}} + \frac{Iv_{dc} M_h e^{I \theta h} e^{\frac{31}{2} \pi h} e^{Ih \varphi}}{2 \pi h} + \frac{v_{dc} M e^{I \theta h} e^{I \varphi}}{\pi} + \frac{v_{dc} M}{\pi e^{I \theta h} e^{I \varphi}} \end{aligned} \quad (17)$$

$$A00 := \text{eval}\left(A00, \left[e^{\frac{31}{2} \pi h} = e^{-\frac{1}{2} \pi h}, e^{-\frac{31}{2} \pi h} = e^{\frac{1}{2} \pi h}\right]\right) \text{ assuming } h :: \text{posint}, h > 2; \# \text{correctionOffset} := \frac{A00}{2}$$

$$\begin{aligned} A00 := & -\frac{Iv_{dc} M_h e^{Ih \Delta_Y} e^{-\frac{1}{2} \pi h}}{2 \pi h e^{Ih \varphi} e^{I \theta h}} + \frac{Iv_{dc} M_h e^{\frac{1}{2} \pi h} e^{I \theta h} e^{Ih \varphi}}{2 \pi h e^{Ih \Delta_Y}} - \frac{Iv_{dc} M_h e^{I \theta h} e^{-\frac{1}{2} \pi h} e^{Ih \varphi}}{2 \pi h e^{Ih \Delta_Y}} + \frac{Iv_{dc} M_h e^{Ih \Delta_Y} e^{\frac{1}{2} \pi h}}{2 \pi h e^{Ih \varphi} e^{I \theta h}} \\ & - \frac{v_{dc} M e^{I \Delta_Y}}{\pi e^{I \theta h} e^{I \varphi}} - \frac{v_{dc} M e^{I \theta h} e^{I \varphi}}{\pi e^{I \Delta_Y}} - \frac{Iv_{dc} M_h e^{\frac{1}{2} \pi h} e^{I \theta h} e^{Ih \varphi}}{2 \pi h} + \frac{Iv_{dc} M_h e^{-\frac{1}{2} \pi h}}{2 \pi h e^{Ih \varphi} e^{I \theta h}} - \frac{Iv_{dc} M_h e^{\frac{1}{2} \pi h}}{2 \pi h e^{Ih \varphi} e^{I \theta h}} \\ & + \frac{Iv_{dc} M_h e^{I \theta h} e^{-\frac{1}{2} \pi h} e^{Ih \varphi}}{2 \pi h} + \frac{v_{dc} M e^{I \theta h} e^{I \varphi}}{\pi} + \frac{v_{dc} M}{\pi e^{I \theta h} e^{I \varphi}} \end{aligned} \quad (18)$$

$A00 := \text{convert}(\text{simplify}(A00), \text{trig})$

$$A00 := \frac{1}{\pi h} \left(v_{dc} \left(2 M h \cos(\varphi + \theta) - 2 M h \cos(\varphi + \theta - \Delta_Y) - M h \sin\left(\frac{(\pi + 2\varphi - 2\Delta_Y) h}{2} + \theta\right) \right) \right. \\ \left. + M h \sin\left(\frac{(-\pi + 2\varphi - 2\Delta_Y) h}{2} + \theta\right) + M h \sin\left(\frac{(\pi + 2\varphi) h}{2} + \theta\right) - M h \sin\left(\frac{(-\pi + 2\varphi) h}{2} + \theta\right) \right) \quad (19)$$

$\text{simplify}(A00)$

$$\frac{1}{\pi h} \left(v_{dc} \left(2 M h \cos(\varphi + \theta) - 2 M h \cos(\varphi + \theta - \Delta_Y) - M h \sin\left(\frac{(\pi + 2\varphi - 2\Delta_Y) h}{2} + \theta\right) \right) \right. \\ \left. + M h \sin\left(\frac{(-\pi + 2\varphi - 2\Delta_Y) h}{2} + \theta\right) + M h \sin\left(\frac{(\pi + 2\varphi) h}{2} + \theta\right) - M h \sin\left(\frac{(-\pi + 2\varphi) h}{2} + \theta\right) \right) \quad (20)$$

Using the approximation Δ_Y

$$\Delta_Y \quad (21)$$

=0

$\text{correctionOffset} := \text{eval}(A00, \text{Delta}[Y] = 0)$

$$\text{correctionOffset} := 0 \quad (22)$$

Conclusions:

- Dead time does affects the Dc component for Trailing-edge

Fundamental component

$\text{Integrand} := \frac{V[dc]}{\pi^2} \cdot \exp(-I \cdot y) :$

$C01 :=$

$$- \text{int} \left(\text{int}(\text{Integrand}, x = x[r](y) .. x[rp](y)), y = -\frac{\pi}{2} + \text{varphi} .. \frac{\pi}{2} + \text{varphi} \right) \\ + \text{int} \left(\text{int}(\text{Integrand}, x = x[f](y) .. x[fp](y)), y = \frac{\pi}{2} + \text{varphi} .. \frac{3\pi}{2} + \text{varphi} \right) :$$

$C01 := (\text{expand}(\text{convert}(C01, \text{exp})))$

$$\begin{aligned}
C01 := & -\frac{2 V_{dc} e^{I\varphi} \Delta_X}{\pi^2} - \frac{V_{dc} M_{-h} h e^{\frac{31}{2} \pi h} e^{I\theta h} e^{Ih\varphi} e^{I\varphi}}{2 \pi (h^2 - 1) e^{Ih\Delta_Y}} + \frac{V_{dc} M_{-h} h e^{-\frac{31}{2} \pi h} e^{Ih\Delta_Y} e^{I\varphi}}{2 \pi (h^2 - 1) e^{I\theta h} e^{Ih\varphi}} \\
& + \frac{V_{dc} M_{-h} h e^{Ih\Delta_Y} e^{-\frac{1}{2} \pi h} e^{I\varphi}}{2 \pi (h^2 - 1) e^{I\theta h} e^{Ih\varphi}} - \frac{V_{dc} M_{-h} h e^{I\theta h} e^{Ih\varphi} e^{\frac{1}{2} \pi h} e^{I\varphi}}{2 \pi (h^2 - 1) e^{Ih\Delta_Y}} + \frac{V_{dc} M h^2 e^{I\Delta_Y}}{2 (h^2 - 1) e^{I\theta h}} \\
& + \frac{V_{dc} M_{-h} e^{\frac{31}{2} \pi h} e^{I\theta h} e^{Ih\varphi} e^{I\varphi}}{2 \pi (h^2 - 1) e^{Ih\Delta_Y}} + \frac{V_{dc} M_{-h} e^{\frac{31}{2} \pi h} e^{I\theta h} e^{Ih\varphi} e^{I\varphi} h}{2 \pi (h^2 - 1)} + \frac{V_{dc} M_{-h} e^{-\frac{31}{2} \pi h} e^{Ih\Delta_Y} e^{I\varphi}}{2 \pi (h^2 - 1) e^{I\theta h} e^{Ih\varphi}} \\
& - \frac{V_{dc} M_{-h} h e^{-\frac{31}{2} \pi h} e^{I\varphi}}{2 \pi (h^2 - 1) e^{I\theta h} e^{Ih\varphi}} + \frac{V_{dc} M_{-h} e^{Ih\Delta_Y} e^{-\frac{1}{2} \pi h} e^{I\varphi}}{2 \pi (h^2 - 1) e^{I\theta h} e^{Ih\varphi}} + \frac{V_{dc} M_{-h} e^{I\theta h} e^{Ih\varphi} e^{\frac{1}{2} \pi h} e^{I\varphi}}{2 \pi (h^2 - 1) e^{Ih\Delta_Y}} \\
& + \frac{V_{dc} M_{-h} e^{I\theta h} e^{Ih\varphi} e^{\frac{1}{2} \pi h} e^{I\varphi} h}{2 \pi (h^2 - 1)} - \frac{V_{dc} M_{-h} h e^{-\frac{1}{2} \pi h} e^{I\varphi}}{2 \pi (h^2 - 1) e^{I\theta h} e^{Ih\varphi}} - \frac{V_{dc} M h^2}{2 (h^2 - 1) e^{I\theta h}} - \frac{V_{dc} M_{-h} e^{\frac{31}{2} \pi h} e^{I\theta h} e^{Ih\varphi} e^{I\varphi}}{2 \pi (h^2 - 1)} \\
& - \frac{V_{dc} M_{-h} e^{-\frac{31}{2} \pi h} e^{I\varphi}}{2 \pi (h^2 - 1) e^{I\theta h} e^{Ih\varphi}} - \frac{V_{dc} M_{-h} e^{I\theta h} e^{Ih\varphi} e^{\frac{1}{2} \pi h} e^{I\varphi}}{2 \pi (h^2 - 1)} - \frac{V_{dc} M_{-h} e^{-\frac{1}{2} \pi h} e^{I\varphi}}{2 \pi (h^2 - 1) e^{I\theta h} e^{Ih\varphi}} - \frac{V_{dc} M e^{I\Delta_Y}}{2 (h^2 - 1) e^{I\theta h}} \\
& + \frac{V_{dc} M}{2 (h^2 - 1) e^{I\theta h}} - \frac{2 V_{dc} e^{I\varphi} h^2 \Delta_X}{\pi^2 (h^2 - 1)} + \frac{2 V_{dc} e^{I\varphi} \Delta_X}{\pi^2 (h^2 - 1)}
\end{aligned} \tag{23}$$

$$C01 := \text{simplify}\left(\text{eval}\left(C01, \left[e^{-\frac{1}{2} \pi h} = e^{\frac{31}{2} \pi h}, e^{-\frac{31}{2} \pi h} = e^{\frac{1}{2} \pi h}\right]\right)\right)$$

$$\begin{aligned}
C01 := & -\frac{1}{(2 h^2 - 2) \pi^2} \left(\left(-\pi M_{-h} (h + 1) e^{\frac{I(3\pi - 2\varphi + 2\Delta_Y)h}{2}} + \frac{I(2\varphi - 2\theta h)}{2} + \pi M_{-h} (h \right. \right. \\
& - 1) e^{\frac{I(3\pi + 2\varphi - 2\Delta_Y)h}{2}} + \frac{I(2\varphi + 2\theta h)}{2} - \pi M_{-h} (h + 1) e^{\frac{I(\pi - 2\varphi + 2\Delta_Y)h}{2}} + \frac{I(2\varphi - 2\theta h)}{2} + \pi M_{-h} (h \\
& - 1) e^{\frac{I(\pi + 2\varphi - 2\Delta_Y)h}{2}} + \frac{I(2\varphi + 2\theta h)}{2} + \pi M_{-h} (h + 1) e^{\frac{I(3\pi - 2\varphi)h}{2}} + \frac{I(2\varphi - 2\theta h)}{2} - \pi M_{-h} (h \\
& - 1) e^{\frac{I(3\pi + 2\varphi)h}{2}} + \frac{I(2\varphi + 2\theta h)}{2} + \pi M_{-h} (h + 1) e^{\frac{I(\pi - 2\varphi)h}{2}} + \frac{I(2\varphi - 2\theta h)}{2} + (h - 1) \left(\right. \\
& \left. - M_{-h} \pi e^{\frac{I(\pi + 2\varphi)h}{2}} + \frac{I(2\varphi + 2\theta h)}{2} + (h + 1) \left(e^{-I\theta h} M \pi^2 - M \pi^2 e^{-I(-\Delta_Y + \theta h)} + 8 e^{I\varphi} \Delta_X \right) \right) \right) V_{dc}
\end{aligned} \tag{24}$$

collect(expand(C01), M)

$$\begin{aligned}
& \left(-\frac{V_{dc} h^2}{(2 h^2 - 2) e^{I\theta h}} + \frac{V_{dc} h^2 e^{I\Delta_Y}}{(2 h^2 - 2) e^{I\theta h}} + \frac{V_{dc}}{(2 h^2 - 2) e^{I\theta h}} - \frac{V_{dc} e^{I\Delta_Y}}{(2 h^2 - 2) e^{I\theta h}} \right) M + \frac{V_{dc} M_{-h} e^{\frac{31}{2} \pi h} e^{Ih\Delta_Y} e^{I\varphi} h}{(2 h^2 - 2) \pi e^{I\theta h} e^{Ih\varphi}} \\
& + \frac{V_{dc} M_{-h} e^{\frac{31}{2} \pi h} e^{Ih\Delta_Y} e^{I\varphi}}{(2 h^2 - 2) \pi e^{I\theta h} e^{Ih\varphi}} - \frac{V_{dc} M_{-h} e^{\frac{31}{2} \pi h} e^{I\theta h} e^{Ih\varphi} e^{I\varphi} h}{(2 h^2 - 2) \pi e^{Ih\Delta_Y}} + \frac{V_{dc} M_{-h} e^{\frac{31}{2} \pi h} e^{I\theta h} e^{Ih\varphi} e^{I\varphi}}{(2 h^2 - 2) \pi e^{Ih\Delta_Y}} \\
& + \frac{V_{dc} M_{-h} e^{Ih\Delta_Y} e^{\frac{1}{2} \pi h} e^{I\varphi} h}{(2 h^2 - 2) \pi e^{I\theta h} e^{Ih\varphi}} + \frac{V_{dc} M_{-h} e^{Ih\Delta_Y} e^{\frac{1}{2} \pi h} e^{I\varphi}}{(2 h^2 - 2) \pi e^{I\theta h} e^{Ih\varphi}} - \frac{V_{dc} M_{-h} e^{I\theta h} e^{Ih\varphi} e^{\frac{1}{2} \pi h} e^{I\varphi} h}{(2 h^2 - 2) \pi e^{Ih\Delta_Y}} \\
& + \frac{V_{dc} M_{-h} e^{I\theta h} e^{Ih\varphi} e^{\frac{1}{2} \pi h} e^{I\varphi}}{(2 h^2 - 2) \pi e^{Ih\Delta_Y}} - \frac{V_{dc} M_{-h} e^{\frac{31}{2} \pi h} e^{I\varphi} h}{(2 h^2 - 2) \pi e^{I\theta h} e^{Ih\varphi}} - \frac{V_{dc} M_{-h} e^{\frac{31}{2} \pi h} e^{I\varphi}}{(2 h^2 - 2) \pi e^{I\theta h} e^{Ih\varphi}}
\end{aligned} \tag{25}$$

$$\begin{aligned}
& + \frac{V_{dc} M_h e^{\frac{31}{2} \pi h} e^{1\theta h} e^{1h\varphi} e^{1\varphi} h}{(2h^2 - 2)\pi} - \frac{V_{dc} M_h e^{\frac{31}{2} \pi h} e^{1\theta h} e^{1h\varphi} e^{1\varphi}}{(2h^2 - 2)\pi} - \frac{V_{dc} M_h e^{\frac{1}{2} \pi h} e^{1\varphi} h}{(2h^2 - 2)\pi e^{1\theta h} e^{1h\varphi}} \\
& - \frac{V_{dc} M_h e^{\frac{1}{2} \pi h} e^{1\varphi}}{(2h^2 - 2)\pi e^{1\theta h} e^{1h\varphi}} + \frac{V_{dc} h M_h e^{1\theta h} e^{1h\varphi} e^{\frac{1}{2} \pi h} e^{1\varphi}}{(2h^2 - 2)\pi} - \frac{8 V_{dc} e^{1\varphi} h^2 \Delta_X}{(2h^2 - 2)\pi^2} - \frac{V_{dc} M_h e^{1\theta h} e^{1h\varphi} e^{\frac{1}{2} \pi h} e^{1\varphi}}{(2h^2 - 2)\pi} \\
& + \frac{8 V_{dc} e^{1\varphi} \Delta_X}{(2h^2 - 2)\pi^2}
\end{aligned}$$

$A01 := \text{evalc}(\text{Re}(C01)) :$

$B01 := \text{evalc}(\text{Im}(C01)) :$

$\text{correctionFundamental} := \text{collect}(\text{combine}(A01 \cos(\omega_o [o] \cdot t) + B01 \sin(\omega_o [o] \cdot t)), \text{Pi})$

$\text{correctionFundamental} :=$

$$\begin{aligned}
& \frac{1}{2h^2 - 2} (-M \cos(\omega_o t + \theta_o) h^2 V_{dc} + M \cos(\omega_o t + \theta_o - \Delta_Y) h^2 V_{dc} + M \cos(\omega_o t + \theta_o) V_{dc} - M \cos(\omega_o t \\
& + \theta_o - \Delta_Y) V_{dc}) + \frac{1}{(2h^2 - 2)\pi} \left(M_h h \cos\left(-\frac{3}{2} \pi h + h \varphi - h \Delta_Y - \varphi + \theta h + \omega_o t\right) h V_{dc} \right. \\
& - M_h h \cos\left(\frac{3}{2} \pi h + h \varphi - h \Delta_Y + \varphi + \theta h - \omega_o t\right) h V_{dc} + M_h h \cos\left(-\frac{1}{2} \pi h + h \varphi - h \Delta_Y - \varphi + \theta h \\
& + \omega_o t\right) h V_{dc} - M_h h \cos\left(\frac{1}{2} \pi h + h \varphi - h \Delta_Y + \varphi + \theta h - \omega_o t\right) h V_{dc} + M_h h \cos\left(\frac{1}{2} \pi h + h \varphi + \varphi + \theta h \\
& - \omega_o t\right) h V_{dc} - M_h h \cos\left(-\frac{3}{2} \pi h + h \varphi - \varphi + \theta h + \omega_o t\right) h V_{dc} + M_h h \cos\left(\frac{3}{2} \pi h + h \varphi + \varphi + \theta h \\
& - \omega_o t\right) h V_{dc} - M_h h \cos\left(-\frac{1}{2} \pi h + h \varphi - \varphi + \theta h + \omega_o t\right) h V_{dc} + M_h h \cos\left(-\frac{3}{2} \pi h + h \varphi - h \Delta_Y - \varphi + \theta h \\
& + \omega_o t\right) V_{dc} + M_h h \cos\left(\frac{3}{2} \pi h + h \varphi - h \Delta_Y + \varphi + \theta h - \omega_o t\right) V_{dc} + M_h h \cos\left(-\frac{1}{2} \pi h + h \varphi - h \Delta_Y - \varphi + \theta h \\
& + \omega_o t\right) V_{dc} + M_h h \cos\left(\frac{1}{2} \pi h + h \varphi - h \Delta_Y + \varphi + \theta h - \omega_o t\right) V_{dc} - M_h h \cos\left(\frac{1}{2} \pi h + h \varphi + \varphi + \theta h \\
& - \omega_o t\right) V_{dc} - M_h h \cos\left(-\frac{3}{2} \pi h + h \varphi - \varphi + \theta h + \omega_o t\right) V_{dc} - M_h h \cos\left(\frac{3}{2} \pi h + h \varphi + \varphi + \theta h - \omega_o t\right) V_{dc} \\
& \left. - M_h h \cos\left(-\frac{1}{2} \pi h + h \varphi - \varphi + \theta h + \omega_o t\right) V_{dc} \right) + \frac{-8 h^2 \Delta_X V_{dc} \cos(\omega_o t - \varphi) + 8 \Delta_X V_{dc} \cos(\omega_o t - \varphi)}{(2h^2 - 2)\pi^2}
\end{aligned} \tag{26}$$

As $T_d \ll \omega_o \wedge T_d \ll 1 \rightarrow \Delta_Y = T_d \omega_o \approx 0$

$\text{correctionFundamentalAprox} := \text{factor}(\text{eval}(\text{correctionFundamental}, \text{Delta}[Y] = 0)) \text{ assuming } h :: \text{posint}, h > 2$

$$\text{correctionFundamentalAprox} := - \frac{4 \Delta_X V_{dc} \cos(\omega_o t - \varphi)}{\pi^2} \tag{27}$$

Conclusions:

- The fundamental component introduced by the dead-time is opposite direction of the current
- The arbitrary phase and magnitude of the modulator nor the carrier phase do not influence the fundamental component of the dead-time
- Proportional to Δ_X and V_{dc} with a proportional constant of $4/\pi^2$
- The injected harmonic do not affect the fundamental component introduced by the dead-time

Base-band harmonics (h≠n)

$$\text{Integrand} := \frac{v[dc]}{\text{Pi}^2} \exp(I \cdot n \cdot y) :$$

$C0n :=$

$$\begin{aligned} & -\text{int}\left(\text{int}(\text{Integrand}, x = x[r](y) \dots x[rp](y)), y = -\frac{\text{Pi}}{2} + \text{varphi} \dots \frac{\text{Pi}}{2} + \text{varphi}\right) \\ & + \text{int}\left(\text{int}(\text{Integrand}, x = x[f](y) \dots x[fp](y)), y = \frac{\text{Pi}}{2} + \text{varphi} \dots \frac{3\text{Pi}}{2} + \text{varphi}\right) \text{ assuming } n :: \text{posint}, h :: \text{posint}, h > 2 : \end{aligned}$$

$C0n := \text{expand}(\text{convert}(C0n, \text{trig})) :$

$\text{factor}(C0n)$

$$\begin{aligned} & - \frac{1}{n^2 (n-1) (n+1) (h-n) (h+n)} \left(\left(-2 \sin\left(\frac{n\pi}{2}\right) \Delta_x n^4 + 2 \sin\left(\frac{n\pi}{2}\right) \Delta_x n^2 - 2 \sin\left(\frac{n\pi}{2}\right) \Delta_x h^2 \right. \right. \\ & + 2 \sin\left(\frac{n\pi}{2}\right) \Delta_x h^2 n^2 + I(-1)^{\frac{3n}{2}} h^2 n^2 \Delta_x - I(-1)^{\frac{n}{2}} h^2 n^2 \Delta_x - I(-1)^{\frac{3n}{2}} M \pi n^4 \cos(\varphi) \cos(\Delta_y) \sin(\theta) \\ & + I(-1)^{\frac{n}{2}} M_h \pi n^2 \cos\left(\frac{\pi h}{2}\right) \cos(h\varphi) \cos(\theta) + I(-1)^{\frac{n}{2}} M_h \pi n^4 \cos\left(\frac{\pi h}{2}\right) \sin(h\varphi) \sin(\theta) \\ & + I(-1)^{\frac{n}{2}} M_h \pi n^4 \sin\left(\frac{\pi h}{2}\right) \sin(h\varphi) \cos(\theta) + I(-1)^{\frac{n}{2}} M_h \pi n^4 \sin\left(\frac{\pi h}{2}\right) \cos(h\varphi) \sin(\theta) \\ & + I(-1)^{\frac{n}{2}} M \pi n^4 \cos(\varphi) \sin(\Delta_y) \cos(\theta) - (-1)^{\frac{n}{2}} \pi M_h h n^3 \sin\left(\frac{\pi h}{2}\right) \cos(h\varphi) \cos(\theta) \\ & + (-1)^{\frac{n}{2}} \pi M_h h n^3 \sin\left(\frac{\pi h}{2}\right) \sin(h\varphi) \sin(\theta) - (-1)^{\frac{n}{2}} \pi M_h h n^3 \cos\left(\frac{\pi h}{2}\right) \sin(h\varphi) \cos(\theta) \\ & - (-1)^{\frac{n}{2}} \pi M_h h n^3 \cos\left(\frac{\pi h}{2}\right) \cos(h\varphi) \sin(\theta) - (-1)^{\frac{n}{2}} \pi M h^2 n \cos(\varphi) \cos(\Delta_y) \cos(\theta) \\ & - (-1)^{\frac{n}{2}} \pi M h^2 n \cos(\varphi) \sin(\Delta_y) \sin(\theta) - (-1)^{\frac{n}{2}} \pi M h^2 n \sin(\varphi) \sin(\Delta_y) \cos(\theta) \\ & + (-1)^{\frac{n}{2}} \pi M h^2 n \sin(\varphi) \cos(\Delta_y) \sin(\theta) + (-1)^{\frac{n}{2}} \pi M_h h n \sin\left(\frac{\pi h}{2}\right) \cos(h\varphi) \cos(\theta) \\ & - (-1)^{\frac{n}{2}} \pi M_h h n \sin\left(\frac{\pi h}{2}\right) \sin(h\varphi) \sin(\theta) + (-1)^{\frac{n}{2}} \pi M_h h n \cos\left(\frac{\pi h}{2}\right) \sin(h\varphi) \cos(\theta) \\ & + (-1)^{\frac{n}{2}} \pi M_h h n \cos\left(\frac{\pi h}{2}\right) \cos(h\varphi) \sin(\theta) + (-1)^{\frac{3n}{2}} M_h \pi h n^3 \sin\left(\frac{3\pi h}{2}\right) \cos(h\varphi) \cos(\theta) \\ & - (-1)^{\frac{3n}{2}} M_h \pi h n^3 \sin\left(\frac{3\pi h}{2}\right) \sin(h\varphi) \sin(\theta) + (-1)^{\frac{3n}{2}} M_h \pi h n^3 \cos\left(\frac{3\pi h}{2}\right) \sin(h\varphi) \cos(\theta) \\ & + (-1)^{\frac{3n}{2}} M_h \pi h n^3 \cos\left(\frac{3\pi h}{2}\right) \cos(h\varphi) \sin(\theta) + I(-1)^{\frac{3n}{2}} M_h \pi n^2 \cos\left(\frac{3\pi h}{2}\right) \sin(h\varphi) \sin(\theta) \\ & + I(-1)^{\frac{3n}{2}} M_h \pi n^2 \sin\left(\frac{3\pi h}{2}\right) \sin(h\varphi) \cos(\theta) + I(-1)^{\frac{3n}{2}} M_h \pi n^2 \sin\left(\frac{3\pi h}{2}\right) \cos(h\varphi) \sin(\theta) \\ & + I(-1)^{\frac{3n}{2}} M \pi n^4 \cos(\varphi) \sin(\Delta_y) \cos(\theta) - (-1)^{\frac{3n}{2}} M_h \pi h n \sin\left(\frac{3\pi h}{2}\right) \cos(h\varphi) \cos(\theta) \\ & + (-1)^{\frac{3n}{2}} M_h \pi h n \sin\left(\frac{3\pi h}{2}\right) \sin(h\varphi) \sin(\theta) - (-1)^{\frac{3n}{2}} M_h \pi h n \cos\left(\frac{3\pi h}{2}\right) \sin(h\varphi) \cos(\theta) \\ & - (-1)^{\frac{3n}{2}} M_h \pi h n \cos\left(\frac{3\pi h}{2}\right) \cos(h\varphi) \sin(\theta) + I(-1)^{\frac{3n}{2}} M_h \pi n^4 \cos\left(\frac{3\pi h}{2}\right) \cos(h\varphi) \cos(\theta) \\ & - (-1)^{\frac{3n}{2}} \pi M h^2 n \cos(\varphi) \cos(\Delta_y) \cos(\theta) - (-1)^{\frac{3n}{2}} \pi M h^2 n \cos(\varphi) \sin(\Delta_y) \sin(\theta) \\ & - (-1)^{\frac{3n}{2}} \pi M h^2 n \sin(\varphi) \sin(\Delta_y) \cos(\theta) + (-1)^{\frac{3n}{2}} \pi M h^2 n \sin(\varphi) \cos(\Delta_y) \sin(\theta) \\ & - I(-1)^{\frac{n}{2}} M \pi h^2 n^2 \cos(\varphi) \sin(\theta) - I(-1)^{\frac{n}{2}} M_h \pi n^2 \cos\left(\frac{\pi h}{2}\right) \sin(h\varphi) \sin(\theta) \end{aligned}$$

$$\begin{aligned}
& -I(-1)^{\frac{n}{2}} M_h \pi n^2 \sin\left(\frac{\pi h}{2}\right) \sin(h\varphi) \cos(\theta h) - I(-1)^{\frac{n}{2}} M_h \pi n^2 \sin\left(\frac{\pi h}{2}\right) \cos(h\varphi) \sin(\theta h) \\
& -I(-1)^{\frac{n}{2}} M \pi h^2 n^2 \sin(\varphi) \cos(\theta) - I(-1)^{\frac{n}{2}} M_h \pi n^4 \cos\left(\frac{\pi h}{2}\right) \cos(h\varphi) \cos(\theta h) \\
& -I(-1)^{\frac{n}{2}} M \pi n^4 \sin(\varphi) \cos(\Delta_Y) \cos(\theta) - I(-1)^{\frac{n}{2}} M \pi n^4 \sin(\varphi) \sin(\Delta_Y) \sin(\theta) \\
& -I(-1)^{\frac{n}{2}} M \pi n^4 \cos(\varphi) \cos(\Delta_Y) \sin(\theta) - I(-1)^{\frac{3n}{2}} M_h \pi n^4 \cos\left(\frac{3\pi h}{2}\right) \sin(h\varphi) \sin(\theta h) \\
& -I(-1)^{\frac{3n}{2}} M_h \pi n^4 \sin\left(\frac{3\pi h}{2}\right) \sin(h\varphi) \cos(\theta h) - I(-1)^{\frac{3n}{2}} M_h \pi n^4 \sin\left(\frac{3\pi h}{2}\right) \cos(h\varphi) \sin(\theta h) \\
& -I(-1)^{\frac{3n}{2}} M_h \pi n^2 \cos\left(\frac{3\pi h}{2}\right) \cos(h\varphi) \cos(\theta h) - I(-1)^{\frac{3n}{2}} M \pi h^2 n^2 \cos(\varphi) \sin(\theta) \\
& -I(-1)^{\frac{3n}{2}} M \pi h^2 n^2 \sin(\varphi) \cos(\theta) - I(-1)^{\frac{3n}{2}} M \pi n^4 \sin(\varphi) \cos(\Delta_Y) \cos(\theta) \\
& -I(-1)^{\frac{3n}{2}} M \pi n^4 \sin(\varphi) \sin(\Delta_Y) \sin(\theta) - (-1)^{\frac{n}{2}} \pi M n^3 \cos(\varphi) \cos(\theta) \\
& + (-1)^{\frac{n}{2}} \pi M n^3 \sin(\varphi) \sin(\theta) - (-1)^{\frac{3n}{2}} \pi M n^3 \cos(\varphi) \cos(\theta) + (-1)^{\frac{3n}{2}} \pi M n^3 \sin(\varphi) \sin(\theta) \\
& - (-1)^{\frac{n}{2}} \pi M n^3 \sin(\varphi) \cos(\Delta_Y) \sin(\theta) + (-1)^{\frac{n}{2}} \pi M h^2 n \cos(\varphi) \cos(\theta) \\
& - (-1)^{\frac{n}{2}} \pi M h^2 n \sin(\varphi) \sin(\theta) + I(-1)^{\frac{n}{2}} M \pi n^4 \sin(\varphi) \cos(\theta) + I(-1)^{\frac{n}{2}} M \pi n^4 \cos(\varphi) \sin(\theta) \\
& + (-1)^{\frac{3n}{2}} \pi M n^3 \cos(\varphi) \cos(\Delta_Y) \cos(\theta) + (-1)^{\frac{3n}{2}} \pi M n^3 \cos(\varphi) \sin(\Delta_Y) \sin(\theta) \\
& + (-1)^{\frac{3n}{2}} \pi M n^3 \sin(\varphi) \sin(\Delta_Y) \cos(\theta) - (-1)^{\frac{3n}{2}} \pi M n^3 \sin(\varphi) \cos(\Delta_Y) \sin(\theta) \\
& + (-1)^{\frac{3n}{2}} \pi M h^2 n \cos(\varphi) \cos(\theta) - (-1)^{\frac{3n}{2}} \pi M h^2 n \sin(\varphi) \sin(\theta) + I(-1)^{\frac{3n}{2}} M \pi n^4 \sin(\varphi) \cos(\theta) \\
& + I(-1)^{\frac{3n}{2}} M \pi n^4 \cos(\varphi) \sin(\theta) + (-1)^{\frac{n}{2}} \pi M n^3 \cos(\varphi) \cos(\Delta_Y) \cos(\theta) \\
& + (-1)^{\frac{n}{2}} \pi M n^3 \cos(\varphi) \sin(\Delta_Y) \sin(\theta) + (-1)^{\frac{n}{2}} \pi M n^3 \sin(\varphi) \sin(\Delta_Y) \cos(\theta) \\
& + (-1)^{\frac{3n}{2}} M_h \pi h n \cos\left(\frac{3\pi h}{2}\right) \sin(h\varphi) \sin(h\Delta_Y) \sin(\theta h) \\
& - (-1)^{\frac{3n}{2}} M_h \pi h n \cos\left(\frac{3\pi h}{2}\right) \cos(h\varphi) \sin(h\Delta_Y) \cos(\theta h) \\
& + (-1)^{\frac{3n}{2}} M_h \pi h n \cos\left(\frac{3\pi h}{2}\right) \cos(h\varphi) \cos(h\Delta_Y) \sin(\theta h) \\
& - (-1)^{\frac{3n}{2}} M_h \pi h n^3 \sin\left(\frac{3\pi h}{2}\right) \cos(h\varphi) \cos(h\Delta_Y) \cos(\theta h) \\
& - (-1)^{\frac{3n}{2}} M_h \pi h n^3 \sin\left(\frac{3\pi h}{2}\right) \cos(h\varphi) \sin(h\Delta_Y) \sin(\theta h) + I(-1)^{\frac{n}{2}} n^4 \Delta_X + I(-1)^{\frac{n}{2}} h^2 \Delta_X \\
& + I(-1)^{\frac{3n}{2}} n^2 \Delta_X - I(-1)^{\frac{n}{2}} n^2 \Delta_X - I(-1)^{\frac{3n}{2}} n^4 \Delta_X - I(-1)^{\frac{3n}{2}} h^2 \Delta_X \\
& - (-1)^{\frac{3n}{2}} M_h \pi h n^3 \sin\left(\frac{3\pi h}{2}\right) \sin(h\varphi) \sin(h\Delta_Y) \cos(\theta h) \\
& + (-1)^{\frac{3n}{2}} M_h \pi h n^3 \sin\left(\frac{3\pi h}{2}\right) \sin(h\varphi) \cos(h\Delta_Y) \sin(\theta h) \\
& - (-1)^{\frac{3n}{2}} M_h \pi h n^3 \cos\left(\frac{3\pi h}{2}\right) \sin(h\varphi) \cos(h\Delta_Y) \cos(\theta h) \\
& - (-1)^{\frac{3n}{2}} M_h \pi h n^3 \cos\left(\frac{3\pi h}{2}\right) \sin(h\varphi) \sin(h\Delta_Y) \sin(\theta h)
\end{aligned}$$

$$\begin{aligned}
& + (-1)^{\frac{3n}{2}} M_{-h} \pi h n^3 \cos\left(\frac{3\pi h}{2}\right) \cos(h\varphi) \sin(h\Delta_Y) \cos(\theta h) \\
& - I(-1)^{\frac{3n}{2}} M_{-h} \pi n^2 \sin\left(\frac{3\pi h}{2}\right) \sin(h\varphi) \cos(h\Delta_Y) \cos(\theta h) \\
& - I(-1)^{\frac{3n}{2}} M_{-h} \pi n^2 \sin\left(\frac{3\pi h}{2}\right) \sin(h\varphi) \sin(h\Delta_Y) \sin(\theta h) \\
& - I(-1)^{\frac{3n}{2}} M_{-h} \pi n^2 \sin\left(\frac{3\pi h}{2}\right) \cos(h\varphi) \cos(h\Delta_Y) \sin(\theta h) \\
& - I(-1)^{\frac{3n}{2}} M_{-h} \pi n^4 \cos\left(\frac{3\pi h}{2}\right) \cos(h\varphi) \cos(h\Delta_Y) \cos(\theta h) \\
& - I(-1)^{\frac{n}{2}} M_{-h} \pi n^4 \cos\left(\frac{\pi h}{2}\right) \sin(h\varphi) \cos(h\Delta_Y) \sin(\theta h) \\
& - I(-1)^{\frac{n}{2}} M_{-h} \pi n^4 \sin\left(\frac{\pi h}{2}\right) \sin(h\varphi) \cos(h\Delta_Y) \cos(\theta h) \\
& - I(-1)^{\frac{n}{2}} M_{-h} \pi n^4 \sin\left(\frac{\pi h}{2}\right) \sin(h\varphi) \sin(h\Delta_Y) \sin(\theta h) \\
& - I(-1)^{\frac{n}{2}} M_{-h} \pi n^4 \sin\left(\frac{\pi h}{2}\right) \cos(h\varphi) \cos(h\Delta_Y) \sin(\theta h) - I(-1)^{\frac{n}{2}} M \pi h^2 n^2 \cos(\varphi) \sin(\Delta_Y) \cos(\theta) \\
& - I(-1)^{\frac{n}{2}} M_{-h} \pi n^2 \sin\left(\frac{\pi h}{2}\right) \cos(h\varphi) \sin(h\Delta_Y) \cos(\theta h) \\
& - I(-1)^{\frac{n}{2}} M_{-h} \pi n^2 \cos\left(\frac{\pi h}{2}\right) \cos(h\varphi) \cos(h\Delta_Y) \cos(\theta h) \\
& - I(-1)^{\frac{n}{2}} M_{-h} \pi n^2 \cos\left(\frac{\pi h}{2}\right) \cos(h\varphi) \sin(h\Delta_Y) \sin(\theta h) \\
& - I(-1)^{\frac{n}{2}} M_{-h} \pi n^2 \cos\left(\frac{\pi h}{2}\right) \sin(h\varphi) \sin(h\Delta_Y) \cos(\theta h) - I(-1)^{\frac{3n}{2}} M \pi h^2 n^2 \cos(\varphi) \sin(\Delta_Y) \cos(\theta) \\
& - I(-1)^{\frac{3n}{2}} M_{-h} \pi n^4 \cos\left(\frac{3\pi h}{2}\right) \cos(h\varphi) \sin(h\Delta_Y) \sin(\theta h) \\
& + I(-1)^{\frac{n}{2}} M_{-h} \pi n^2 \sin\left(\frac{\pi h}{2}\right) \sin(h\varphi) \sin(h\Delta_Y) \sin(\theta h) \\
& - I(-1)^{\frac{3n}{2}} M_{-h} \pi n^4 \cos\left(\frac{3\pi h}{2}\right) \sin(h\varphi) \sin(h\Delta_Y) \cos(\theta h) \\
& - I(-1)^{\frac{3n}{2}} M_{-h} \pi n^4 \sin\left(\frac{3\pi h}{2}\right) \cos(h\varphi) \sin(h\Delta_Y) \cos(\theta h) \\
& - I(-1)^{\frac{3n}{2}} M_{-h} \pi n^2 \cos\left(\frac{3\pi h}{2}\right) \sin(h\varphi) \cos(h\Delta_Y) \sin(\theta h) \\
& - (-1)^{\frac{n}{2}} \pi M_{-h} h n \sin\left(\frac{\pi h}{2}\right) \cos(h\varphi) \cos(h\Delta_Y) \cos(\theta h) \\
& - (-1)^{\frac{n}{2}} \pi M_{-h} h n \sin\left(\frac{\pi h}{2}\right) \cos(h\varphi) \sin(h\Delta_Y) \sin(\theta h) \\
& + I(-1)^{\frac{n}{2}} M_{-h} \pi n^4 \cos\left(\frac{\pi h}{2}\right) \cos(h\varphi) \sin(h\Delta_Y) \sin(\theta h) \\
& + I(-1)^{\frac{n}{2}} M_{-h} \pi n^4 \cos\left(\frac{\pi h}{2}\right) \sin(h\varphi) \sin(h\Delta_Y) \cos(\theta h) + I(-1)^{\frac{3n}{2}} M \pi h^2 n^2 \sin(\varphi) \cos(\Delta_Y) \cos(\theta) \\
& + I(-1)^{\frac{3n}{2}} M \pi h^2 n^2 \sin(\varphi) \sin(\Delta_Y) \sin(\theta) + I(-1)^{\frac{3n}{2}} M \pi h^2 n^2 \cos(\varphi) \cos(\Delta_Y) \sin(\theta) \\
& + I(-1)^{\frac{3n}{2}} M_{-h} \pi n^2 \cos\left(\frac{3\pi h}{2}\right) \cos(h\varphi) \cos(h\Delta_Y) \cos(\theta h) \\
& + I(-1)^{\frac{3n}{2}} M_{-h} \pi n^2 \cos\left(\frac{3\pi h}{2}\right) \cos(h\varphi) \sin(h\Delta_Y) \sin(\theta h) \\
& + I(-1)^{\frac{3n}{2}} M_{-h} \pi n^2 \cos\left(\frac{3\pi h}{2}\right) \sin(h\varphi) \sin(h\Delta_Y) \cos(\theta h)
\end{aligned} \tag{28}$$

$$\begin{aligned}
& + I (-1)^{\frac{3n}{2}} M_h \pi n^2 \sin\left(\frac{3\pi h}{2}\right) \cos(h\varphi) \sin(h\Delta_Y) \cos(\theta h) \\
& - (-1)^{\frac{3n}{2}} M_h \pi h n^3 \cos\left(\frac{3\pi h}{2}\right) \cos(h\varphi) \cos(h\Delta_Y) \sin(\theta h) \\
& + (-1)^{\frac{3n}{2}} M_h \pi h n \sin\left(\frac{3\pi h}{2}\right) \cos(h\varphi) \cos(h\Delta_Y) \cos(\theta h) \\
& + (-1)^{\frac{3n}{2}} M_h \pi h n \sin\left(\frac{3\pi h}{2}\right) \cos(h\varphi) \sin(h\Delta_Y) \sin(\theta h) \\
& + (-1)^{\frac{3n}{2}} M_h \pi h n \sin\left(\frac{3\pi h}{2}\right) \sin(h\varphi) \sin(h\Delta_Y) \cos(\theta h) \\
& - (-1)^{\frac{3n}{2}} M_h \pi h n \sin\left(\frac{3\pi h}{2}\right) \sin(h\varphi) \cos(h\Delta_Y) \sin(\theta h) \\
& + (-1)^{\frac{3n}{2}} M_h \pi h n \cos\left(\frac{3\pi h}{2}\right) \sin(h\varphi) \cos(h\Delta_Y) \cos(\theta h) \\
& - (-1)^{\frac{n}{2}} \pi M_h h n \sin\left(\frac{\pi h}{2}\right) \sin(h\varphi) \sin(h\Delta_Y) \cos(\theta h) \\
& + (-1)^{\frac{n}{2}} \pi M_h h n \sin\left(\frac{\pi h}{2}\right) \sin(h\varphi) \cos(h\Delta_Y) \sin(\theta h) \\
& - (-1)^{\frac{n}{2}} \pi M_h h n \cos\left(\frac{\pi h}{2}\right) \sin(h\varphi) \cos(h\Delta_Y) \cos(\theta h) \\
& - (-1)^{\frac{n}{2}} \pi M_h h n \cos\left(\frac{\pi h}{2}\right) \sin(h\varphi) \sin(h\Delta_Y) \sin(\theta h) \\
& + (-1)^{\frac{n}{2}} \pi M_h h n \cos\left(\frac{\pi h}{2}\right) \cos(h\varphi) \sin(h\Delta_Y) \cos(\theta h) \\
& - (-1)^{\frac{n}{2}} \pi M_h h n \cos\left(\frac{\pi h}{2}\right) \cos(h\varphi) \cos(h\Delta_Y) \sin(\theta h) \\
& + (-1)^{\frac{n}{2}} \pi M_h h n^3 \sin\left(\frac{\pi h}{2}\right) \cos(h\varphi) \cos(h\Delta_Y) \cos(\theta h) \\
& + (-1)^{\frac{n}{2}} \pi M_h h n^3 \sin\left(\frac{\pi h}{2}\right) \cos(h\varphi) \sin(h\Delta_Y) \sin(\theta h) \\
& + (-1)^{\frac{n}{2}} \pi M_h h n^3 \sin\left(\frac{\pi h}{2}\right) \sin(h\varphi) \sin(h\Delta_Y) \cos(\theta h) \\
& - (-1)^{\frac{n}{2}} \pi M_h h n^3 \sin\left(\frac{\pi h}{2}\right) \sin(h\varphi) \cos(h\Delta_Y) \sin(\theta h) \\
& + (-1)^{\frac{n}{2}} \pi M_h h n^3 \cos\left(\frac{\pi h}{2}\right) \sin(h\varphi) \cos(h\Delta_Y) \cos(\theta h) \\
& + (-1)^{\frac{n}{2}} \pi M_h h n^3 \cos\left(\frac{\pi h}{2}\right) \sin(h\varphi) \sin(h\Delta_Y) \sin(\theta h) \\
& - (-1)^{\frac{n}{2}} \pi M_h h n^3 \cos\left(\frac{\pi h}{2}\right) \cos(h\varphi) \sin(h\Delta_Y) \cos(\theta h) \\
& + (-1)^{\frac{n}{2}} \pi M_h h n^3 \cos\left(\frac{\pi h}{2}\right) \cos(h\varphi) \cos(h\Delta_Y) \sin(\theta h) \\
& + I (-1)^{\frac{n}{2}} M_h \pi n^2 \cos\left(\frac{\pi h}{2}\right) \sin(h\varphi) \cos(h\Delta_Y) \sin(\theta h) \\
& + I (-1)^{\frac{n}{2}} M_h \pi n^2 \sin\left(\frac{\pi h}{2}\right) \sin(h\varphi) \cos(h\Delta_Y) \cos(\theta h) \\
& + I (-1)^{\frac{3n}{2}} M_h \pi n^4 \cos\left(\frac{3\pi h}{2}\right) \sin(h\varphi) \cos(h\Delta_Y) \sin(\theta h) \\
& + I (-1)^{\frac{3n}{2}} M_h \pi n^4 \sin\left(\frac{3\pi h}{2}\right) \sin(h\varphi) \cos(h\Delta_Y) \cos(\theta h) \\
& + I (-1)^{\frac{3n}{2}} M_h \pi n^4 \sin\left(\frac{3\pi h}{2}\right) \sin(h\varphi) \sin(h\Delta_Y) \sin(\theta h)
\end{aligned}$$

$$\begin{aligned}
& +I(-1)^{\frac{3n}{2}} M_h \pi n^4 \sin\left(\frac{3\pi h}{2}\right) \cos(h\varphi) \cos(h\Delta_Y) \sin(\theta h) \\
& +I(-1)^{\frac{n}{2}} M_h \pi n^2 \sin\left(\frac{\pi h}{2}\right) \cos(h\varphi) \cos(h\Delta_Y) \sin(\theta h) \\
& +I(-1)^{\frac{n}{2}} M_h \pi n^4 \sin\left(\frac{\pi h}{2}\right) \cos(h\varphi) \sin(h\Delta_Y) \cos(\theta h) + I(-1)^{\frac{n}{2}} M \pi h^2 n^2 \sin(\varphi) \cos(\Delta_Y) \cos(\theta v) \\
& +I(-1)^{\frac{n}{2}} M \pi h^2 n^2 \sin(\varphi) \sin(\Delta_Y) \sin(\theta v) + I(-1)^{\frac{n}{2}} M \pi h^2 n^2 \cos(\varphi) \cos(\Delta_Y) \sin(\theta v) \\
& +I(-1)^{\frac{n}{2}} M_h \pi n^4 \cos\left(\frac{\pi h}{2}\right) \cos(h\varphi) \cos(h\Delta_Y) \cos(\theta h) \left(\cos(n\varphi) + I \sin(n\varphi) \right) v_{dc}
\end{aligned}$$

Analysis simplifying periodic terms

$$\begin{aligned}
& seq\left((-1)^{-\frac{n}{2}}, n = 2..10, 1 \right) \\
& \qquad \qquad \qquad -1, I, 1, -I, -1, I, 1, -I, -1
\end{aligned} \tag{29}$$

$$\begin{aligned}
& seq\left((-1)^{\frac{3n}{2}}, n = 2..10, 1 \right) \\
& \qquad \qquad \qquad -1, I, 1, -I, -1, I, 1, -I, -1
\end{aligned} \tag{30}$$

$$\begin{aligned}
& seq\left(\sin\left(\frac{\pi h}{2}\right), h = 2..10, 1 \right) \\
& \qquad \qquad \qquad 0, -1, 0, 1, 0, -1, 0, 1, 0
\end{aligned} \tag{31}$$

$$\begin{aligned}
& seq\left(\sin\left(\frac{3\pi h}{2}\right), h = 2..10, 1 \right) \\
& \qquad \qquad \qquad 0, 1, 0, -1, 0, 1, 0, -1, 0
\end{aligned} \tag{32}$$

$$\begin{aligned}
& seq\left(\cos\left(\frac{\pi h}{2}\right), h = 2..10, 1 \right) \\
& \qquad \qquad \qquad -1, 0, 1, 0, -1, 0, 1, 0, -1
\end{aligned} \tag{33}$$

$$\begin{aligned}
& seq\left(\cos\left(\frac{3\pi h}{2}\right), h = 2..10, 1 \right) \\
& \qquad \qquad \qquad -1, 0, 1, 0, -1, 0, 1, 0, -1
\end{aligned} \tag{34}$$

$$\begin{aligned}
C0n &:= \text{factor} \left(\text{eval} \left(C0n, \left[(-1)^{\frac{3n}{2}} = (-1)^{-\frac{n}{2}}, \cos \left(\frac{3\pi h}{2} \right) = \cos \left(\frac{\pi h}{2} \right), \sin \left(\frac{3\pi h}{2} \right) = -\sin \left(\frac{\pi h}{2} \right), \text{Delta}[Y] \right. \right. \right. \\
&= 0 \left. \left. \left. \right) \right) \right) \\
C0n &:= \frac{\text{I} \left(2 \text{I} \sin \left(\frac{n\pi}{2} \right) - (-1)^{-\frac{n}{2}} + (-1)^{\frac{n}{2}} \right) (\cos(n\varphi) + \text{I} \sin(n\varphi)) \Delta_X v_{dc}}{n\pi^2} \quad (35)
\end{aligned}$$

$$\begin{aligned}
&\text{seq} \left((-1)^{-\frac{n}{2}}, n = 2..10, 2 \right) \\
&\qquad\qquad\qquad -1, 1, -1, 1, -1 \quad (36)
\end{aligned}$$

$$\begin{aligned}
&\text{seq} \left((-1)^{\frac{n}{2}}, n = 2..10, 2 \right) \\
&\qquad\qquad\qquad -1, 1, -1, 1, -1 \quad (37)
\end{aligned}$$

For even values of n

$$\begin{aligned}
C0n_{\text{even}} &:= \text{factor} \left(\text{eval} \left(C0n, \left[(-1)^{-\frac{n}{2}} = (-1)^{\frac{n}{2}} \right] \right) \right) \text{assuming } n :: \text{posint}, n :: \text{even}; \\
\text{correctionBasebandHarmonics}_{\text{even}} &:= 0; \\
C0n_{\text{even}} &:= 0 \\
\text{correctionBasebandHarmonics}_{\text{even}} &:= 0 \quad (38)
\end{aligned}$$

For odd values of n

$$\begin{aligned}
C0n_{\text{odd}} &:= \text{factor} \left(\text{eval} \left(C0n, \left[(-1)^{-\frac{n}{2}} = -(-1)^{\frac{n}{2}} \right] \right) \right) \text{assuming } n :: \text{posint}, n :: \text{odd}; \text{convert}(C0n_{\text{odd}}, \text{exp}); \\
C0n_{\text{odd}} &:= \frac{2 \left(\text{I} (-1)^{\frac{n}{2}} - (-1)^{\frac{n}{2} - \frac{1}{2}} \right) (\cos(n\varphi) + \text{I} \sin(n\varphi)) \Delta_X v_{dc}}{n\pi^2}
\end{aligned}$$

$$\frac{2 \left(\mathbf{I} e^{\frac{1}{2} \pi n} - e^{\mathbf{I} \pi \left(\frac{n}{2} - \frac{1}{2} \right)} \right) e^{\mathbf{I} n \varphi} \Delta_X v_{dc}}{n \pi^2} \quad (39)$$

analysing the periodic terms:

$$\begin{aligned} \text{seq} \left(\mathbf{I} e^{\frac{1}{2} \pi n}, n = 1..10, 2 \right) \\ -1, 1, -1, 1, -1 \end{aligned} \quad (40)$$

$$\begin{aligned} \text{seq} \left(-e^{\mathbf{I} \pi \left(\frac{n}{2} - \frac{1}{2} \right)}, n = 1..10, 2 \right) \\ -1, 1, -1, 1, -1 \end{aligned} \quad (41)$$

$$\begin{aligned} C0n_odd := \text{eval} \left(C0n_odd \left[\mathbf{I} e^{\frac{1}{2} \pi n} - e^{\mathbf{I} \pi \left(\frac{n}{2} - \frac{1}{2} \right)} \right] \right) \\ C0n_odd := \frac{2 \left(\mathbf{I} (-1)^{\frac{n}{2}} - (-1)^{\frac{n}{2} - \frac{1}{2}} \right) (\cos(n \varphi) + \mathbf{I} \sin(n \varphi)) \Delta_X v_{dc}}{n \pi^2} \end{aligned} \quad (42)$$

analysing the periodic terms:

$$\begin{aligned} \text{seq} \left(\mathbf{I} (-1)^{\frac{n}{2}}, n = 1..10, 2 \right) \\ -1, 1, -1, 1, -1 \end{aligned} \quad (43)$$

$$\begin{aligned} \text{seq} \left(-(-1)^{\frac{n}{2} - \frac{1}{2}}, n = 1..10, 2 \right) \\ -1, 1, -1, 1, -1 \end{aligned} \quad (44)$$

$$C0n_odd := \text{eval} \left(C0n_odd \left[\mathbf{I} (-1)^{\frac{n}{2}} - (-1)^{\frac{n}{2} - \frac{1}{2}} \right] \right)$$

$$C0n_odd := - \frac{4 (-1)^{\frac{n}{2} - \frac{1}{2}} (\cos(n \varphi) + I \sin(n \varphi)) \Delta_X v_{dc}}{n \pi^2} \quad (45)$$

Calculating Fourier coefficient

$A0n := \text{evalc}(\text{Re}(C0n_odd))$ assuming $v_{dc} :: \text{real}, M :: \text{real}, \Delta_{\phi} :: \text{real}, \Delta_{\theta} :: \text{real}, \varphi :: \text{real}, n :: \text{posint}$;

$B0n := \text{evalc}(\text{Im}(C0n_odd))$ assuming $v_{dc} :: \text{real}, M :: \text{real}, \Delta_{\phi} :: \text{real}, \Delta_{\theta} :: \text{real}, \varphi :: \text{real}, n :: \text{posint}$;

$n\text{Harmonics} := A0n \cos(n \cdot \text{omega}[o] \cdot t) + B0n \sin(n \cdot \text{omega}[o] \cdot t)$;

$\text{correctionBasebandHarmonics_odd} := \text{combine}(n\text{Harmonics})$

$$A0n := - \frac{4 v_{dc} \left(\sin\left(\frac{n \pi}{2}\right) \Delta_X \cos(n \varphi) + \cos\left(\frac{n \pi}{2}\right) \Delta_X \sin(n \varphi) \right)}{n \pi^2}$$

$$B0n := - \frac{4 v_{dc} \left(-\cos\left(\frac{n \pi}{2}\right) \Delta_X \cos(n \varphi) + \sin\left(\frac{n \pi}{2}\right) \Delta_X \sin(n \varphi) \right)}{n \pi^2}$$

$$\text{correctionBasebandHarmonics_odd} := \frac{4 v_{dc} \Delta_X \sin\left(-\frac{1}{2} n \pi - n \varphi + n \omega_o t\right)}{n \pi^2} \quad (46)$$

Conclusions:

- The arbitrary phase of the voltage does not influence the baseband component of the dead-time
- It is proportional to DeltaX and Vdc with a proportional constant of $4/\pi^2$
- It is inverse proportional to the harmonic number
- The injected harmonic do not affects the baseband harmonics introduced by the dead time

C.2 MapleTM2019 worksheet for Double-edge Naturally Sampled PWM

[doubleEdgeNaturallySampledPwm.mw](#)

Ideal Part

restart;

restart (1)

with(plots):

*testParameters := [M=0.6, θo = $\frac{30 \cdot \text{Pi}}{180}$, θc = $\frac{45 \cdot \text{Pi}}{180}$, M_h=0.1, θh = $\frac{15 \cdot \text{Pi}}{180}$, h=7, V[dc]=1, M[f]=21, ω_o=2
·Pi·60, ω_c = ω_o·M[f], T_d=0.0001, varphi = $\frac{30 \cdot \text{Pi}}{180}$, Δ[X]=2·Pi·60·21·0.0001, Δ[Y]=2·Pi·60·0.0001]:*

Carrier wave form

$$c(x) := \begin{cases} c_n(x) & -\pi \leq x < 0 \\ c_p(x) & 0 \leq x < \pi \end{cases}$$

$$c := x \mapsto \begin{cases} c_n(x) & -\pi \leq x < 0 \\ c_p(x) & 0 \leq x < \pi \end{cases} \quad (2)$$

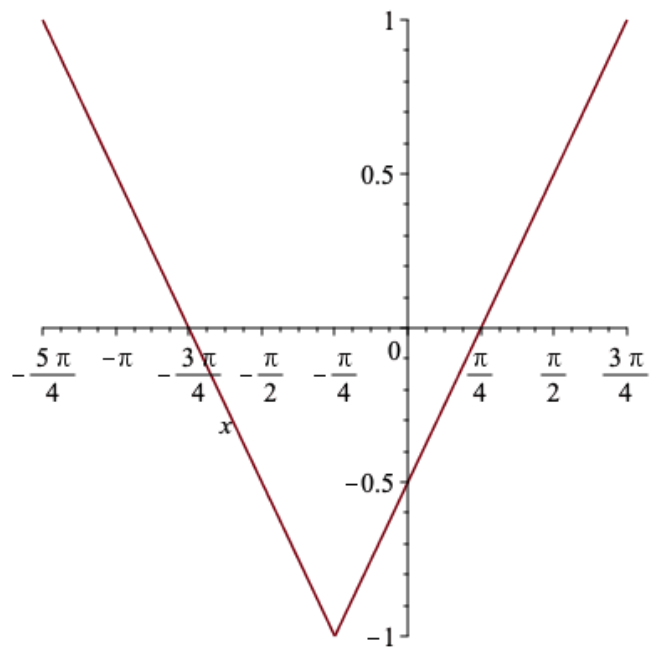
where $c_n(x) := -\frac{2}{\pi} \cdot (x + \theta_c) - 1$

$$c_n := x \mapsto -\frac{2(x + \theta_c)}{\pi} - 1 \quad (3)$$

and $c_p(x) := \frac{2}{\pi} \cdot (x + \theta_c) - 1$

$$c_p := x \mapsto \frac{2(x + \theta_c)}{\pi} - 1 \quad (4)$$

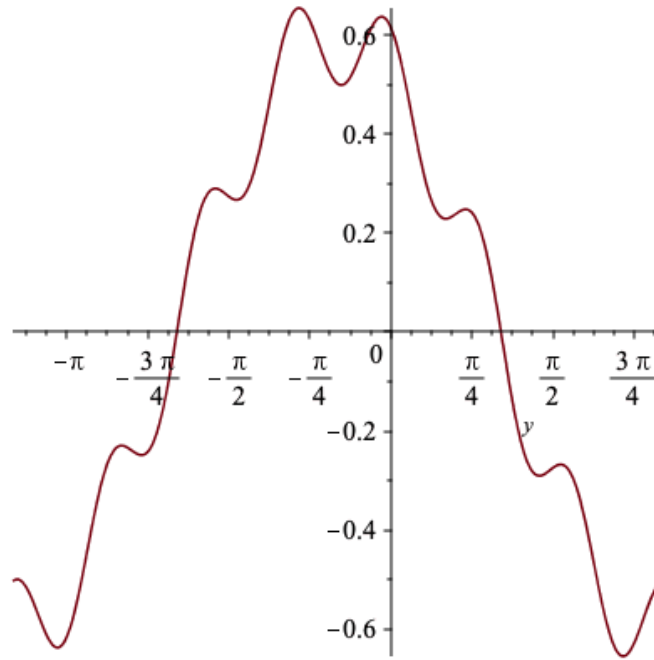
plot_cn := plot(eval(c[n](x), testParameters), x = eval(-Pi - θc..0 - θc, testParameters)):
plot_cp := plot(eval(c[p](x), testParameters), x = eval(0 - θc..Pi - θc, testParameters)):
display(plot_cn, plot_cp)



Modulator waveform $v_o(y) := M \cos(y + \theta_o) + M_h \cos(h \cdot y + \theta_h)$;

$$v_o := y \mapsto M \cos(y + \theta_o) + M_h \cos(h y + \theta_h) \quad (5)$$

`plot(eval(v[o])(y), testParameters), eval(y = -Pi - theta_o..Pi - theta_o, testParameters))`



PWM Definition

The rising function can be found by comparing $c_n(x) := -\frac{2}{\pi} \cdot (x + \theta_c) - 1$ and

$v_o(y) := M \cos(y + \theta_o) + M_h \cos(h \cdot y + \theta_h)$; and solving for x

$x[r](y) := \text{solve}(c[n](x) = v[o](y), x) : \text{factor}(x[r](y))$

$$-\frac{M \cos(y + \theta_o) \pi}{2} - \frac{M_h \cos(h y + \theta_h) \pi}{2} - \frac{\pi}{2} - \theta_c \quad (6)$$

and the falling function $x[f](y) := \text{solve}(c[p](x) = v[o](y), x) : \text{factor}(x[f](y))$

$$\frac{M \cos(y + \theta_o) \pi}{2} + \frac{M_h \cos(h y + \theta_h) \pi}{2} + \frac{\pi}{2} - \theta_c \quad (7)$$

$F(x, y) := \text{piecewise}(x[r](y) \leq x \leq x[f](y), V[dc], 0)$

$$F := (x, y) \mapsto \begin{cases} V_{dc} & x_r(y) \leq x \leq x_f(y) \\ 0 & \text{otherwise} \end{cases} \quad (8)$$

3-D Model of the Ideal Term $\text{numContours} := 2$:

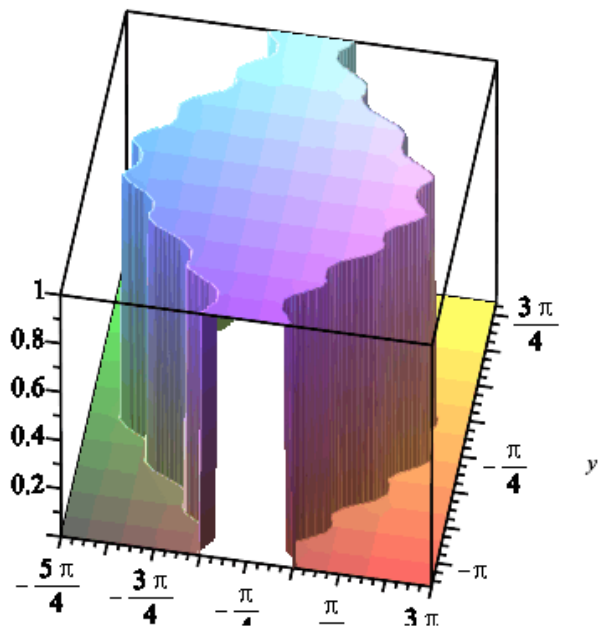
$\text{limits} := [\text{eval}(-\pi - \theta_c.. \pi - \theta_c, \text{testParameters}), \text{eval}(-\pi - \theta_o.. \pi - \theta_o, \text{testParameters}), 0..1]$:

```

numOfpoints := 150 :
gridPoints := [numOfpoints, numOfpoints] :
initialOrientation := [280, 40, 0] :

plot3d( eval( F( x, y ), testParameters ), eval( x = -pi - 2c .. pi - 2c, testParameters ), eval( y = -pi - 2o .. pi - 2o,
testParameters ),
contours = numContours,
orientation = initialOrientation,
view = limits,
style = surface,
grid = gridPoints )

```



Low Frequency Spectrum of the Ideal Term

DC component

```

Integrand :=  $\frac{v[dc]}{\pi^2}$  :
A00 := int( int( Integrand, x = x[r](y) .. x[f](y) ), y = -Pi .. Pi ) :
idealA00 := eval( A00 ) assuming h :: posint :
idealOffset :=  $\frac{idealA00}{2}$ 

```

$$idealOffset := v_{dc} \quad (9)$$

Conclusions:

- the DC component only depends of the Vdc

Fundamental component

$$\begin{aligned}
 \text{Integrand} &:= \frac{v[dc]}{\pi^2} \cdot \exp(I \cdot y) : \\
 C01 &:= \text{int}(\text{int}(\text{Integrand}, x = x[r](y) .. x[f](y)), y = -\pi .. \pi) : \\
 \text{idealA01} &:= \text{evalc}(\text{Re}(C01)) ; \\
 \text{idealB01} &:= \text{evalc}(\text{Im}(C01)) ; \\
 \text{idealFundamental} &:= \text{combine}(\text{idealA01} \cdot \cos(\omega[o] t) + \text{idealB01} \cdot \sin(\omega[o] t)) \text{ assuming } h :: \text{posint}
 \end{aligned}$$

$$\begin{aligned}
 \text{idealA01} &:= - \frac{v_{dc} \left(-M \pi \cos(\Theta_o) h^2 + 2 M_h h \sin(\pi h) \cos(\Theta_h) + M \pi \cos(\Theta_o) \right)}{\pi (h^2 - 1)} \\
 \text{idealB01} &:= - \frac{v_{dc} \left(M \sin(\Theta_o) \pi h^2 - M \sin(\Theta_o) \pi - 2 M_h \sin(\pi h) \sin(\Theta_h) \right)}{\pi (h^2 - 1)} \\
 \text{idealFundamental} &:= M v_{dc} \cos(\omega_o t + \Theta) \tag{10}
 \end{aligned}$$

Conclusions:

- the fundamental component only depends of the fundamental component of the modulator signal and it is proportional to Vdc

Base-band harmonics (n≠h)

$$\begin{aligned}
 \text{Integrand} &:= \frac{v[dc]}{\pi^2} \cdot \exp(I \cdot n \cdot y) : \\
 C0n &:= \text{int}(\text{int}(\text{Integrand}, x = x[r](y) .. x[f](y)), y = -\pi .. \pi) \text{ assuming } n :: \text{posint} : \\
 \text{idealA0n} &:= \text{evalc}(\text{Re}(C0n)) : \\
 \text{idealB0n} &:= \text{evalc}(\text{Im}(C0n)) : \\
 \text{idealBasebandHarmonics} &:= \text{combine}(\text{idealA0n} \cdot \cos(n \cdot \omega[o] \cdot t) + \text{idealB0n} \cdot \sin(n \cdot \omega[o] \cdot t)) \text{ assuming } h \\
 &:: \text{posint}
 \end{aligned}$$

$$\text{idealBasebandHarmonics} := 0 \tag{11}$$

Conclusions:

- for the ideal case there is not baseband harmonics for the frequencies different of the h harmonic.

Base-band harmonics (n=h)

$$\begin{aligned}
 \text{Integrand} &:= \frac{v[dc]}{\pi^2} \cdot \exp(I \cdot h \cdot y) : \\
 C0h &:= \text{int}(\text{int}(\text{Integrand}, x = x[r](y) .. x[f](y)), y = -\pi .. \pi) \text{ assuming } n :: \text{posint} :
 \end{aligned}$$

$idealA_{\theta h} := evalc(\text{Re}(C_{\theta h})) :$
 $idealB_{\theta h} := evalc(\text{Im}(C_{\theta h})) :$

$idealBaseband_h := combine(idealA_{\theta h} \cos(h \cdot \omega_o [o] \cdot t) + idealB_{\theta h} \sin(h \cdot \omega_o [o] \cdot t))$ assuming $h :: posint$

$$idealBaseband_h := \cos(h \omega_o t + \Theta_h) (-1)^{2h} v_{dc} M_h \quad (12)$$

$idealBaseband_h := eval(idealBaseband_h, (-1)^{2h} = 1)$

$$idealBaseband_h := \cos(h \omega_o t + \Theta_h) v_{dc} M_h \quad (13)$$

Conclusions:

- the h harmonic only depends of the h component of the modulator and it is proportional to Vdc

(Correction Part)

PWM Defintion

The correction on the rising function can be found by

$x[rp](y) := solve(c[n](x - \text{Delta}[X]) = v[o](y - \text{Delta}[Y]), x) : factor(x[rp](y))$

$$-\frac{M \cos(y - \Delta_Y + \Theta_o) \pi}{2} - \frac{M_h \cos(h y - h \Delta_Y + \Theta_h) \pi}{2} - \frac{\pi}{2} - \Theta_c + \Delta_X \quad (14)$$

and the falling function

$x[fp](y) := solve(c[p](x - \text{Delta}[X]) = v[o](y - \text{Delta}[Y]), x) : factor(x[fp](y))$

$$\frac{M \cos(y - \Delta_Y + \Theta_o) \pi}{2} + \frac{M_h \cos(h y - h \Delta_Y + \Theta_h) \pi}{2} + \frac{\pi}{2} - \Theta_c + \Delta_X \quad (15)$$

$Fcor(x, y) := piecewise\left(x[r](y) \leq x \leq x[rp](y) \wedge -\frac{\pi}{2} + \varphi + \Theta_o \leq y < \frac{\pi}{2} + \varphi + \Theta_o, -V[dc],\right.$

$x[f](y) \leq x \leq x[fp](y) \wedge \frac{\pi}{2} + \varphi + \Theta_o \leq y < \frac{3 \cdot \pi}{2} + \varphi + \Theta_o, V[dc],$

0)

$$Fcor := (x, y) \mapsto \begin{cases} -V_{dc} & x_r(y) \leq x \leq x_{rp}(y) \text{ and } -\frac{\pi}{2} + \varphi + \Theta_o \leq y \text{ and } y < \frac{\pi}{2} + \varphi + \Theta_o \\ V_{dc} & x_f(y) \leq x \leq x_{fp}(y) \text{ and } \frac{\pi}{2} + \varphi + \Theta_o \leq y \text{ and } y < \frac{3\pi}{2} + \varphi + \Theta_o \\ 0 & \text{otherwise} \end{cases} \quad (16)$$

3-D Model of the Corrected Term $numOfpoints := 250$:

```

xRange := eval(-π - θc..π - θc, testParameters) :
yRange := eval(-π/2 + φ + θo + 0.001..3π/2 + φ + θo, testParameters) :
# xTick:= [eval(-π - θc, testParameters) = typeset(-π - θ[c]), eval(-θc, testParameters) = typeset(-θ[c]), eval(π - θc, testParameters) = typeset(π - θ[c])] :
# yTick:= [eval(-π/2 + φ + θo + 0.001, testParameters) = typeset(A), eval(π/2 + φ + θo, testParameters) = typeset(B), eval(3π/2 + φ + θo, testParameters) = typeset(C)] :
xTick := [eval(-π - θc, testParameters) = typeset( ), eval(-θc, testParameters) = typeset( ), eval(π - θc, testParameters) = typeset( )] :
yTick := [eval(-π/2 + φ + θo + 0.001, testParameters) = typeset( ), eval(π/2 + φ + θo, testParameters) = typeset( ), eval(3π/2 + φ + θo, testParameters) = typeset( )] :

plotOptions := contours = 2, orientation = [280, 40, 0], style = surface, grid = [numOfpoints, numOfpoints], axes = framed, scaling = constrained, labels = [x, y, Vdc], font = [Helvetica, italic, 16], labelfont = [Helvetica, italic, 16] :

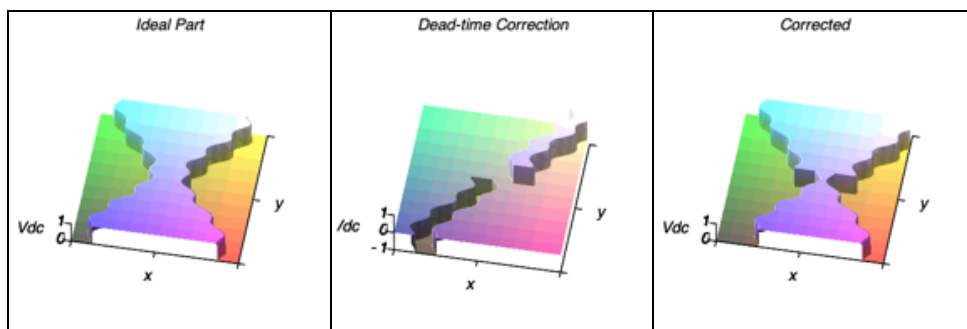
#plotsetup(wmf, plotoutput = `ideal3D.wmf`, plotoptions = `portrait, noborder, width=2.33in, height=2.33in`) :
plotsetup(bmp, plotoutput = `ideal3D.bmp`, plotoptions = `portrait, noborder, width=4.66in, height=4.66in`) :
plotIdeal := plot3d(eval(F(x, y), testParameters), x = xRange, y = yRange, plotOptions, tickmarks = [xTick, yTick, 2], view = [xRange, yRange, 0..1], title = "Ideal Part");

plotsetup(bmp, plotoutput = `correction3D.bmp`, plotoptions = `portrait, noborder, width=4.66in, height=4.66in`) :
plotCorrection := plot3d(eval(Fcor(x, y), testParameters), x = xRange, y = yRange, plotOptions, tickmarks = [xTick, yTick, 3], view = [xRange, yRange, -1..1], title = "Dead-time Correction");

plotsetup(bmp, plotoutput = `corrected3D.bmp`, plotoptions = `portrait, noborder, width=4.66in, height=4.66in`) :
plotCorrected := plot3d(eval(F(x, y) + Fcor(x, y), testParameters), x = xRange, y = yRange, plotOptions, tickmarks = [xTick, yTick, 2], view = [xRange, yRange, 0..1], title = "Corrected");

plotsetup(default) :
Arr := Array(1..3) :
Arr[1] := plotIdeal :
Arr[2] := plotCorrection :
Arr[3] := plotCorrected :
display(Arr);

```



DC component

$$\begin{aligned}
Integrand &:= \frac{v[dc]}{\text{Pi}^2} : \\
A00 &:= \\
&-int\left(int(Integrand, x=x[r](y)..x[rp](y)), y=-\frac{\text{Pi}}{2} + \text{varphi}..\frac{\text{Pi}}{2} + \text{varphi}\right) \\
&+ int\left(int(Integrand, x=x[f](y)..x[fp](y)), y=\frac{\text{Pi}}{2} + \text{varphi}..\frac{3\text{Pi}}{2} + \text{varphi}\right) \text{ assuming } h::\text{posint}, h > 2 : \\
A00 &:= \text{factor}(\text{expand}(\text{convert}(A00, \text{exp}))) \\
A00 &:= \\
&\frac{\frac{1}{4} M_h \left(-e^{-\frac{1}{2}\pi h} (e^{1h\varphi})^2 (e^{1\theta})^2 + (e^{1h\varphi})^2 (e^{1\theta})^2 e^{\frac{31}{2}\pi h} + e^{1h\Delta_Y} e^{-\frac{31}{2}\pi h} - e^{\frac{1}{2}\pi h} e^{1h\Delta_Y} \right) (e^{1h\Delta_Y} - 1) v_{dc}}{\pi h e^{1h\varphi} e^{1\theta} e^{1h\Delta_Y}} \quad (17)
\end{aligned}$$

$$\begin{aligned}
A00 &:= \text{eval}\left(A00, \left[e^{-\frac{1}{2}\pi h} = e^{\frac{31}{2}\pi h}, e^{-\frac{31}{2}\pi h} = e^{\frac{1}{2}\pi h} \right]\right) : \text{correctionOffset} := \frac{A00}{2} \\
&\text{correctionOffset} := 0 \quad (18)
\end{aligned}$$

Conclusions:

- the dead time does not affects the Dc component

Fundamental component

$$\begin{aligned}
Integrand &:= \frac{V[dc]}{\text{Pi}^2} \cdot \exp(I \cdot y) : \\
C01 &:= \\
&-int\left(int(Integrand, x=x[r](y)..x[rp](y)), y=-\frac{\text{Pi}}{2} + \text{varphi}..\frac{\text{Pi}}{2} + \text{varphi}\right) \\
&+ int\left(int(Integrand, x=x[f](y)..x[fp](y)), y=\frac{\text{Pi}}{2} + \text{varphi}..\frac{3\text{Pi}}{2} + \text{varphi}\right) : \\
C01 &:= (\text{expand}(\text{convert}(C01, \text{exp}))) \\
C01 &:= -\frac{V_{dc} M_h h e^{1\varphi} e^{\frac{1}{2}\pi h} e^{1h\Delta_Y}}{4(h^2-1)\pi e^{1h\varphi} e^{1\theta}} + \frac{V_{dc} M_h h e^{1\varphi} e^{1h\Delta_Y} e^{-\frac{31}{2}\pi h}}{4(h^2-1)\pi e^{1h\varphi} e^{1\theta}} + \frac{V_{dc} M_h h e^{1\varphi} e^{-\frac{1}{2}\pi h} e^{1h\varphi} e^{1\theta}}{4(h^2-1)\pi e^{1h\Delta_Y}} \\
&- \frac{V_{dc} M_h h e^{1\varphi} e^{1h\varphi} e^{1\theta} e^{\frac{31}{2}\pi h}}{4(h^2-1)\pi e^{1h\Delta_Y}} + \frac{V_{dc} M h^2 e^{1\Delta_Y}}{2(h^2-1)e^{1\theta}} - \frac{V_{dc} M_h e^{1\varphi} e^{\frac{1}{2}\pi h} e^{1h\Delta_Y}}{4(h^2-1)\pi e^{1h\varphi} e^{1\theta}} + \frac{V_{dc} M_h h e^{1\varphi} e^{\frac{1}{2}\pi h}}{4(h^2-1)\pi e^{1h\varphi} e^{1\theta}} \\
&+ \frac{V_{dc} M_h e^{1\varphi} e^{1h\Delta_Y} e^{-\frac{31}{2}\pi h}}{4(h^2-1)\pi e^{1h\varphi} e^{1\theta}} - \frac{V_{dc} M_h h e^{1\varphi} e^{-\frac{31}{2}\pi h}}{4(h^2-1)\pi e^{1h\varphi} e^{1\theta}} - \frac{V_{dc} M_h e^{1\varphi} e^{-\frac{1}{2}\pi h} e^{1h\varphi} e^{1\theta}}{4(h^2-1)\pi e^{1h\Delta_Y}} \\
&- \frac{V_{dc} M_h e^{1\varphi} e^{-\frac{1}{2}\pi h} e^{1h\varphi} e^{1\theta} h}{4(h^2-1)\pi} + \frac{V_{dc} M_h e^{1\varphi} e^{1h\varphi} e^{1\theta} e^{\frac{31}{2}\pi h}}{4(h^2-1)\pi e^{1h\Delta_Y}} + \frac{V_{dc} M_h e^{1\varphi} e^{1h\varphi} e^{1\theta} e^{\frac{31}{2}\pi h} h}{4(h^2-1)\pi} \quad (19)
\end{aligned}$$

$$\begin{aligned}
& -\frac{V_{dc} h^2 M}{2 (h^2 - 1) e^{1\theta}} + \frac{V_{dc} M_{-h} e^{1\varphi} e^{\frac{1}{2} \pi h}}{4 (h^2 - 1) \pi e^{1h\varphi} e^{1\theta}} - \frac{V_{dc} M_{-h} e^{1\varphi} e^{-\frac{31}{2} \pi h}}{4 (h^2 - 1) \pi e^{1h\varphi} e^{1\theta}} + \frac{V_{dc} M_{-h} e^{1\varphi} e^{-\frac{1}{2} \pi h} e^{1h\varphi} e^{1\theta}}{4 (h^2 - 1) \pi} \\
& - \frac{V_{dc} M_{-h} e^{1\varphi} e^{1h\varphi} e^{1\theta} e^{\frac{31}{2} \pi h}}{4 (h^2 - 1) \pi} - \frac{V_{dc} M e^{1\Delta_Y}}{2 (h^2 - 1) e^{1\theta}} + \frac{V_{dc} M}{2 (h^2 - 1) e^{1\theta}} - \frac{4 V_{dc} e^{1\varphi} h^2 \Delta_X}{(h^2 - 1) \pi^2} + \frac{4 V_{dc} e^{1\varphi} \Delta_X}{(h^2 - 1) \pi^2} \\
C01 := & \text{simplify} \left(\text{eval} \left(C01, \left[e^{-\frac{1}{2} \pi h} = e^{\frac{31}{2} \pi h}, e^{-\frac{31}{2} \pi h} = e^{\frac{1}{2} \pi h} \right] \right) \right) \\
C01 := & \frac{V_{dc} \left(M \pi^2 e^{-1(-\Delta_Y + \theta)} - M \pi^2 e^{-1\theta} - 8 e^{1\varphi} \Delta_X \right)}{2 \pi^2} \tag{20}
\end{aligned}$$

`collect(expand(C01), M)`

$$\left(\frac{V_{dc} e^{1\Delta_Y}}{2 e^{1\theta}} - \frac{V_{dc}}{2 e^{1\theta}} \right) M - \frac{4 V_{dc} e^{1\varphi} \Delta_X}{\pi^2} \tag{21}$$

`A01 := evalc(Re(C01)) :`

`B01 := evalc(Im(C01)) :`

`correctionFundamental := collect(combine(A01*cos(omega[o]*t) + B01*sin(omega[o]*t), Pi)`

$$\text{correctionFundamental} := \frac{M \cos(\omega_o t + \theta - \Delta_Y) V_{dc}}{2} - \frac{M \cos(\omega_o t + \theta) V_{dc}}{2} - \frac{4 \Delta_X V_{dc} \cos(\omega_o t - \varphi)}{\pi^2} \tag{22}$$

As $T_d \ll \omega_o \wedge T_d \ll 1 \rightarrow \Delta_Y = T_d \omega_o \approx 0$

`correctionFundamentalAprox := eval(correctionFundamental, Delta[Y] = 0)`

$$\text{correctionFundamentalAprox} := - \frac{4 \Delta_X V_{dc} \cos(\omega_o t - \varphi)}{\pi^2} \tag{23}$$

Conclusions:

- the fundamental component introduced by the dead-time is oppoive direction of the current
- the arbitrary phase and magnitud of the modulator nor the carrier phase do not influence the fundamental component of the dead-time
- it is proportional to DeltaX and Vdc with a proportional constand of 4/Pi^2
- the injected harmonic do not affect the fundamental component introduced by the dead-time

Base-band harmonics (h≠n)

$$\text{Integrand} := \frac{v[dc]}{\text{Pi}^2} \cdot \exp(I \cdot n \cdot y) :$$

$C0n :=$

$$\begin{aligned} & -\text{int}\left(\text{int}(\text{Integrand}, x = x[r](y) \dots x[rp](y)), y = -\frac{\text{Pi}}{2} + \text{varphi} \dots \frac{\text{Pi}}{2} + \text{varphi}\right) \\ & + \text{int}\left(\text{int}(\text{Integrand}, x = x[f](y) \dots x[fp](y)), y = \frac{\text{Pi}}{2} + \text{varphi} \dots \frac{3\text{Pi}}{2} + \text{varphi}\right) \text{ assuming } n :: \text{posint}, h :: \text{posint}, h > 2 : \end{aligned}$$

$C0n := \text{expand}(\text{convert}(C0n, \text{trig})) :$

$\text{factor}(C0n);$

$$\begin{aligned} & -\frac{1}{2 \pi^2 n (n-1) (n+1) (h-n) (h+n)} \left(\left(-2 I (-1)^{-\frac{n}{2}} \Delta_X h^2 + 2 I (-1)^{-\frac{n}{2}} \Delta_X n^2 + 4 I (-1)^{\frac{n}{2}} \Delta_X h^2 \right. \right. \\ & - 4 I (-1)^{\frac{n}{2}} \Delta_X n^2 - 2 I (-1)^{-\frac{n}{2}} \Delta_X n^4 + 4 I (-1)^{\frac{n}{2}} \Delta_X n^4 - I M \pi \cos(\theta) (-1)^{-\frac{n}{2}} \cos(\varphi) \sin(\Delta_Y) n^4 \\ & + I M \sin(\theta) \pi (-1)^{-\frac{n}{2}} \cos(\varphi) \cos(\Delta_Y) n^4 + I M \sin(\theta) \pi (-1)^{-\frac{n}{2}} \sin(\varphi) \sin(\Delta_Y) n^4 \\ & + I M \pi \cos(\theta) (-1)^{-\frac{n}{2}} \sin(\varphi) \cos(\Delta_Y) n^4 + I M_h \pi \cos\left(\frac{\pi h}{2}\right) \cos(\theta h) \cos(h \varphi) (-1)^{-\frac{n}{2}} \cos(h \Delta_Y) n^4 \\ & + I M_h \pi \cos\left(\frac{\pi h}{2}\right) \sin(\theta h) \cos(h \varphi) (-1)^{-\frac{n}{2}} \sin(h \Delta_Y) n^4 \\ & + I M_h \pi \sin\left(\frac{\pi h}{2}\right) \cos(\theta h) \sin(h \varphi) (-1)^{-\frac{n}{2}} \cos(h \Delta_Y) n^4 \\ & + (-1)^{-\frac{n}{2}} M_h \pi h n^3 \cos\left(\frac{\pi h}{2}\right) \sin(h \varphi) \cos(h \Delta_Y) \cos(\theta h) \\ & + (-1)^{-\frac{n}{2}} M_h \pi h n^3 \cos\left(\frac{\pi h}{2}\right) \sin(h \varphi) \sin(h \Delta_Y) \sin(\theta h) \\ & - (-1)^{-\frac{n}{2}} M_h \pi h n^3 \cos\left(\frac{\pi h}{2}\right) \cos(h \varphi) \sin(h \Delta_Y) \cos(\theta h) \\ & + (-1)^{-\frac{n}{2}} M_h \pi h n^3 \cos\left(\frac{\pi h}{2}\right) \cos(h \varphi) \cos(h \Delta_Y) \sin(\theta h) \\ & - (-1)^{-\frac{n}{2}} M_h \pi h n^3 \sin\left(\frac{\pi h}{2}\right) \cos(h \varphi) \cos(h \Delta_Y) \cos(\theta h) \\ & - (-1)^{-\frac{n}{2}} M_h \pi h n^3 \sin\left(\frac{\pi h}{2}\right) \cos(h \varphi) \sin(h \Delta_Y) \sin(\theta h) \\ & - (-1)^{-\frac{n}{2}} M_h \pi h n^3 \sin\left(\frac{\pi h}{2}\right) \sin(h \varphi) \sin(h \Delta_Y) \cos(\theta h) \\ & - I M_h \pi \cos\left(\frac{\pi h}{2}\right) \cos(\theta h) \sin(h \varphi) (-1)^{-\frac{n}{2}} \sin(h \Delta_Y) n^2 \\ & - I M_h \pi \cos\left(\frac{\pi h}{2}\right) \cos(\theta h) \cos(h \varphi) (-1)^{-\frac{n}{2}} \cos(h \Delta_Y) n^2 \\ & - I M_h \pi \cos\left(\frac{\pi h}{2}\right) \sin(\theta h) \cos(h \varphi) (-1)^{-\frac{n}{2}} \sin(h \Delta_Y) n^2 \\ & - I M_h \pi \sin\left(\frac{\pi h}{2}\right) \cos(\theta h) \sin(h \varphi) (-1)^{-\frac{n}{2}} \cos(h \Delta_Y) n^2 \\ & - I M_h \pi \sin\left(\frac{\pi h}{2}\right) \sin(\theta h) \sin(h \varphi) (-1)^{-\frac{n}{2}} \sin(h \Delta_Y) n^2 \\ & - I M_h \pi \sin\left(\frac{\pi h}{2}\right) \sin(\theta h) \cos(h \varphi) (-1)^{-\frac{n}{2}} \cos(h \Delta_Y) n^2 \\ & - I M_h \pi \cos\left(\frac{\pi h}{2}\right) \sin(\theta h) \sin(h \varphi) (-1)^{-\frac{n}{2}} \cos(h \Delta_Y) n^4 - I M \sin(\theta) \pi (-1)^{-\frac{n}{2}} \cos(\varphi) \cos(\Delta_Y) h^2 n^2 \\ & - I M \sin(\theta) \pi (-1)^{-\frac{n}{2}} \sin(\varphi) \sin(\Delta_Y) h^2 n^2 - I M \pi \cos(\theta) (-1)^{-\frac{n}{2}} \sin(\varphi) \cos(\Delta_Y) h^2 n^2 \end{aligned}$$

$$\begin{aligned}
& +IM\pi\cos(\theta\varphi)(-1)^{-\frac{n}{2}}\cos(\varphi)\sin(\Delta_Y)h^2n^2+IM_h\pi\sin\left(\frac{\pi h}{2}\right)\sin(\theta h)\sin(h\varphi)(-1)^{-\frac{n}{2}}\sin(h\Delta_Y)n^4 \\
& +IM_h\pi\sin\left(\frac{\pi h}{2}\right)\sin(\theta h)\cos(h\varphi)(-1)^{-\frac{n}{2}}\cos(h\Delta_Y)n^4 \\
& +IM_h\pi\cos\left(\frac{\pi h}{2}\right)\sin(\theta h)\sin(h\varphi)(-1)^{-\frac{n}{2}}\cos(h\Delta_Y)n^2 \\
& +IM_h\pi\sin\left(\frac{\pi h}{2}\right)\cos(\theta h)\cos(h\varphi)(-1)^{-\frac{n}{2}}\sin(h\Delta_Y)n^2 \\
& +IM_h\pi\cos\left(\frac{\pi h}{2}\right)\cos(\theta h)\sin(h\varphi)(-1)^{-\frac{n}{2}}\sin(h\Delta_Y)n^4 \\
& -IM_h\pi\sin\left(\frac{\pi h}{2}\right)\cos(\theta h)\cos(h\varphi)(-1)^{-\frac{n}{2}}\sin(h\Delta_Y)n^4 \\
& -IM_h\pi\cos\left(\frac{\pi h}{2}\right)\cos(\theta h)\cos(h\varphi)(-1)^{-\frac{n}{2}}n^4-IM_h\pi\sin\left(\frac{\pi h}{2}\right)\cos(\theta h)\sin(h\varphi)(-1)^{-\frac{n}{2}}n^4 \\
& -IM_h\pi\sin\left(\frac{\pi h}{2}\right)\sin(\theta h)\cos(h\varphi)(-1)^{-\frac{n}{2}}n^4-IM_h\pi\cos\left(\frac{\pi h}{2}\right)\sin(\theta h)\sin(h\varphi)(-1)^{-\frac{n}{2}}n^2 \\
& +2I(-1)^{\frac{3n}{2}}n^2\Delta_X-IM\sin(\theta\varphi)\pi(-1)^{-\frac{n}{2}}\cos(\varphi)n^4-IM\pi\cos(\theta\varphi)(-1)^{-\frac{n}{2}}\sin(\varphi)n^4 \\
& -2I(-1)^{\frac{3n}{2}}n^4\Delta_X-2I(-1)^{\frac{3n}{2}}h^2\Delta_X+2I(-1)^{-\frac{n}{2}}\Delta_Xh^2n^2-4I(-1)^{\frac{n}{2}}\Delta_Xh^2n^2 \\
& +IM\sin(\theta\varphi)\pi(-1)^{-\frac{n}{2}}\cos(\varphi)h^2n^2+IM\pi\cos(\theta\varphi)(-1)^{-\frac{n}{2}}\sin(\varphi)h^2n^2 \\
& +IM_h\pi\cos\left(\frac{\pi h}{2}\right)\sin(\theta h)\sin(h\varphi)(-1)^{-\frac{n}{2}}n^4+IM_h\pi\cos\left(\frac{\pi h}{2}\right)\cos(\theta h)\cos(h\varphi)(-1)^{-\frac{n}{2}}n^2 \\
& +IM_h\pi\sin\left(\frac{\pi h}{2}\right)\cos(\theta h)\sin(h\varphi)(-1)^{-\frac{n}{2}}n^2+IM_h\pi\sin\left(\frac{\pi h}{2}\right)\sin(\theta h)\cos(h\varphi)(-1)^{-\frac{n}{2}}n^2 \\
& +(-1)^{-\frac{n}{2}}M_h\pi hn^3\sin\left(\frac{\pi h}{2}\right)\sin(h\varphi)\cos(h\Delta_Y)\sin(\theta h) \\
& +(-1)^{-\frac{n}{2}}M_h\pi hn\sin\left(\frac{\pi h}{2}\right)\cos(h\varphi)\cos(h\Delta_Y)\cos(\theta h) \\
& +(-1)^{-\frac{n}{2}}M_h\pi hn\sin\left(\frac{\pi h}{2}\right)\cos(h\varphi)\sin(h\Delta_Y)\sin(\theta h) \\
& +(-1)^{-\frac{n}{2}}M_h\pi hn\sin\left(\frac{\pi h}{2}\right)\sin(h\varphi)\sin(h\Delta_Y)\cos(\theta h) \\
& -(-1)^{-\frac{n}{2}}M_h\pi hn\sin\left(\frac{\pi h}{2}\right)\sin(h\varphi)\cos(h\Delta_Y)\sin(\theta h) \\
& -(-1)^{-\frac{n}{2}}M_h\pi hn\cos\left(\frac{\pi h}{2}\right)\sin(h\varphi)\cos(h\Delta_Y)\cos(\theta h) \\
& -(-1)^{-\frac{n}{2}}M_h\pi hn\cos\left(\frac{\pi h}{2}\right)\sin(h\varphi)\sin(h\Delta_Y)\sin(\theta h) \\
& +(-1)^{-\frac{n}{2}}M_h\pi hn\cos\left(\frac{\pi h}{2}\right)\cos(h\varphi)\sin(h\Delta_Y)\cos(\theta h) \\
& -(-1)^{-\frac{n}{2}}M_h\pi hn\cos\left(\frac{\pi h}{2}\right)\cos(h\varphi)\cos(h\Delta_Y)\sin(\theta h)+2I(-1)^{\frac{3n}{2}}h^2n^2\Delta_X \\
& +(-1)^{-\frac{n}{2}}M\pi n^3\cos(\varphi)\cos(\theta\varphi)-(-1)^{-\frac{n}{2}}M\pi n^3\sin(\varphi)\sin(\theta\varphi) \\
& -(-1)^{\frac{3n}{2}}M_h\pi hn\cos\left(\frac{3\pi h}{2}\right)\sin(h\varphi)\cos(\theta h)-(-1)^{\frac{3n}{2}}M_h\pi hn\cos\left(\frac{3\pi h}{2}\right)\cos(h\varphi)\sin(\theta h) \\
& +(-1)^{\frac{3n}{2}}M_h\pi hn^3\sin\left(\frac{3\pi h}{2}\right)\cos(h\varphi)\cos(\theta h)+I(-1)^{\frac{3n}{2}}M_h\pi n^4\cos\left(\frac{3\pi h}{2}\right)\cos(h\varphi)\cos(\theta h) \\
& +I(-1)^{\frac{3n}{2}}M_h\pi n^2\cos\left(\frac{3\pi h}{2}\right)\sin(h\varphi)\sin(\theta h)+I(-1)^{\frac{3n}{2}}M_h\pi n^2\sin\left(\frac{3\pi h}{2}\right)\sin(h\varphi)\cos(\theta h)
\end{aligned}$$

$$\begin{aligned}
& + I(-1)^{\frac{3n}{2}} M_- h \pi n^2 \sin\left(\frac{3\pi h}{2}\right) \cos(h\varphi) \sin(\theta h) - I(-1)^{\frac{3n}{2}} M \pi h^2 n^2 \sin(\varphi) \cos(\theta\varphi) \\
& - I(-1)^{\frac{3n}{2}} M_- h \pi n^4 \cos\left(\frac{3\pi h}{2}\right) \sin(h\varphi) \sin(\theta h) - I(-1)^{\frac{3n}{2}} M_- h \pi n^4 \sin\left(\frac{3\pi h}{2}\right) \sin(h\varphi) \cos(\theta h) \\
& - I(-1)^{\frac{3n}{2}} M_- h \pi n^4 \sin\left(\frac{3\pi h}{2}\right) \cos(h\varphi) \sin(\theta h) - I(-1)^{\frac{3n}{2}} M_- h \pi n^2 \cos\left(\frac{3\pi h}{2}\right) \cos(h\varphi) \cos(\theta h) \\
& - I(-1)^{\frac{3n}{2}} M \pi h^2 n^2 \cos(\varphi) \sin(\theta\varphi) + I(-1)^{\frac{3n}{2}} M \pi n^4 \cos(\varphi) \sin(\Delta_\gamma) \cos(\theta\varphi) \\
& - (-1)^{\frac{3n}{2}} M \pi h^2 n \cos(\varphi) \cos(\Delta_\gamma) \cos(\theta\varphi) - (-1)^{\frac{3n}{2}} M \pi h^2 n \cos(\varphi) \sin(\Delta_\gamma) \sin(\theta\varphi) \\
& - (-1)^{\frac{3n}{2}} M \pi h^2 n \sin(\varphi) \sin(\Delta_\gamma) \cos(\theta\varphi) + (-1)^{\frac{3n}{2}} M \pi h^2 n \sin(\varphi) \cos(\Delta_\gamma) \sin(\theta\varphi) \\
& - (-1)^{\frac{3n}{2}} M_- h \pi h n^3 \sin\left(\frac{3\pi h}{2}\right) \sin(h\varphi) \sin(\theta h) + (-1)^{\frac{3n}{2}} M_- h \pi h n^3 \cos\left(\frac{3\pi h}{2}\right) \sin(h\varphi) \cos(\theta h) \\
& + (-1)^{\frac{3n}{2}} M_- h \pi h n^3 \cos\left(\frac{3\pi h}{2}\right) \cos(h\varphi) \sin(\theta h) - (-1)^{\frac{3n}{2}} M_- h \pi h n \sin\left(\frac{3\pi h}{2}\right) \cos(h\varphi) \cos(\theta h) \\
& + (-1)^{\frac{3n}{2}} M_- h \pi h n \sin\left(\frac{3\pi h}{2}\right) \sin(h\varphi) \sin(\theta h) - I(-1)^{\frac{3n}{2}} M \pi n^4 \sin(\varphi) \cos(\Delta_\gamma) \cos(\theta\varphi) \\
& - I(-1)^{\frac{3n}{2}} M \pi n^4 \sin(\varphi) \sin(\Delta_\gamma) \sin(\theta\varphi) - I(-1)^{\frac{3n}{2}} M \pi n^4 \cos(\varphi) \cos(\Delta_\gamma) \sin(\theta\varphi) \\
& + (-1)^{-\frac{n}{2}} M \pi h^2 n \sin(\varphi) \sin(\theta\varphi) - (-1)^{-\frac{n}{2}} M \pi n^3 \cos(\varphi) \cos(\Delta_\gamma) \cos(\theta\varphi) \\
& - (-1)^{-\frac{n}{2}} M \pi n^3 \cos(\varphi) \sin(\Delta_\gamma) \sin(\theta\varphi) - (-1)^{-\frac{n}{2}} M \pi n^3 \sin(\varphi) \sin(\Delta_\gamma) \cos(\theta\varphi) \\
& + (-1)^{-\frac{n}{2}} M \pi n^3 \sin(\varphi) \cos(\Delta_\gamma) \sin(\theta\varphi) - (-1)^{-\frac{n}{2}} M \pi h^2 n \cos(\varphi) \cos(\theta\varphi) \\
& + (-1)^{-\frac{n}{2}} M_- h \pi h n^3 \sin\left(\frac{\pi h}{2}\right) \cos(h\varphi) \cos(\theta h) - (-1)^{-\frac{n}{2}} M_- h \pi h n^3 \sin\left(\frac{\pi h}{2}\right) \sin(h\varphi) \sin(\theta h) \\
& - (-1)^{-\frac{n}{2}} M_- h \pi h n \sin\left(\frac{\pi h}{2}\right) \cos(h\varphi) \cos(\theta h) + (-1)^{-\frac{n}{2}} M_- h \pi h n \sin\left(\frac{\pi h}{2}\right) \sin(h\varphi) \sin(\theta h) \\
& + (-1)^{-\frac{n}{2}} M_- h \pi h n \cos\left(\frac{\pi h}{2}\right) \sin(h\varphi) \cos(\theta h) + (-1)^{-\frac{n}{2}} M_- h \pi h n \cos\left(\frac{\pi h}{2}\right) \cos(h\varphi) \sin(\theta h) \\
& - (-1)^{-\frac{n}{2}} M_- h \pi h n^3 \cos\left(\frac{\pi h}{2}\right) \sin(h\varphi) \cos(\theta h) - (-1)^{-\frac{n}{2}} M_- h \pi h n^3 \cos\left(\frac{\pi h}{2}\right) \cos(h\varphi) \sin(\theta h) \\
& + (-1)^{-\frac{n}{2}} M \pi h^2 n \cos(\varphi) \cos(\Delta_\gamma) \cos(\theta\varphi) + (-1)^{-\frac{n}{2}} M \pi h^2 n \cos(\varphi) \sin(\Delta_\gamma) \sin(\theta\varphi) \\
& + (-1)^{-\frac{n}{2}} M \pi h^2 n \sin(\varphi) \sin(\Delta_\gamma) \cos(\theta\varphi) - (-1)^{-\frac{n}{2}} M \pi h^2 n \sin(\varphi) \cos(\Delta_\gamma) \sin(\theta\varphi) \\
& - (-1)^{\frac{3n}{2}} M \pi n^3 \cos(\varphi) \cos(\theta\varphi) + (-1)^{\frac{3n}{2}} M \pi n^3 \sin(\varphi) \sin(\theta\varphi) \\
& + (-1)^{\frac{3n}{2}} M \pi n^3 \cos(\varphi) \cos(\Delta_\gamma) \cos(\theta\varphi) + (-1)^{\frac{3n}{2}} M \pi n^3 \cos(\varphi) \sin(\Delta_\gamma) \sin(\theta\varphi) \\
& + (-1)^{\frac{3n}{2}} M \pi n^3 \sin(\varphi) \sin(\Delta_\gamma) \cos(\theta\varphi) - (-1)^{\frac{3n}{2}} M \pi n^3 \sin(\varphi) \cos(\Delta_\gamma) \sin(\theta\varphi) \\
& + (-1)^{\frac{3n}{2}} M \pi h^2 n \cos(\varphi) \cos(\theta\varphi) - (-1)^{\frac{3n}{2}} M \pi h^2 n \sin(\varphi) \sin(\theta\varphi) + I(-1)^{\frac{3n}{2}} M \pi n^4 \sin(\varphi) \cos(\theta\varphi) \\
& + I(-1)^{\frac{3n}{2}} M \pi n^4 \cos(\varphi) \sin(\theta\varphi) - I(-1)^{\frac{3n}{2}} M_- h \pi n^4 \cos\left(\frac{3\pi h}{2}\right) \sin(h\varphi) \sin(h\Delta_\gamma) \cos(\theta h) \\
& + (-1)^{\frac{3n}{2}} M_- h \pi h n \sin\left(\frac{3\pi h}{2}\right) \cos(h\varphi) \sin(h\Delta_\gamma) \sin(\theta h) \\
& + (-1)^{\frac{3n}{2}} M_- h \pi h n \sin\left(\frac{3\pi h}{2}\right) \sin(h\varphi) \sin(h\Delta_\gamma) \cos(\theta h)
\end{aligned} \tag{24}$$

$$\begin{aligned}
& - (-1)^{\frac{3n}{2}} M_h \pi h n \sin\left(\frac{3\pi h}{2}\right) \sin(h\varphi) \cos(h\Delta_y) \sin(\theta h) \\
& + (-1)^{\frac{3n}{2}} M_h \pi h n \cos\left(\frac{3\pi h}{2}\right) \sin(h\varphi) \cos(h\Delta_y) \cos(\theta h) \\
& + (-1)^{\frac{3n}{2}} M_h \pi h n \cos\left(\frac{3\pi h}{2}\right) \sin(h\varphi) \sin(h\Delta_y) \sin(\theta h) \\
& - (-1)^{\frac{3n}{2}} M_h \pi h n \cos\left(\frac{3\pi h}{2}\right) \cos(h\varphi) \sin(h\Delta_y) \cos(\theta h) \\
& + (-1)^{\frac{3n}{2}} M_h \pi h n \cos\left(\frac{3\pi h}{2}\right) \cos(h\varphi) \cos(h\Delta_y) \sin(\theta h) \\
& - (-1)^{\frac{3n}{2}} M_h \pi h n^3 \sin\left(\frac{3\pi h}{2}\right) \cos(h\varphi) \cos(h\Delta_y) \cos(\theta h) \\
& + (-1)^{\frac{3n}{2}} M_h \pi h n^3 \sin\left(\frac{3\pi h}{2}\right) \sin(h\varphi) \cos(h\Delta_y) \sin(\theta h) \\
& - (-1)^{\frac{3n}{2}} M_h \pi h n^3 \cos\left(\frac{3\pi h}{2}\right) \sin(h\varphi) \cos(h\Delta_y) \cos(\theta h) \\
& - (-1)^{\frac{3n}{2}} M_h \pi h n^3 \cos\left(\frac{3\pi h}{2}\right) \sin(h\varphi) \sin(h\Delta_y) \sin(\theta h) \\
& + (-1)^{\frac{3n}{2}} M_h \pi h n^3 \cos\left(\frac{3\pi h}{2}\right) \cos(h\varphi) \sin(h\Delta_y) \cos(\theta h) \\
& - (-1)^{\frac{3n}{2}} M_h \pi h n^3 \cos\left(\frac{3\pi h}{2}\right) \cos(h\varphi) \cos(h\Delta_y) \sin(\theta h) \\
& + I (-1)^{\frac{3n}{2}} M \pi h^2 n^2 \sin(\varphi) \cos(\Delta_y) \cos(\theta\varphi) \\
& - (-1)^{\frac{3n}{2}} M_h \pi h n^3 \sin\left(\frac{3\pi h}{2}\right) \cos(h\varphi) \sin(h\Delta_y) \sin(\theta h) \\
& - (-1)^{\frac{3n}{2}} M_h \pi h n^3 \sin\left(\frac{3\pi h}{2}\right) \sin(h\varphi) \sin(h\Delta_y) \cos(\theta h) \\
& + I (-1)^{\frac{3n}{2}} M \pi h^2 n^2 \sin(\varphi) \sin(\Delta_y) \sin(\theta\varphi) + I (-1)^{\frac{3n}{2}} M \pi h^2 n^2 \cos(\varphi) \cos(\Delta_y) \sin(\theta\varphi) \\
& - I (-1)^{\frac{3n}{2}} M_h \pi n^4 \sin\left(\frac{3\pi h}{2}\right) \cos(h\varphi) \sin(h\Delta_y) \cos(\theta h) \\
& - I (-1)^{\frac{3n}{2}} M \pi h^2 n^2 \cos(\varphi) \sin(\Delta_y) \cos(\theta\varphi) \\
& - I (-1)^{\frac{3n}{2}} M_h \pi n^2 \cos\left(\frac{3\pi h}{2}\right) \sin(h\varphi) \cos(h\Delta_y) \sin(\theta h) \\
& - I (-1)^{\frac{3n}{2}} M_h \pi n^2 \sin\left(\frac{3\pi h}{2}\right) \sin(h\varphi) \cos(h\Delta_y) \cos(\theta h) \\
& - I (-1)^{\frac{3n}{2}} M_h \pi n^2 \sin\left(\frac{3\pi h}{2}\right) \sin(h\varphi) \sin(h\Delta_y) \sin(\theta h) \\
& - I (-1)^{\frac{3n}{2}} M_h \pi n^2 \sin\left(\frac{3\pi h}{2}\right) \cos(h\varphi) \cos(h\Delta_y) \sin(\theta h) \\
& - I (-1)^{\frac{3n}{2}} M_h \pi n^4 \cos\left(\frac{3\pi h}{2}\right) \cos(h\varphi) \cos(h\Delta_y) \cos(\theta h) \\
& - I (-1)^{\frac{3n}{2}} M_h \pi n^4 \cos\left(\frac{3\pi h}{2}\right) \cos(h\varphi) \sin(h\Delta_y) \sin(\theta h) \\
& + I (-1)^{\frac{3n}{2}} M_h \pi n^2 \sin\left(\frac{3\pi h}{2}\right) \cos(h\varphi) \sin(h\Delta_y) \cos(\theta h) \\
& + I (-1)^{\frac{3n}{2}} M_h \pi n^4 \cos\left(\frac{3\pi h}{2}\right) \sin(h\varphi) \cos(h\Delta_y) \sin(\theta h) \\
& + I (-1)^{\frac{3n}{2}} M_h \pi n^4 \sin\left(\frac{3\pi h}{2}\right) \sin(h\varphi) \cos(h\Delta_y) \cos(\theta h)
\end{aligned}$$

$$\begin{aligned}
& + I (-1)^{\frac{3n}{2}} M_h \pi n^4 \sin\left(\frac{3\pi h}{2}\right) \sin(h\varphi) \sin(h\Delta_y) \sin(\theta h) \\
& + I (-1)^{\frac{3n}{2}} M_h \pi n^4 \sin\left(\frac{3\pi h}{2}\right) \cos(h\varphi) \cos(h\Delta_y) \sin(\theta h) \\
& + I (-1)^{\frac{3n}{2}} M_h \pi n^2 \cos\left(\frac{3\pi h}{2}\right) \cos(h\varphi) \cos(h\Delta_y) \cos(\theta h) \\
& + I (-1)^{\frac{3n}{2}} M_h \pi n^2 \cos\left(\frac{3\pi h}{2}\right) \cos(h\varphi) \sin(h\Delta_y) \sin(\theta h) \\
& + I (-1)^{\frac{3n}{2}} M_h \pi n^2 \cos\left(\frac{3\pi h}{2}\right) \sin(h\varphi) \sin(h\Delta_y) \cos(\theta h) \\
& + (-1)^{\frac{3n}{2}} M_h \pi h n \sin\left(\frac{3\pi h}{2}\right) \cos(h\varphi) \cos(h\Delta_y) \cos(\theta h) \left(\cos(n\varphi) + I \sin(n\varphi) \right) v_{dc}
\end{aligned}$$

Analysis simplifying periodic terms

$$\begin{aligned}
& seq\left((-1)^{-\frac{n}{2}}, n = 2..10, 1 \right) \\
& \qquad \qquad \qquad -1, I, 1, -I, -1, I, 1, -I, -1
\end{aligned} \tag{25}$$

$$\begin{aligned}
& seq\left((-1)^{\frac{3n}{2}}, n = 2..10, 1 \right) \\
& \qquad \qquad \qquad -1, I, 1, -I, -1, I, 1, -I, -1
\end{aligned} \tag{26}$$

$$\begin{aligned}
& seq\left(\sin\left(\frac{\pi h}{2}\right), h = 2..10, 1 \right) \\
& \qquad \qquad \qquad 0, -1, 0, 1, 0, -1, 0, 1, 0
\end{aligned} \tag{27}$$

$$\begin{aligned}
& seq\left(\sin\left(\frac{3\pi h}{2}\right), h = 2..10, 1 \right) \\
& \qquad \qquad \qquad 0, 1, 0, -1, 0, 1, 0, -1, 0
\end{aligned} \tag{28}$$

$$\begin{aligned}
& seq\left(\cos\left(\frac{\pi h}{2}\right), h = 2..10, 1 \right) \\
& \qquad \qquad \qquad -1, 0, 1, 0, -1, 0, 1, 0, -1
\end{aligned} \tag{29}$$

$$\begin{aligned}
& seq\left(\cos\left(\frac{3\pi h}{2}\right), h = 2..10, 1 \right) \\
& \qquad \qquad \qquad -1, 0, 1, 0, -1, 0, 1, 0, -1
\end{aligned} \tag{30}$$

$$C0n := \text{factor} \left(\text{eval} \left(C0n, \left[(-1)^{\frac{3n}{2}} = (-1)^{-\frac{n}{2}}, \cos \left(\frac{3\pi h}{2} \right) = \cos \left(\frac{\pi h}{2} \right), \sin \left(\frac{3\pi h}{2} \right) = -\sin \left(\frac{\pi h}{2} \right) \right] \right) \right)$$

$$C0n := \frac{-2 I (\cos(n \varphi) + I \sin(n \varphi)) \left((-1)^{-\frac{n}{2}} - (-1)^{\frac{n}{2}} \right) \Delta_X v_{dc}}{n \pi^2} \quad (31)$$

$$\text{seq} \left((-1)^{-\frac{n}{2}}, n = 2..10, 1 \right)$$

$$-1, I, 1, -I, -1, I, 1, -I, -1 \quad (32)$$

$$\text{seq} \left((-1)^{\frac{n}{2}}, n = 2..10, 1 \right)$$

$$-1, -I, 1, I, -1, -I, 1, I, -1 \quad (33)$$

For even values of n

$$C0n_even := \text{factor} \left(\text{eval} \left(C0n, \left[(-1)^{-\frac{n}{2}} = (-1)^{\frac{n}{2}} \right] \right) \right); \text{correctionBasebandHarmonics_even} := 0;$$

$$C0n_even := 0$$

$$\text{correctionBasebandHarmonics_even} := 0 \quad (34)$$

For odd values of n

$$C0n_odd := \text{factor} \left(\text{eval} \left(C0n, \left[(-1)^{-\frac{n}{2}} = -(-1)^{\frac{n}{2}} \right] \right) \right);$$

$$\text{convert}(C0n_odd, \text{exp});$$

$$A0n := \text{evalc}(\text{Re}(C0n_odd)) \text{ assuming } v_{dc} :: \text{real}, M :: \text{real}, \Delta_{\ominus} :: \text{real}, \Delta_{\ominus} :: \text{real}, \varphi :: \text{real}, n :: \text{posint};$$

$$B0n := \text{evalc}(\text{Im}(C0n_odd)) \text{ assuming } v_{dc} :: \text{real}, M :: \text{real}, \Delta_{\ominus} :: \text{real}, \Delta_{\ominus} :: \text{real}, \varphi :: \text{real}, n :: \text{posint};$$

$$n\text{Harmonics} := A0n \cos(n \cdot \text{omega}[o] \cdot t) + B0n \sin(n \cdot \text{omega}[o] \cdot t);$$

$$\text{correctionBasebandHarmonics_odd} := \text{combine}(n\text{Harmonics})$$

$$\begin{aligned}
C0n_odd &:= \frac{4 I (\cos(n \varphi) + I \sin(n \varphi)) (-1)^{\frac{n}{2}} \Delta_X v_{dc}}{n \pi^2} \\
&\frac{4 I e^{I n \varphi} e^{\frac{I}{2} \pi n} \Delta_X v_{dc}}{n \pi^2} \\
A0n &:= - \frac{4 v_{dc} \left(\sin\left(\frac{n \pi}{2}\right) \Delta_X \cos(n \varphi) + \cos\left(\frac{n \pi}{2}\right) \Delta_X \sin(n \varphi) \right)}{n \pi^2} \\
B0n &:= \frac{4 v_{dc} \left(\cos\left(\frac{n \pi}{2}\right) \Delta_X \cos(n \varphi) - \sin\left(\frac{n \pi}{2}\right) \Delta_X \sin(n \varphi) \right)}{n \pi^2} \\
correctionBasebandHarmonics_odd &:= \frac{4 \Delta_X v_{dc} \sin\left(-\frac{1}{2} n \pi - n \varphi + n \omega_o t\right)}{n \pi^2} \quad (35)
\end{aligned}$$

Conclusions:

- the arbitrary phase of the voltage does not influence the baseband component of the dead-time
- it is proportional to DeltaX and Vdc with a proportional constant of 4/Pi^2
- it is inverse proportional to the harmonic number
- the injected harmonic do not affects the baseband harmonics introduced by the dead time

Single-phase Converter (three-level)

Ideal VaN

$$ideal_v[aN] := idealOffset + idealFundamental + idealBaseband_h$$

$$ideal_v_{aN} := v_{dc} + M v_{dc} \cos(\omega_o t + \theta_o) + \cos(h t \omega_o + \Theta h) v_{dc} M_h \quad (36)$$

$$\text{Correction VaN } correction_v[aN] := correctionOffset + correctionBasebandHarmonics_odd$$

$$correction_v_{aN} := \frac{4 \Delta_X v_{dc} \sin\left(-\frac{1}{2} n \pi - n \varphi + n \omega_o t\right)}{n \pi^2} \quad (37)$$

$$\text{VaN } v[aN] := ideal_v[aN] + correction_v[aN]$$

$$v_{aN} := v_{dc} + M v_{dc} \cos(\omega_o t + \Theta_o) + \cos(h t \omega_o + \Theta_h) v_{dc} M_h + \frac{4 \Delta_X v_{dc} \sin\left(-\frac{1}{2} n \pi - n \varphi + n \omega_o t\right)}{n \pi^2} \quad (38)$$

Ideal VbN $ideal_v[bN] := eval(ideal_v[aN], [\omega_o t = \omega_o t + \text{Pi}, h \omega_o t = h \omega_o t + h \text{Pi}])$

$$ideal_v_{bN} := v_{dc} - M v_{dc} \cos(\omega_o t + \Theta_o) + \cos(h t \omega_o + \pi h + \Theta_h) v_{dc} M_h \quad (39)$$

Correction VbN

$correction_v[bN] := eval(correction_v[aN], [n \omega_o t = n \omega_o t + n \text{Pi}])$

$$correction_v_{bN} := \frac{4 \Delta_X v_{dc} \sin\left(\frac{1}{2} n \pi - n \varphi + n \omega_o t\right)}{n \pi^2} \quad (40)$$

Ideal Vab

$ideal_v[ab] := ideal_v[aN] - ideal_v[bN]$

$$ideal_v_{ab} := 2 M v_{dc} \cos(\omega_o t + \Theta_o) + \cos(h t \omega_o + \Theta_h) v_{dc} M_h - \cos(h t \omega_o + \pi h + \Theta_h) v_{dc} M_h \quad (41)$$

$seq(-\cos(h t \omega_o + \pi h + \Theta_h), h = 3..9, 1)$

$$\cos(3 \omega_o t + \Theta_h), -\cos(4 \omega_o t + \Theta_h), \cos(5 \omega_o t + \Theta_h), -\cos(6 \omega_o t + \Theta_h), \cos(7 \omega_o t + \Theta_h), -\cos(8 \omega_o t + \Theta_h), \cos(9 \omega_o t + \Theta_h) \quad (42)$$

$ideal_v[ab] := (simplify(eval(ideal_v[ab], [h t \omega_o + \Theta_h = u, h t \omega_o + \pi h + \Theta_h = u + \pi h]))) \text{ assuming } h::\text{posint}$

$$ideal_v_{ab} := 2 \left(M \cos(\omega_o t + \Theta_o) - \frac{M_h \cos(u) \left((-1)^h - 1 \right)}{2} \right) v_{dc} \quad (43)$$

$seq((-1)^h - 1, h = 1..9, 1)$

$$-2, 0, -2, 0, -2, 0, -2, 0, -2 \quad (44)$$

$idealOdd_v[ab] := eval(ideal_v[ab], [(-1)^h - 1 = -2, u = h t \omega_o + \Theta_h])$

$$idealOdd_v_{ab} := 2 (M \cos(\omega_o t + \Theta_o) + M_h \cos(h t \omega_o + \Theta_h)) v_{dc} \quad (45)$$

Appendix D

PSCADTM Simulation Diagrams

This appendix shows the implementation of all simulations performed in this thesis using *PSCADTM* blocks.

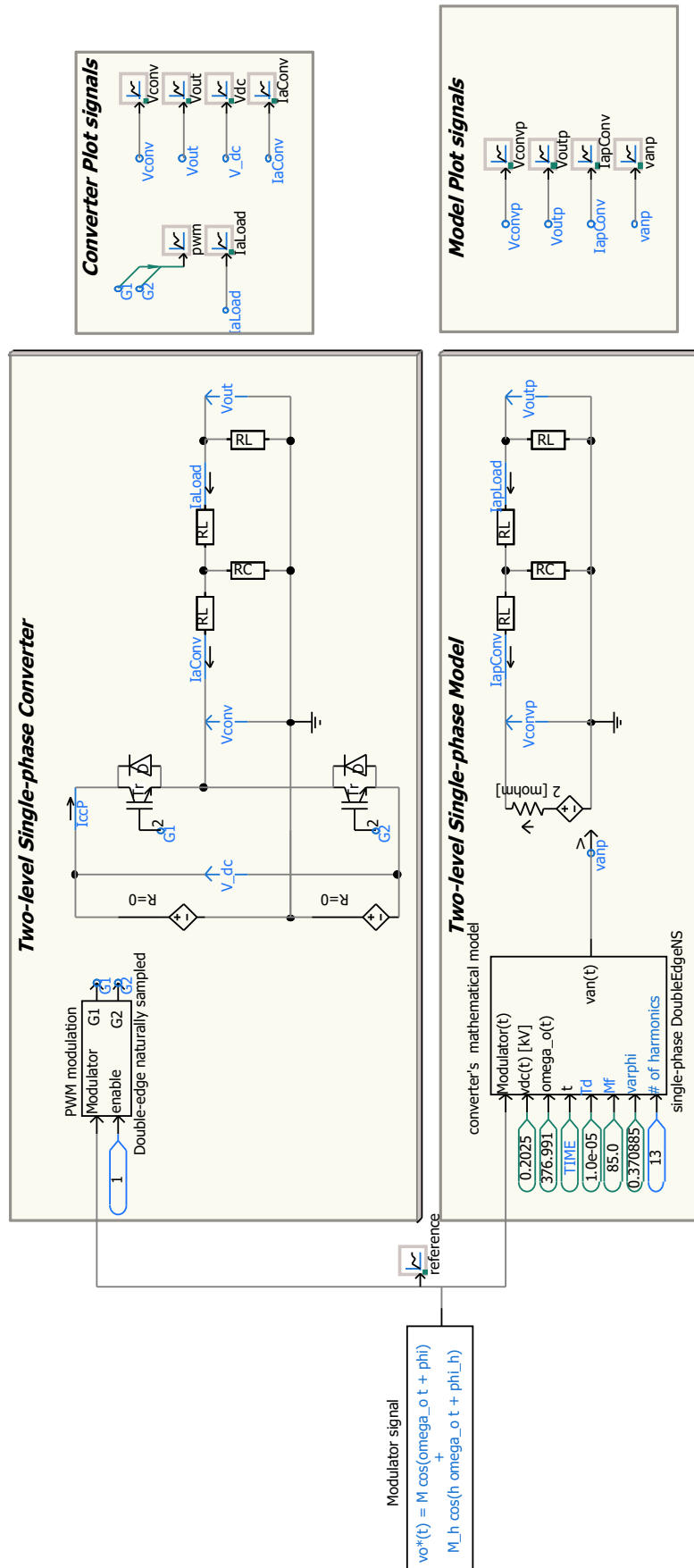


Figure D.1 - PSCADTM simulation of the two-levels single-phase VSI used in chapter 3.

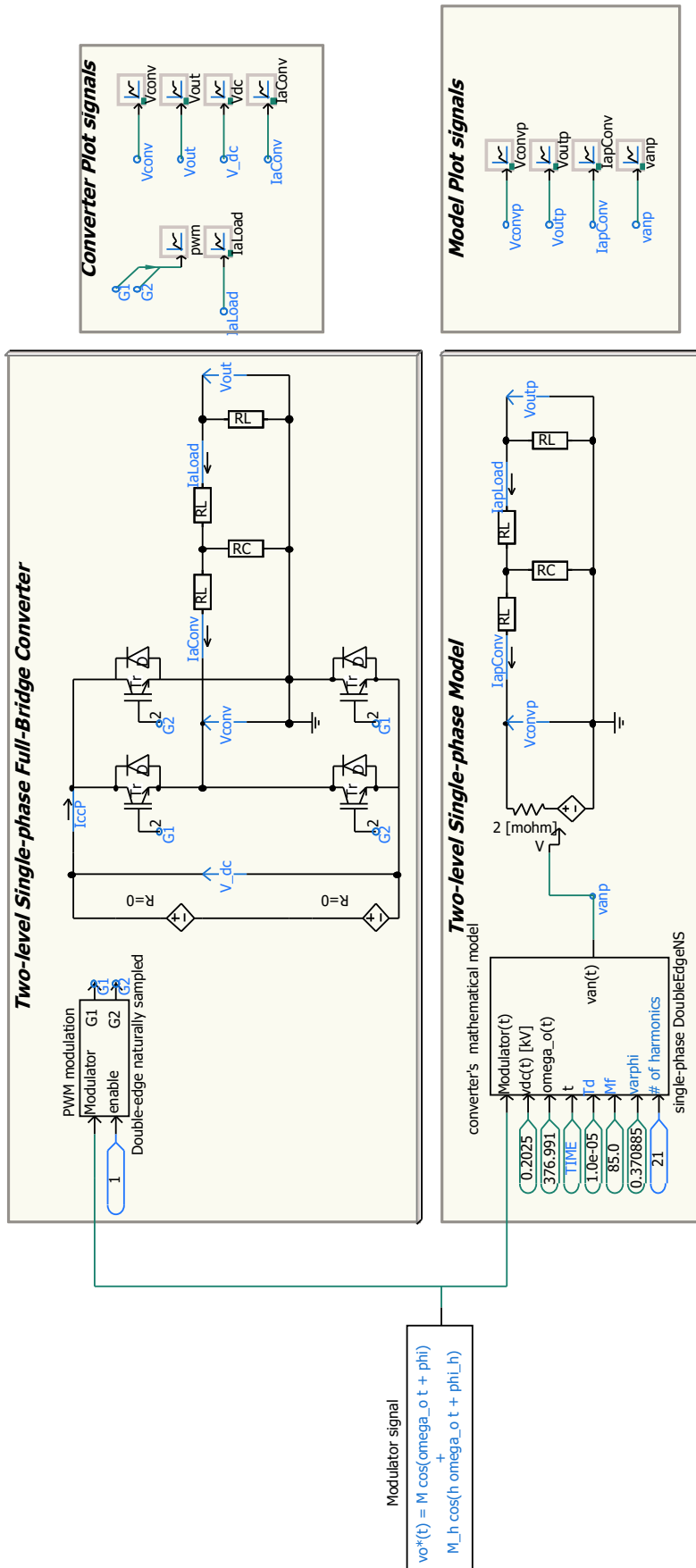


Figure D.2 - PSCADTM simulation of the two levels single-phase full-bridge VSI used in chapter 3.

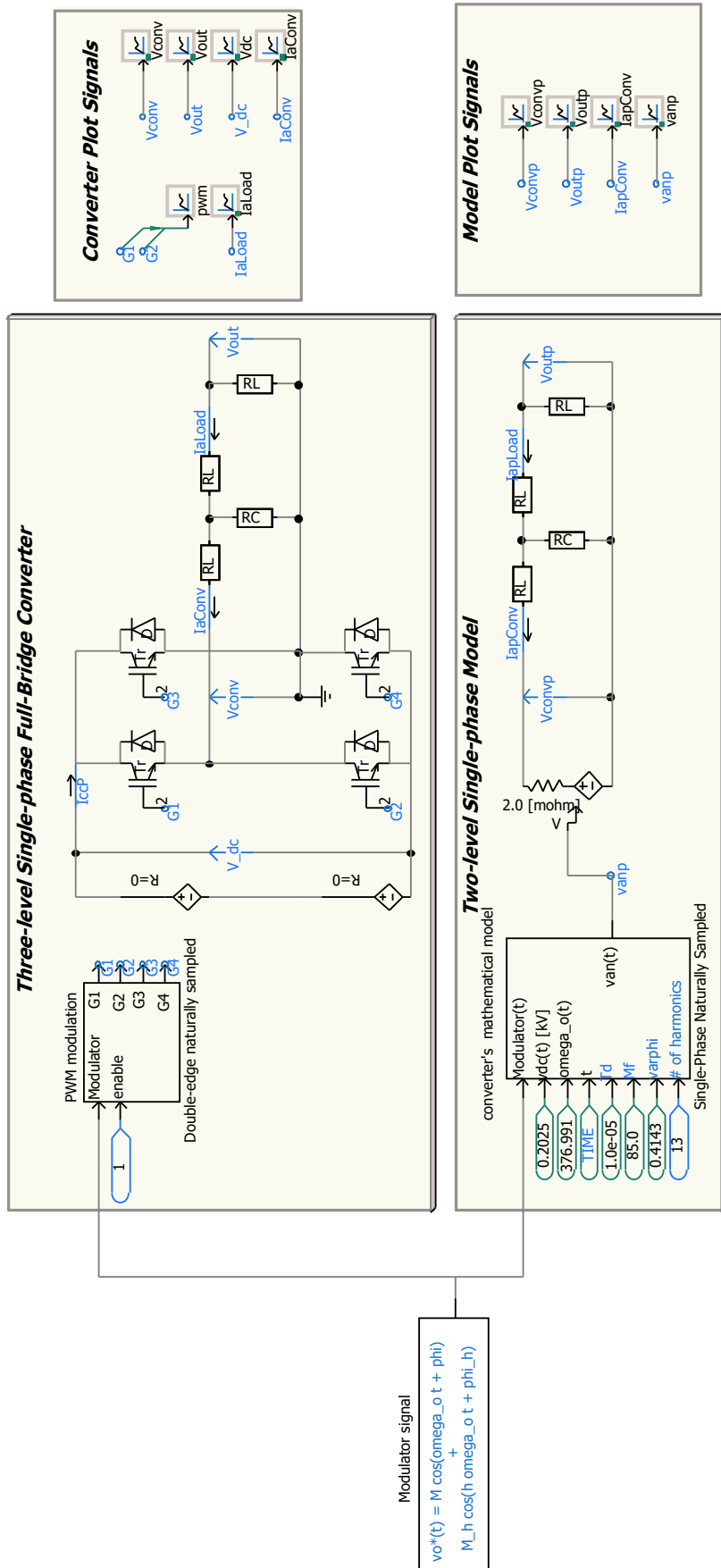


Figure D.3 - PSCADTM simulation of the three levels single-phase full-bridge VSI used in chapter 3.

Appendix E

PwmSpectra Package

Using the theoretical development presented in Chapter 3, a *Wolfram Mathematica*[®] package application called *PwmSpectra* was built. This application provides simple analytical and numerical functions to facilitate the study of digital and analog *PWM* schemes. *PwmSpectra* was published as an open software project available for download and development under the *Academic Free License v3.0 (AFL3)* [46].

This appendix details the structure and provides several examples of *PwmSpectra* applications.

E.1 *PwmSpectra* Details

PwmSpectra is an open project of a *Wolfram Mathematica*[®] package application developed to provide a quick and straightforward framework for studying analog and digital *PWM* schemes. The principal characteristics are listed below:

- *Test Driven Development (TDD)* with up to one hundred and ten built-in unit-tests.
- Numerical results for a set of harmonic components.
- Analytical expressions for the low-frequency spectra of analog *PWM* schemes.
- Analytical boundary expressions for Naturally and regular sampled *PWM* schemes.
- Plot function to understand the numerical distribution of the samples used by the numerical integration method.
- Vectors plot of the ideal, correction, and corrected terms for a specific component.
- Multiple spectra of a selected *PWM* scheme for a linear variation of any parameter.
- Multiple plots of the behavior of each component for a given parameter variation.
- Export analytical expression to *MATLAB*[®] symbolic toolbox.
- Pre-defined single- and multiple-frequency test case scenarios.
- Dark-mode option in all plot functions.
- *PwmSpectra* is available for download and development in a *GIT* public repository, <https://github.com/jrgcaicedo/PwmSpectra>.
- license: *Academic Free License v3.0 (AFL3)*.

The initial diagram of the architecture of *PwmSpectra* and an illustrative example using this package application is shown in the following sections.

E.2 UML Diagram V1.0

Figure E.1 uses a class representation to illustrate the relationship of the *PwmSpectra* packages.

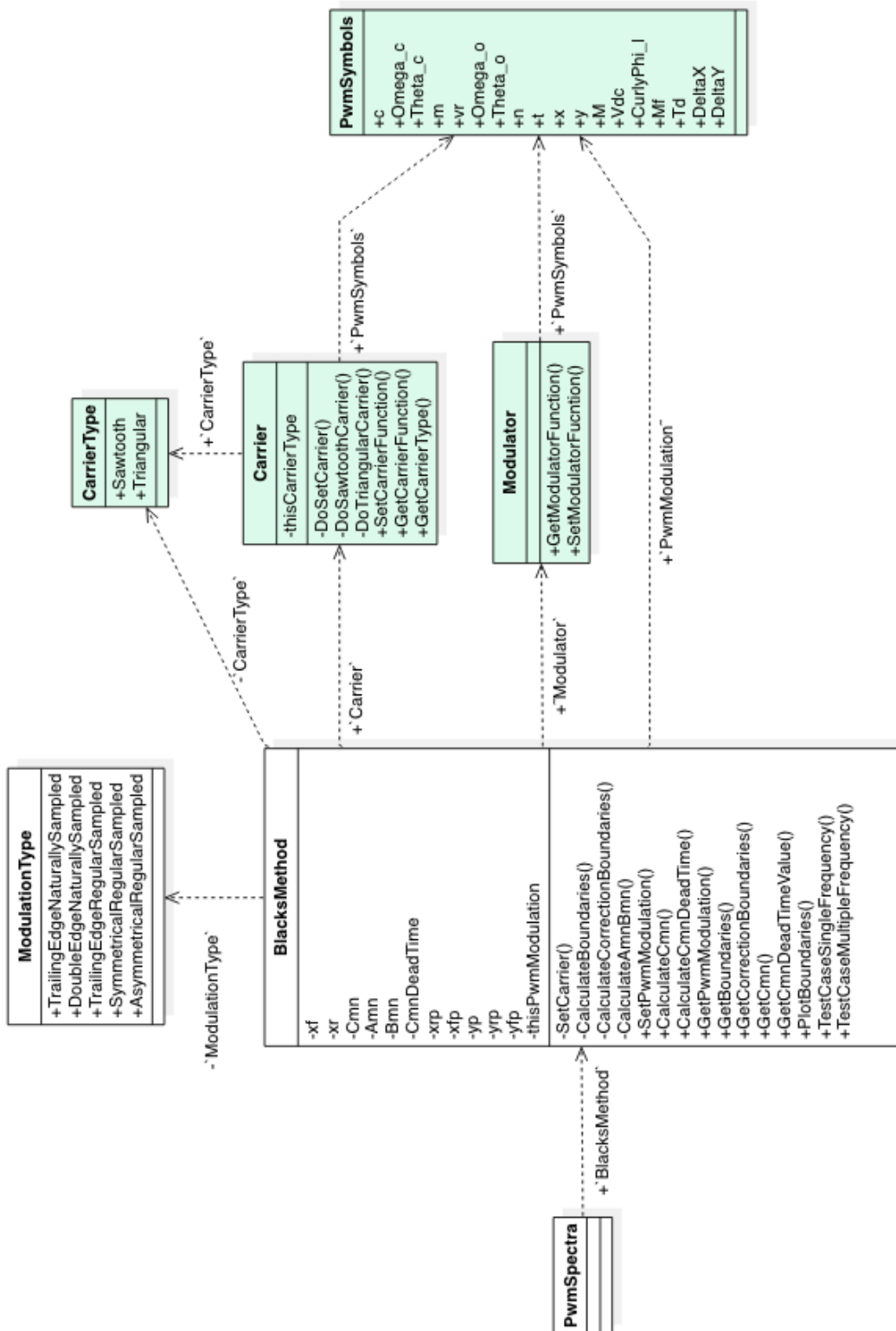


Figure E.1 - UML diagram of *PwmSpectra* V1.0.

E.3 Wolfram Mathematica[®] Notebook of a *PwmSpectra* Examples

Analytical harmonic study of PWM with Multiple-frequency input and dead-time

```
In[703]:= << PwmSpectra`
```

```
In[704]:= Remove["Global`*"]
```

■ PWM Definition set-up

Attributes

Auxiliary Functions

Main Constructor

```
In[714]:= setPwmModulation[DoubleEdgeNaturallySampled];
setTestCase[multipleFrequency];
setIntegralLimits[idealPwm];
```

■ Numerical Analysis

Calculating the magnitude of the corrected fundamental-frequency component.

```
In[717]:= ClearAllSymbols[];
setPwmModulation[DoubleEdgeNaturallySampled];
setTestCase[multipleFrequency];
callTestCase[];
TestParameters[];
m = 0;
n = 1;
correction = CalculateCorrectedCmnValue[] // Norm
```

```
Out[724]= 0.642253
```

Calculating ideal spectra values.

```
In[725]:= Table[m; CalculateCmnValue[] // Norm, {m, 0, 3, 1}, {n, 1, 5, 1}] // MatrixForm
```

```
Out[725]//MatrixForm=
```

$$\begin{pmatrix} 0.8 & 4.9381 \times 10^{-7} & 6.93889 \times 10^{-17} & 6.93889 \times 10^{-18} & 0.05 \\ 1.03657 \times 10^{-7} & 0.217635 & 3.04984 \times 10^{-8} & 0.0179649 & 2.23534 \times 10^{-8} \\ 0.315943 & 1.03458 \times 10^{-7} & 0.160925 & 1.97089 \times 10^{-8} & 0.00985449 \\ 3.64229 \times 10^{-8} & 0.152662 & 3.22367 \times 10^{-8} & 0.101835 & 2.642 \times 10^{-8} \end{pmatrix}$$

Calculating correction spectra values.

```
In[726]:= Table[m;
n;
CalculateCorrectionCmnValue[] // Norm, {m, 0, 3, 1}, {n, 1, 5, 1}] // MatrixForm
```

```
Out[726]//MatrixForm=
```

$$\begin{pmatrix} 0.257625 & 7.13949 \times 10^{-17} & 0.0865804 & 7.009 \times 10^{-17} & 0.0526061 \\ 3.53816 \times 10^{-17} & 0.118379 & 9.81308 \times 10^{-18} & 0.0701632 & 6.74761 \times 10^{-17} \\ 0.147178 & 4.56334 \times 10^{-17} & 0.0694447 & 5.05159 \times 10^{-17} & 0.0291387 \\ 5.92859 \times 10^{-17} & 0.0567346 & 8.61269 \times 10^{-17} & 0.057589 & 6.05913 \times 10^{-17} \end{pmatrix}$$

- Frequency Plot

Parametric Variation Spectra

Auxiliary Functions

Calculate the effects of the parameter variation in the ideal, correction, and corrected Spectra

```
In[732]:= ClearAllSymbols[];
callTestCase[];
TestParameters[];
numberOfBaseBandHarmonics = 7;
numberOfCarrierHarmonics = 1;
numberOfSideBandHarmonics = 3;
darkMode = True;
SetParameterVariation["Td"];

showMatrixEnable = False;
CalculateVariationSpectra[showMatrixEnable]
```

Plot spectra of a parameter variations

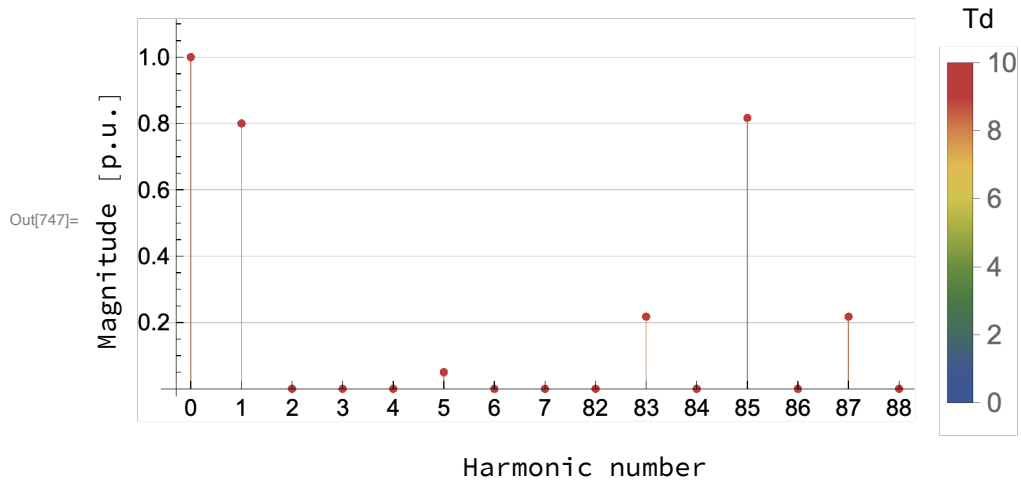
```
In[742]:= darkMode = False;
parameterLabel = StringJoin[{parameter, parameterUnits}];
xAxisLogScaleEnable = False;
parameterRange = {initialValue, finalValue}/parameterBase;

Print["Ideal spectra"]
PlotParameterSpectra[idealSpectra, parameter,
  parameterUnits, parameterRange, darkMode, xAxisLogScaleEnable]
Print["Correction spectra"]
PlotParameterSpectra[correctionSpectra, parameter,
  parameterUnits, parameterRange, darkMode, xAxisLogScaleEnable]
Print["Corrected spectra"]
PlotParameterSpectra[correctedSpectra, parameter,
  parameterUnits, parameterRange, darkMode, xAxisLogScaleEnable]
```

Ideal spectra

Double-Edge Naturally Sampled PWM Modulation

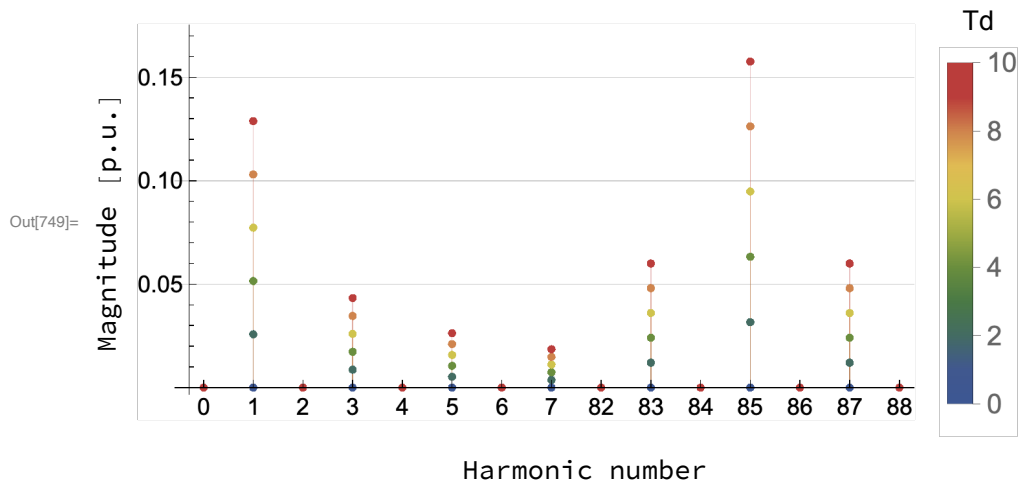
Parameters: $\omega_o=376.991[\text{rad/s}]$, $\omega_c=32044.2[\text{rad/s}]$, $M_f=85.$,
 $M=0.8[\text{p.u.}]$, $M_h=0.05[\text{p.u.}]$, $\varphi_l=0.785398[\text{rad/s}]$, $V_{dc}=1.[\text{p.u.}]$, $T_d=\text{variable}$



Correction spectra

Double-Edge Naturally Sampled PWM Modulation

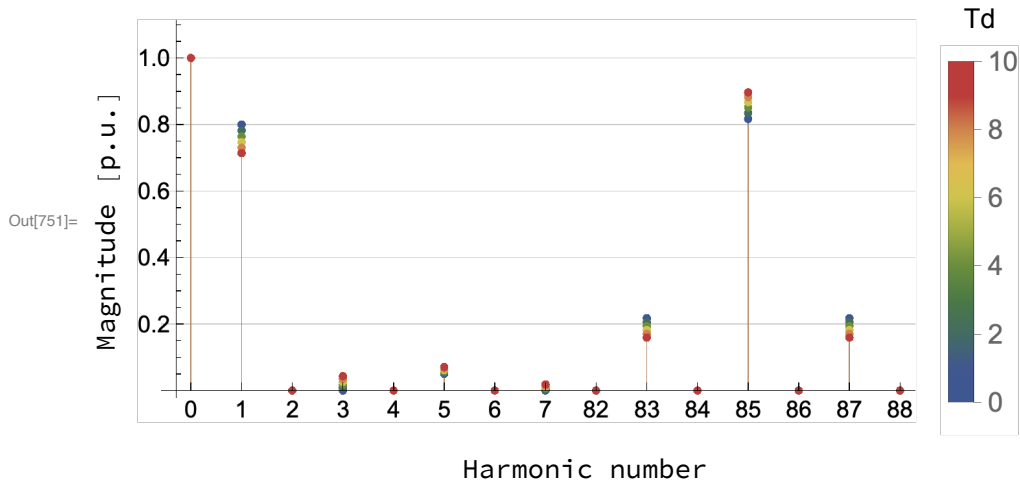
Parameters: $\omega_0=376.991$ [rad/s], $\omega_c=32044.2$ [rad/s], $M_f=85.$,
 $M=0.8$ [p.u.], $M_h=0.05$ [p.u.], $\phi_l=0.785398$ [rad/s], $V_{dc}=1.$ [p.u.], $T_d=variable$



Corrected spectra

Double-Edge Naturally Sampled PWM Modulation

Parameters: $\omega_0=376.991$ [rad/s], $\omega_c=32044.2$ [rad/s], $M_f=85.$,
 $M=0.8$ [p.u.], $M_h=0.05$ [p.u.], $\phi_l=0.785398$ [rad/s], $V_{dc}=1.$ [p.u.], $T_d=variable$



In[751]:=

Plot Matrix of component due to a parameter variation

In[753]:=

```
Print["Corrected spectra"]
parameterRange = {initialValue, finalValue}/parameterBase;
```

```
subPlotSize = 150;
initialComponent = 1;
componentIncrement = 1;
```

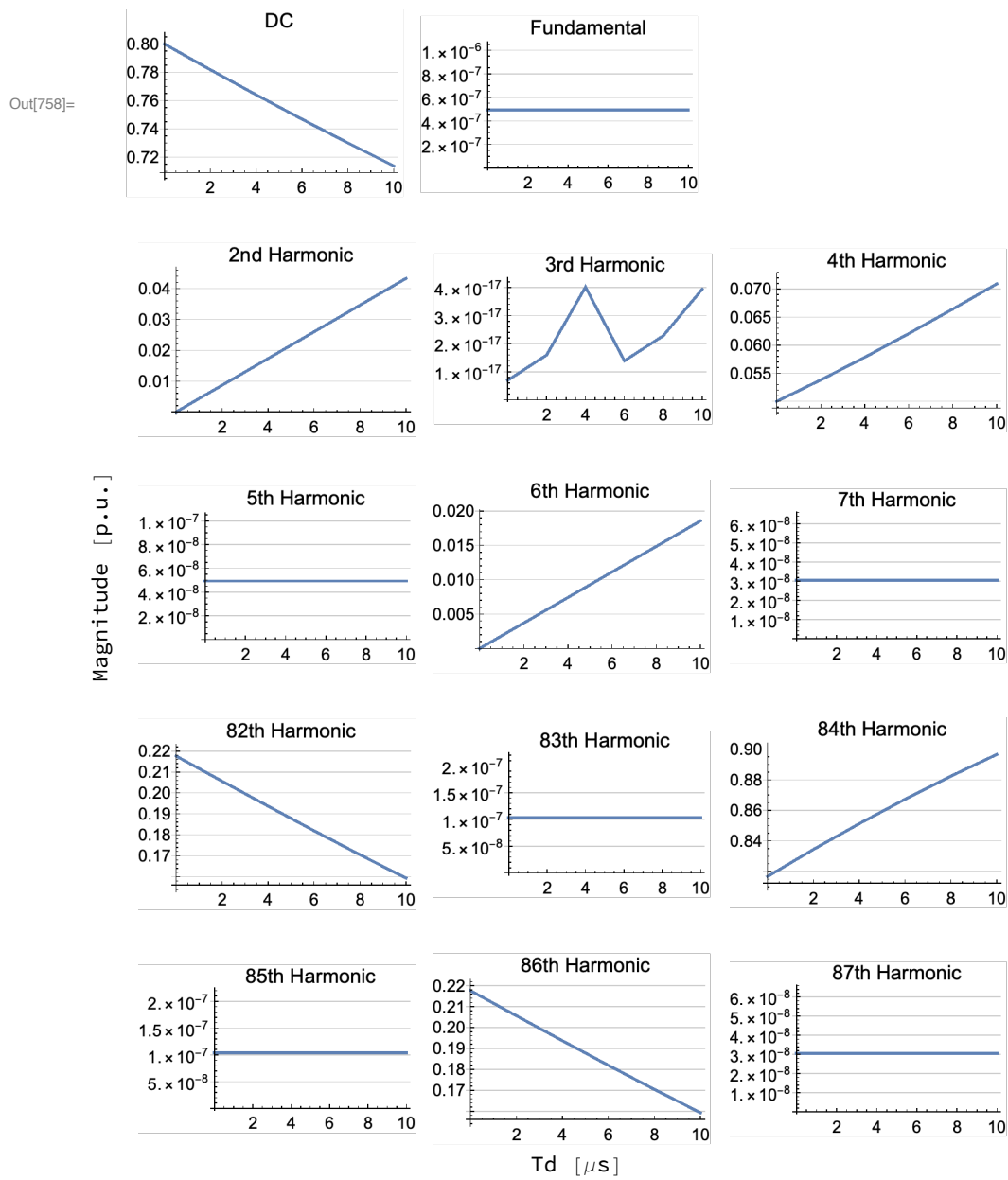
```
PlotComponentMatrixWithParameterVariation[
  correctedSpectra
  , parameter
  , parameterUnits
  , parameterRange
  , darkMode
  , xAxisLogScaleEnable
  , subPlotSize
  , initialComponent
  , componentIncrement
]
```

Corrected spectra

15

Double-Edge Naturally Sampled PWM Modulation

Parameters: $\omega_0=376.991$ [rad/s], $\omega_c=32044.2$ [rad/s], $M_f=85.$,
 $M=0.8$ [p.u], $M_h=0.05$ [p.u], $\varphi_l=0.785398$ [rad/s], $V_{dc}=1.$ [p.u], $T_d=variable$



- Calculating component expressions (analytically and numerically)

Auxiliary functions

DC

The ideal an correction part is given by

In[772]:= `calculateDcInnerIntegralSolutions[]`

Out[772]= `{0.31831 Vdc (1. + 1. M Cos[y] + 0.05 Cos[5. y]), 0.31831 Vdc (1. + 1. M Cos[y] + 0.05 Cos[5. y])}`

```
In[773]:= ConvertToMatlabExpression[dcInnerIntegralSolutions[[1]]]
ConvertToMatlabExpression[dcInnerIntegralSolutions[[2]]]

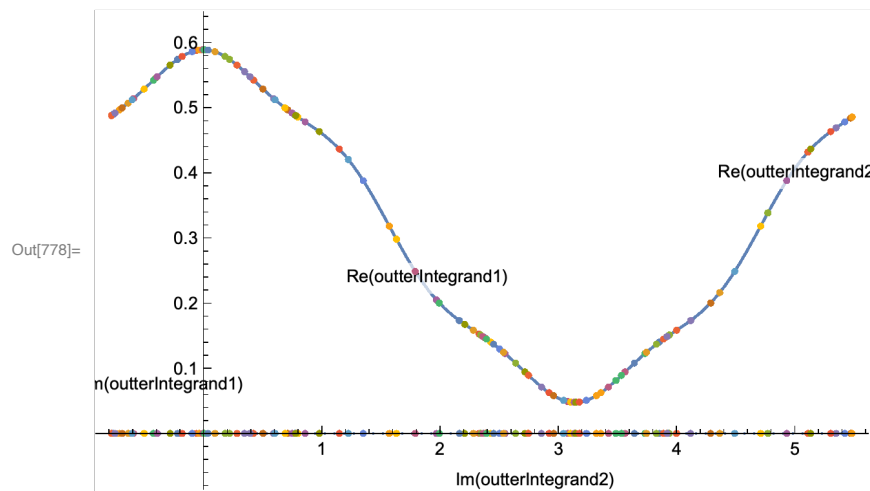
Out[773]= 0.3183098861837907.*Vdc.*(1. + 1.*M.*cos(y) + 0.04999999999999996.*cos(5.*y))

Out[774]= 0.3183098861837907.*Vdc.*(1. + 1.*M.*cos(y) + 0.04999999999999996.*cos(5.*y))
```

Performance Test

```
In[775]:= callTestCase[];
TestParameters[];
Print[C00 // AbsoluteTiming];
PlotEvaluationPointsOfOuterIntegral[dcInnerIntegralSolutions, yIntegralLimit]
```

{0.028866, 2.}



Fundamental

The fundamental component is given by

```
In[779]:= calculateFundamentalInnerIntegralSolutions[]

Out[779]= {0.31831 e^{i y} (1. Vdc + 1. M Vdc Cos[y] + 0.05 Vdc Cos[5. y]),
0.31831 e^{i y} (1. Vdc + 1. M Vdc Cos[y] + 0.05 Vdc Cos[5. y])}

In[780]:= ConvertToMatlabExpression[fundamentalInnerIntegralSolutions[[1]]]
ConvertToMatlabExpression[fundamentalInnerIntegralSolutions[[2]]]

Out[780]= 0.3183098861837907.*exp(1i.*y).*(1.*Vdc +
1.*M.*Vdc.*cos(y) + 0.04999999999999996.*Vdc.*cos(5.*y))

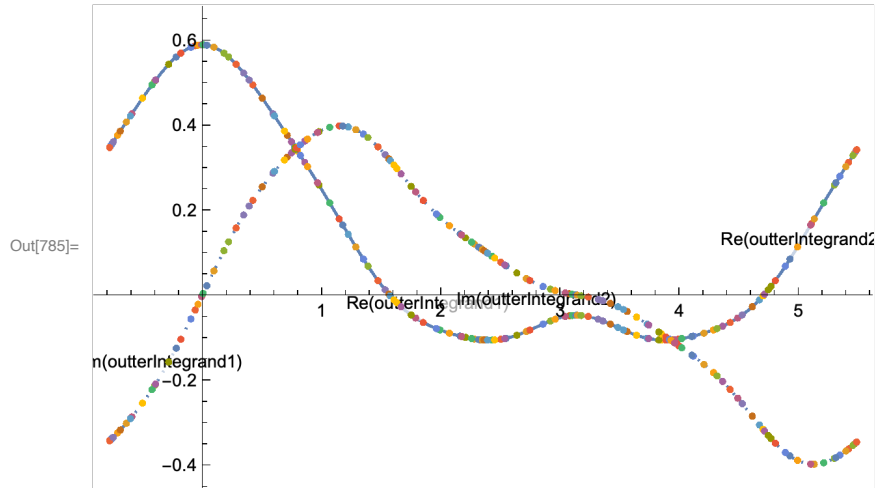
Out[781]= 0.3183098861837907.*exp(1i.*y).*(1.*Vdc +
1.*M.*Vdc.*cos(y) + 0.04999999999999996.*Vdc.*cos(5.*y))
```

Performance Test

```

In[782]:= callTestCase[];
TestParameters[];
Print[C01 // AbsoluteTiming];
PlotEvaluationPointsOfOuterIntegral[fundamentalInnerIntegralSolutions, yIntegralLimit]
{0.011046, {0.8, 5.55112 × 10-17}}

```



Baseband Harmonics

The fundamental harmonics are given by

```
In[786]:= calculateSignalHarmonicsInnerIntegralSolutions[]
```

```
Out[786]:= {0.31831 ei n y (1. Vdc + 1. M Vdc Cos [y] + 0.05 Vdc Cos [5. y]),
0.31831 ei n y (1. Vdc + 1. M Vdc Cos [y] + 0.05 Vdc Cos [5. y])}
```

```
In[787]:= ConvertToMatlabExpression[signalHarmonicsInnerIntegralSolutions[[1]]]
ConvertToMatlabExpression[signalHarmonicsInnerIntegralSolutions[[2]]]
```

```
Out[787]:= 0.3183098861837907.*exp(1i.*n.*y).*(1.*Vdc
+ 1.*M.*Vdc.*cos(y) + 0.04999999999999996.*Vdc.*cos(5.*y))
```

```
Out[788]:= 0.3183098861837907.*exp(1i.*n.*y).*(1.*Vdc
+ 1.*M.*Vdc.*cos(y) + 0.04999999999999996.*Vdc.*cos(5.*y))
```

Performance Test

```

In[789]:= callTestCase[];
TestParameters[];
n = 3;
Print[C0n[n] // AbsoluteTiming];
PlotEvaluationPointsOfOuterIntegral[
  signalHarmonicsInnerIntegralSolutions, yIntegralLimit]

```

```
{0.01284, {8.04912 × 10-16, 8.32667 × 10-17}}
```

